Universität Hamburg

DER FORSCHUNG | DER LEHRE | DER BILDUNG

Characterization of HN1L: a novel signaling protein connecting NAADP and Ca^{2+} microdomain formation in T cells

Dissertation

Zur Erlangung der Würde des Doktors der Naturwissenschaften des Fachbereichs Biologie der Fakultät für Mathematik, Informatik und Naturwissenschaften der Universität Hamburg

vorgelegt von

Imrankhan Khansahib

aus Sivaganga, India

Hamburg, 2022

Folgende Gutachter empfehlen die Annahme der Dissertation:

Prof. Dr. rer. nat. Dr. med. habil. Andreas H. Guse
Prof. Dr. rer. nat. Hans Willi Mitrücker

Datum der Disputation: 10.06.2022

ABSTRACT

Nicotinic acid adenine dinucleotide phosphate (NAADP) is the most potent calcium ion (Ca^{2+}) mobilizing secondary messenger targeting ryanodine receptor type 1 (RYR1) for Ca^{2+} release from ER in T cells. It has been reported to evoke the earliest local Ca^{2+} signals, also termed Ca^{2+} microdomains, during activation of T cells. Photoaffinity labelling (PAL) revealed that NAADP binds to a small cytosolic protein (NAADP-binding protein) of 22/23 kDa size, which then together activates the RYR1 localized on membrane of the endoplasmic reticulum (ER). Our group identified the 22/23 kDa protein to be hematological and neurological expressed 1–like protein (HN1L), also called jupiter microtubule-associated homolog 2 (JPT2). This thesis further characterizes the identified protein, HN1L, by assessing its binding towards NAADP and elucidating its role in NAADP-mediated Ca^{2+} signaling in T cells.

PAL with recombinant HN1L showed strong labelling by the probe which was displaced by NAADP in nanomolar range suggesting that HN1L is a highly specific NAADP-binding protein. Further, PAL with deletion mutants of HN1L provided insights that NAADP binds to latter half of HN1L close to the C-terminal end. Functional knockout of *hn1l* in Jurkat T cells resulted in delayed onset and reduced amplitude of global Ca^{2+} signaling. Fast and local Ca^{2+} imaging of *hn1l*$^{-/-}$ Jurkat T cells showed that the number of initial Ca^{2+} microdomains reduced significantly upon activation. Similar effects on both local and global Ca^{2+} signals were obtained by knocking out *hn1l* in rat primary T cells. Impaired Ca^{2+} signaling in the absence of HN1L in two different systems strongly claims that it has an important signaling function in NAADP signalosome in T cells.

Super-resolution via optical reassignment (SoRa) imaging showed that HN1L and RYR colocalize at ER-plasma membrane (PM)-junction and upon stimulation, HN1L was found to translocate towards the PM suggesting a role of HN1L at ER-PM junction during activation of T cells. The structural data showed that HN1L and NAADP interact with SPRY2 (domain 2 found in splA kinase and ryanodine receptors) and bridging solenoid (Bsol) domains of RYR1, strongly supporting the colocalization findings. Furthermore, the open probability (P_o) of RYR1 increased significantly in the presence of HN1L and NAADP. Overall, a strong association between HN1L and RYR1 has been shown.

Taken together, the data presented in this thesis demonstrates that HN1L functions as a NAADP-binding protein enabling NAADP to evoke Ca^{2+} release from ER via RYR1 in T cells.

ZUSAMMENFASSUNG

Nicotinsäureadenindinukleotidphosphat (NAADP) ist der potenteste, Calciumion (Ca^{2+}) mobilisierende sekundäre Botenstoff, der den Ryanodinrezeptor Typ 1 (RYR1) öffnet und so die Ca^{2+} Freisetzung aus dem ER in T-Zellen vermittelt. Es wurde berichtet, dass NAADP die frühesten lokalen Ca^{2+} Signale während der Aktivierung von T-Zellen hervorruft, die auch als Ca^{2+} Mikrodomänen bezeichnet werden. Durch Photoaffinitätsmarkierung (PAL) konnte gezeigt werden, dass NAADP an ein kleines zytosolisches Protein (NAADP-bindendes Protein) mit einer Größe von 22/23 kDa bindet, das dann gemeinsam den RYR1 an der Membran des Endoplasmatischen Retikulums (ER) aktiviert. Unsere Gruppe konnte ein 22/23 kDa großes Protein als hematological and neurological expressed 1–like protein (HN1L) identifizieren, das auch als jupiter microtubule-associated homolog 2 (JPT2) bezeichnet wird. In dieser Arbeit wurde das identifizierte Protein, HN1L, weiter charakterisiert indem seine Bindung an NAADP und seine Signalfunktion bei der NAADP-vermittelten Ca^{2+} Signalübertragung in T-Zellen untersucht wurde.

PAL mit rekombinantem HN1L zeigte eine starke Bande durch die Sonde, welche durch NAADP im nanomolaren Bereich verdrängt werden konnte, was darauf schließen lässt, dass HN1L ein hochspezifisches NAADP-bindendes Protein ist. Darüber hinaus wurden PAL-Experimente mit Deletionsmutanten von HN1L durchgeführt, wodurch das C-terminale Ende als NAADP bindende Stelle identifiziert wurde. Der funktionelle Knockout von *hn1l* in Jurkat-T-Zellen führte zu einem verzögerten Einsetzen und einer reduzierten Amplitude von globalen Ca^{2+} Signalen. Schnelle und lokale Ca^{2+} Mikroskopie von *hn1l*$^{-/-}$ Jurkat T-Zellen zeigte, dass die Anzahl der initialen Ca^{2+} Mikrodomänen nach der Aktivierung deutlich abnahm. Ähnliche Auswirkungen auf lokale und globale Ca^{2+} Signale wurden durch KO von *hn1l* in primären T-Zellen der Ratte verifiziert. Die Beeinträchtigung der Ca^{2+} Signalübertragung in Abwesenheit von HN1L in zwei verschiedenen Systemen deutet darauf hin, dass es eine wichtige Funktion im NAADP-Signalosom in T-Zellen hat.

Super-Resolution via Optical Reassignment (SoRa) Mikroskopie zeigte, dass HN1L und RYR an der ER-Plasmamembran (PM)-Kontaktstelle ko-lokalisieren und dass HN1L bei Stimulation in Richtung PM transloziert, was auf eine Rolle von HN1L während der Aktivierung von T-Zellen an der ER-PM-Kontaktstelle schließen lässt. Zusätzlich zeigten Strukturdaten, dass HN1L zusammen mit NAADP mit den SPRY2 (domain 2 found in splA kinase and ryanodine receptors)- und bridging solenoid (Bsol)-Domänen von RYR1 interagieren, was die Ergebnisse der Ko-lokalisierung weiter unterstützt. Außerdem stieg die Öffnungswahrscheinlichkeit (P_o) von RYR1 in Gegenwart von HN1L und NAADP deutlich an. Insgesamt konnte eine starke Verbindung zwischen HN1L und RYR1 nachgewiesen werden.

Insgesamt zeigen die in dieser Arbeit vorgelegten Daten, dass HN1L als NAADP-bindendes Protein fungiert, welches die Ca^{2+} Freisetzung aus dem ER über RYR1 durch Bindung an NAADP in T-Zellen vermittelt.

TABLE OF CONTENTS

LIST OF ABBREVIATIONS

Å	Angstrom
%	Percentage
°C	Celsius degree
µg	Microgram
µL	Microlitre
µM	Micromolar
AHT	Anhydrotetracycline
APC	Antigen presenting cell
ATP	Adenosine triphosphate
bs	Beam splitter
BSA	Bovine serum albumin
Ca^{2+}	Calcium
cADPR	Cyclic adenosine diphosphate ribose
CICR	Calcium induced calcium release
CO_2	Carbon dioxide
CRISPR	Clustered regularly interspaced short palindromic repeats
DAG	Diacylglycerol
DNA	Deoxyribonucleic acid
DNAse	Deoxyribonuclease
DTT	Dithiothreitol
DUOX	Dual NADPH oxidase
E	Elution buffer
E.coli	Escherichia coli
e.g.	Example
EC	Excitation-contraction
EDTA	Ethylenediaminetetraacetic acid
EGTA	Ethylene glycol-bis(β-aminoethyl ether)-N,N,N′,N′-tetraacetic acid
em	Emission
Epac	Exchange protein directly activated by cAMP
ER	Endoplasmic reticulum
ex	Excitation
FACS	Fluorescence-activated cell sorting

FBS	Fetal bovine serum
GLC-6-P-DH	Glucose-6-phosphate dehydrogenase
g	Gram
HCl	Hydrochloric Acid
HEPES	4-(2-hydroxyethyl)-1-piperazineethanesulfonic acid
His	Histidine
HN1L	Hematological and neurological expressed 1-like protein
HRP	Horseradish peroxide
IP_3	D-*myo*-inositol-1,4,5-triphosphate
IP_3R	D-*myo*-inositol-1,4,5-triphosphate receptor
KCl	Potassium chloride
kDa	Kilo dalton
LGCC	Ligand-gated calcium channel
LSM12	Sm-like protein 12
M	Molar
mA	Milliampere
mAb	Monoclonal antibody
mg	Milligram
$MgCl_2$	Magnesium chloride
$MgSO_4$	Magnesium sulphate
MHC	Major histocompatibility complexes
mL	Millilitre
mM	Millimolar
MS	Mass spectroscopy
NaH_2PO_4	Monosodium dihydrogen phosphate
NADP	Nicotinamide adenine dinucleotide phosphate
NADPH	Reduced nicotinamide adenine dinucleotide phosphate
NAADP	Nicotinic acid adenine dinucleotide phosphate
NAADPH	Reduced nicotinic acid adenine dinucleotide phosphate
NAADP-BP	NAADP binding protein
Ni-NTA	Nickel-Nitriloacetic acid
ng	Nanogram
nm	Nanometer
nM	Nanomolar
OD	Optical density

OKT3	Muromonab-CD3
ORAI	Calcium Release-Activated Calcium Modulator
pH	Power of hydrogen
PCR	Polymerase chain reaction
PIP2	Phosphatidylinositol 4,5- bisphosphate
PLCγ1	Phospholipase C γ1
PLL	Poly-l-lysine
PM	Plasma membrane
PMCA	Plasma membrane Ca^{2+} ATPase
PVDF	Polyvinylidene Fluoride
R	Regeneration buffer
RNA	Ribonucleic acid
RNAse	Ribonuclease
RSB	Reticulocyte standard buffer
RYR	Ryanodine receptor
SDS	Sodium dodecyl sulfate
SERCA	Sarco/endoplasmic reticulum Ca^{2+} ATPase
SOB	Super optimal broth
SOC	Super optimal broth with catabolite repression
SOCE	Store operated Ca^{2+} entry
SR	Sarcoplasmic reticulum
STIM	Stromal interaction molecule
TAE	Tris-acetate-ethylnediaminetetraacetic acid
TBS	Tris buffered saline
TBST	Tris buffered saline tween
TCR	T cell receptor
TPC	Two pore channel
tRNA	Transfer RNA
V	Voltage
v/v	Volume/volume
VGCC	Voltage-gated calcium channel
W	Wash buffer
w/v	Weight/volume

LIST OF FIGURES

LIST OF TABLES

1 INTRODUCTION

1.1 CALCIUM SIGNALING

Calcium is considered as one of the abundant elements found in human with majority of it deposited in teeth and bones. Calcium ions (Ca^{2+}) are recognized as an essential and universal messenger that control various cellular processes such as fertilization, cell proliferation and development, muscle contraction, exocytosis, gene transcription etc. (Berridge et al., 2000). A gradient of Ca^{2+} concentration is observed between the cells and extracellular space with free cytosolic Ca^{2+} concentrations ($[Ca^{2+}]_i$) at around 100 nM and extracellular Ca^{2+} concentrations ($[Ca^{2+}]_{ex}$) at around 1 mM (Berridge et al., 2000). Several pumps and exchangers on the plasma membrane (Lewis et al., 2012), Ca^{2+} binding proteins such as calmodulin, and compartmentalization of Ca^{2+} in internal Ca^{2+} stores, help the cells to maintain such concentration gradient across the PM (Clapham, 2007). In resting cells, plasma membrane Ca^{2+} ATPase (PMCA) at PM (Carafoli, 1991) and sarco/endoplasmic reticulum Ca^{2+} ATPases (SERCAs) at intracellular membranes (Toyoshima & Nomura, 2002) actively participate to maintain around 100 nM Ca^{2+} in cytosol by pumping out Ca^{2+} to extracellular space and by replenishing the intracellular Ca^{2+} stores respectively. Furthermore, Ca^{2+} binding proteins, such as for examples (e.g.) calmodulin, calretinin or parvalbumins (α and β isoforms) are involved in Ca^{2+} buffering to control Ca^{2+} persistence` in the cytosol (Gilabert, 2012). In activated cells (stimulated by a signal to perform particular function), several classes of (i) Ca^{2+} selective channel at PM, such as voltage-gated calcium channels (VGCCs), ligand-gated calcium channels (LGCCs) and (ii) channels at intracellular Ca^{2+} store membranes, e.g. ryanodine receptors (RYRs) or D-*myo*-inositol-1,4,5-triphosphate receptors (IP_3Rs), actively participate to rapidly increase the $[Ca^{2+}]_i$ to around 1 mM (Berridge et al., 2000).

1.2 CALCIUM SIGNALING IN T LYMPHOCYTES

The immune system in mammals helps to fight pathogens bacteria, viruses and parasites by innate and adaptive immunity. The adaptive immune system consists of T lymphocytes, which are involved in cell-mediated immunity and B lymphocytes, that are responsible for humoral immunity. This thesis focuses on T lymphocytes, hereafter referred to as T cells, and their initial mechanism(s) of activation. Accordingly, Ca^{2+} signaling in T cells is described in more detail below.

Ca^{2+} signaling plays a crucial role in immunity by regulating effector functions in T cells such as metabolism, proliferation, differentiation, antibody production, cytokine secretion and cytotoxicity (Trebak & Kinet, 2019). Activation of a T cell requires a specific antigenic peptide that is bound to major

histocompatibility complexes (MHC) found at the surface of antigen-presenting cells (APCs) and a T cell receptor (TCR). TCR comprises of a α:β heterodimer with four invariant signaling chains collectively called as CD3, at the surface of the T cells that is specific to the antigen presented by APCs. Such TCR-MHC interaction leads to rise of $[Ca^{2+}]_i$ initiated by Ca^{2+} mobilizing secondary messengers formed in cytosol of T cells. In addition to the TCR-MHC ligation, co-stimulation by binding of CD80 and CD86 (expressed on APCs) to CD28 (their receptor, expressed on T cells) is required to fully activate the T cells and such contacts have to last for some time to instigate gene expression changes in T cells (Feske, 2007).

1.2.1 Secondary Messengers

Three intracellular secondary messengers mobilize Ca^{2+} during activation of T cells with distinct signaling pathways namely D-*myo*-inositol-1,4,5-triphosphate (IP_3), cyclic ADP-ribose (cADPR) and nicotinic acid adenine dinucleotide phosphate (NAADP). These three secondary messengers show distinct formation kinetics upon activation of T cells. Figure 1 shows concentrations of secondary messengers formed in Jurkat T cells upon stimulation with a monoclonal antibody against CD3 (Muromonab-CD3 / OKT3) with their corresponding involvement in increase of $[Ca^{2+}]_i$.

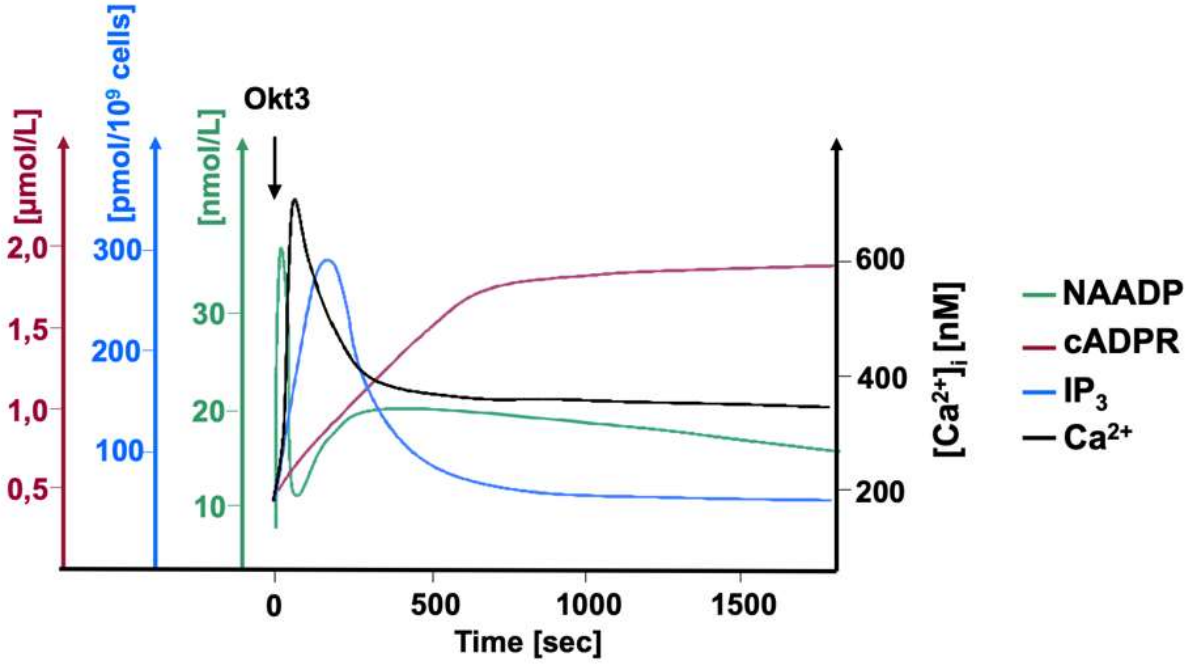

Figure 1: Concentrations of secondary messengers over time upon activation of T cells with OKT3: A comparison of concentrations of secondary messengers formed and their involvement in increasing cytosolic Ca^{2+} concentration upon stimulation of T cells with OKT3. Addition of OKT3 is indicated by an arrow. (modified from Gasser et al., 2006; Guse et al., 1999; Guse et al., 1993).

1.2.1.1 D-myo-inositol-1,4,5-triphosphate (IP_3)

IP_3 was first reported as Ca^{2+} mobilizing secondary messenger in pancreatic acinar cells almost 4 decades ago (Streb et al., 1983) and since then it was well studied and characterized. Figure 2 shows the chemical

structure of IP_3. Upon activation of T cells, phospholipase C γ1 (PLCγ1) cleaves phospholipid phosphatidylinositol 4,5-bisphosphate (PIP_2) to form two products namely diacylglycerol (DAG) and IP_3 (Feske, 2007). It is clear from Figure 1 that IP_3 is formed in 2-3 minutes post stimulation of T cells followed by activation of IP_3R, which is a ligand-activated Ca^{2+} channel located on the membrane of endoplasmic reticulum (ER). Such interaction of IP_3 with IP_3R evokes Ca^{2+} release from ER (Foskett et al., 2007). IP_3R is expressed in T cells as three subtypes namely IP_3R1, IP_3R2 and IP_3R3 (Nagaleekar et al., 2008), which form homo- and hetero-tetrameric complexes (Taylor et al., 1999). It was previously reported that IP_3 binds to all IP_3R subtypes with highest affinity towards IP_3R2 (Iwai et al., 2007). Moreover, Ca^{2+} actively regulates all three subtypes of IP_3R displaying a bell-shaped relationship: low Ca^{2+} concentrations (< 300 nM) open the channel for Ca^{2+} release whereas high concentrations of Ca^{2+} (> 300 nM) inhibit the Ca^{2+} release from ER (Bezprozvanny et al., 1991). Among the three subtypes, IP_3R3 shows the highest affinity to Ca^{2+} and IP_3R1 displaying the lowest affinity (Tu et al., 2005).

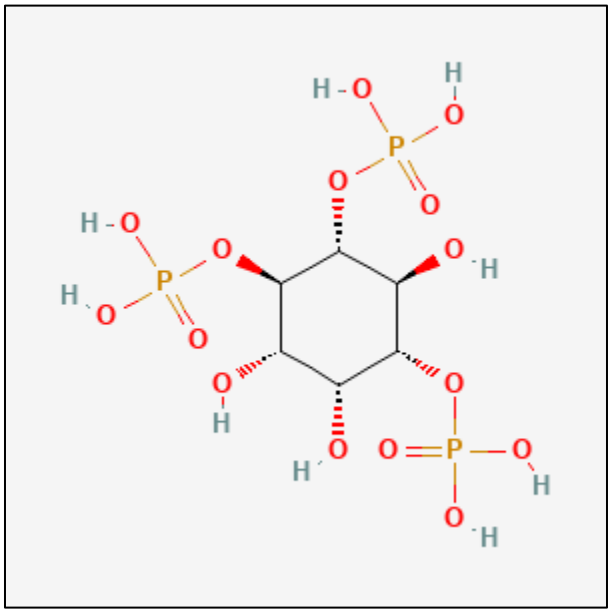

Figure 2: Atomic structure of IP_3: IP_3 has a molecular mass of 420.10 g/mol and is composed of an inositol ring three phosphate groups at carbon positions 1, 4 and 5 (https://pubchem.ncbi.nlm.nih.gov)

1.2.1.2 Cyclic ADP-ribose (cADPR)

cADPR was first discovered as a Ca^{2+} mobilizing secondary messenger in sea urchin egg homogenates showing distinct Ca^{2+} release as compared to IP_3-mediated Ca^{2+} release (Clapper et al., 1987). It has been reported that cADPR evokes Ca^{2+} release in approximately 40 different cell types (Galione & Churchill, 2002). Lee et al. (1995) reported that cADPR is synthesized by cyclization of β-NAD catalysed by ADP-ribosyl cyclase, also known as CD38. Figure 3 shows the chemical structure of cADPR. Upon activation of T cells, cADPR contributes to the global Ca^{2+} signals much later than IP_3 (Figure 1). cADPR activates RYR on the ER to evoke Ca^{2+} release and enhances the Ca^{2+} induced Ca^{2+} release (CICR) (Galione et al., 1991).

Accordingly, Schwarzmann et al. (2002) reported that cADPR showed supressed Ca^{2+} signals in *ryr* knockdown T cells.

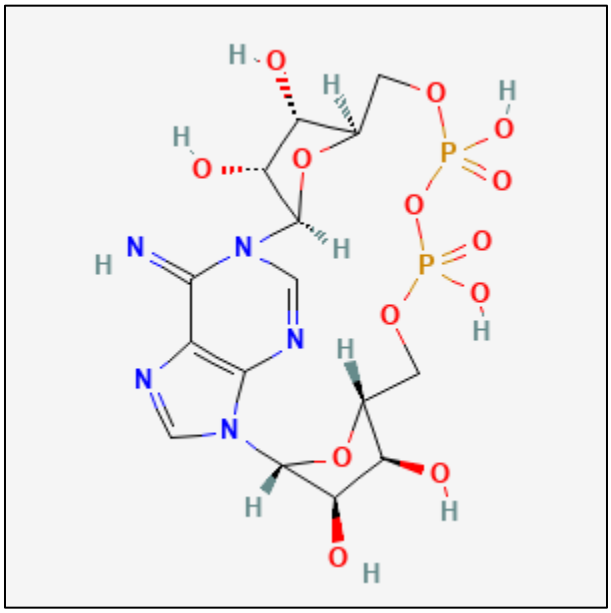

Figure 3: Atomic structure of cyclic ADP-ribose (cADPR): cADPR is a cyclic adenine nucleotide with two phosphate groups at 5`OH group of adenosine. The second phosphate group is further connected to a ribose at its 5` position. This ribose closes the cycle by attaching to the nitrogen at position 1 of adenine using a glycosidic linkage. Molecular mass of cADPR is 541.30 g/mol. (https://pubchem.ncbi.nlm.nih.gov)

1.2.1.3 Nicotinic Acid Adenine Dinucleotide Phosphate (NAADP)

NAADP was the latest member of secondary messengers discovered that mobilizes Ca^{2+}. It was first discovered as an impurity in commercial nicotinamide adenine dinucleotide (NADP) that could evoke Ca^{2+} release in sea urchin homogenates (Clapper et al., 1987). Later in 1995, by performing HPLC, ^{1}H NMR and mass spectroscopy, the Ca^{2+}-releasing compound was identified to be NAADP (Lee & Aarhus, 1995). Figure 4 shows the atomic structural differences between NADP and NAADP. It is intriguing that the substitution of amide group by carboxylic group in NADP provides a novel signaling function to the molecule. It was also reported that EC_{50} of NAADP was around 30 nM to evoke Ca^{2+} release in sea urchin egg homogenates whereas the NAADP analogues such as NADP and NAAD could not evoke Ca^{2+} release at 1.1 µM and 4 µM respectively suggesting that NAADP is the most potent Ca^{2+} mobilizing secondary messengers as compared to IP_3 and cADPR (Lee & Aarhus, 1995). As shown in Figure 1, NAADP evokes Ca^{2+} release from intracellular Ca^{2+} stores already at nanomolar concentrations with in first few seconds after activation of T cells. Moreover, NAADP has been shown to initiate short-lived and localized Ca^{2+} signals, termed as Ca^{2+} microdomains, readily in the first seconds after activation of T cells (Wolf et al., 2015).

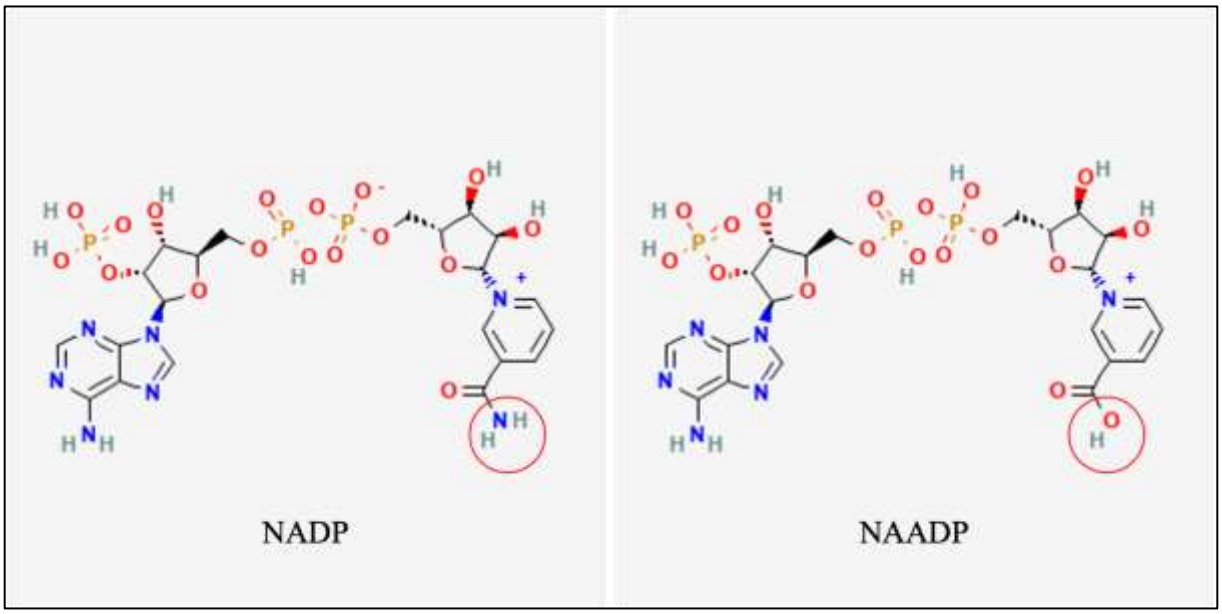

Figure 4: Atomic structural differences between NADP and NAADP: NADP and NAADP are the members of adenine dinucleotide with an amide and carboxylic group at 3` position of the pyridine ring respectively. The molecular mass of NAADP is 745.40 g/mol (https://pubchem.ncbi.nlm.nih.gov)

1.3 NAADP-MEDIATED Ca^{2+} SIGNALING

1.3.1 Synthesis of NAADP

Several groups have reported that NAADP is produced upon specific extracellular stimulation in different types of cells such as mouse pancreatic acinar cells (Yamasaki et al., 2005), adipocytes (Song et al., 2012), pancreatic beta cells (Masgrau et al., 2003), myocytes (Lewis et al., 2012) or human T cells (Gasser et al., 2006). However, production of NAADP in the cells was controversially discussed. Chini and Dousa (1995) showed that NAADP can be synthesized by incubating NADP with nicotinic acid in multiple tissue homogenates. Later that year, Aarhus et al. (1995) suggested that Aplysia ADP-ribosyl cyclase and mammalian CD38 can synthesize NAADP by catalysing the base exchange reaction between NADP and nicotinic acid. These enzymes have also been reported to synthesize cADPR *in vitro* (Howard et al., 1993; Lee & Aarhus, 1991). Figure 5 shows the synthesis of adenine derived secondary messengers (NAADP and cADPR) catalysed by mammalian CD38. The base exchange reaction catalysed by CD38 requires high concentration of nicotinic acid (in mM range) and acidic pH 4-5 to synthesize NAADP suggesting that CD38 cannot synthesize NAADP at physiological conditions (Aarhus et al., 1995).

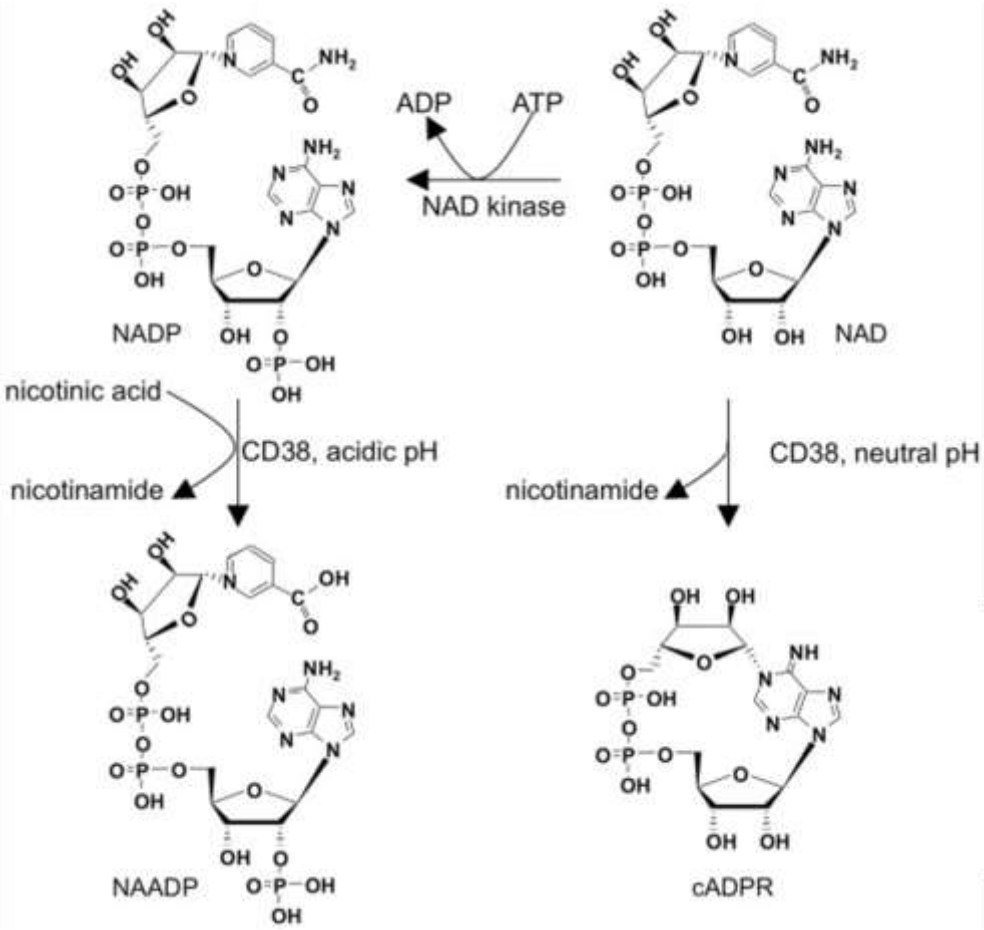

Figure 5: Synthesis of NAADP and cADPR catalyzed by CD38: CD38 catalyzes a base exchange reaction between NADP and excess amount of nicotinic acid at acidic pH to synthesize NAADP. While cADPR is synthesized by CD38 from NAD at neutral pH. (modified from (Ernst et al., 2013).

Recently, Gu et al., (2021) showed that knockout of *cd38* in T cells did not affect Ca^{2+} signaling upon stimulation. Furthermore, they demonstrated that Dual NADPH oxidase 2 (DUOX 2) is the responsible enzyme at PM to synthesize NAADP from NAADPH upon activation of T cells (Gu et al., 2021). They also claim that about 85 to 100-fold excess of NAADPH is likely present under reduced conditions in the cytosol suggesting the involvement of glucose-6-phosphate dehydrogenase (GLC-6-P-DH) forming a DUOX2- and GLC-6-P-DH–catalysed redox cycle to produce and degrade NAADP through NAADPH as an inactive intermediate (Gu et al., 2021). In addition, functional knockout of *duox2* in T cells affected Ca^{2+} signaling upon activation of T cells (Gu et al., 2021).

1.3.2 Organelles targeted by NAADP

When Lee and Aarhus (1995) initially discovered Ca^{2+} releasing activity of NAADP in sea urchin egg homogenates, they reported that the yolk fraction, separated by Percoll density gradient centrifugation, showed explicit responses to NAADP. Furthermore, they claimed the reserve granule from the yolk fraction

to be the organelle targeted by NAADP (Lee & Aarhus, 1995). Later, Churchill et al. (2002) showed that the identified reserve granule in sea urchin egg homogenates is highly comparable to lysosomes in mammalian cells suggesting lysosomes to be the NAADP-sensitive organelle s in mammalian cells. To support these findings, three independent groups reported evidence showing lysosomes were targeted by NAADP via two pore channels (TPCs) that are expressed on membranes of lysosomes (Brailoiu et al., 2009; Calcraft et al., 2009; Zong et al., 2009). However, by performing lipid planar bilayer experiments, Hohenegger et al. (2002) identified that RYR1, which is expressed on membranes of ER or sarcoplasmic reticulum (SR) in mammalian cells, potentially responded to NAADP, claiming ER/SR to be the organelles targeted by NAADP. Furthermore, microinjection of NAADP in T cells evoked Ca^{2+} release from ER, but not from lysosomes as the inhibitor of vacuolar type H^+- ATPase, bafilomycin A, had no effect in Ca^{2+} signaling evoked by NAADP (Steen et al., 2007). Contrastingly, Gerasimenko et al. (2006) showed that NAADP evoked Ca^{2+} release from both ER and acidic vesicles in pancreatic acinar cells indicating that NAADP may target more than one organelle, perhaps in a cell-type specific manner.

1.3.3 NAADP sensitive ion channels

Conflicting research propose that either ER/SR or lysosomes or even both organelles respond to NAADP via RYR1 or TPCs respectively. RYRs are the largest known ion channels with molecular mass of > 2 MDa and they are expressed as homotetramers on membranes of ER/SR (Zalk et al., 2007). Like IP_3Rs, RYRs are expressed in mammalian cells as three subtypes with approximately 70 % sequence identity: RYR1, 2 and 3 (Rossi & Sorrentino, 2002). Ledbetter et al. (1994) showed that RYR1 is predominantly expressed in skeletal muscles mediating excitation-contraction (EC) coupling, while RYR2 and RYR3 are mainly expressed in cardiac muscles and brain cells respectively. Moreover, several groups have reported the expression of RYRs in various immune cells such as dendritic cells, T and B cells and their roles in Ca^{2+} signaling and proliferation (Guse et al., 1999; Hosoi et al., 2001; O'Connell et al., 2002; Sei et al., 1999).

Mojzisová et al. (2001) provided the initial evidence that the open probability of RYR2 from cardiac microsomes increased in presence of 1 μM NAADP using lipid planar bilayer recordings. However, 1 μM of NAADP is considered non-physiological as several groups have reported that the cytosolic concentration of NAADP in mammalian cells lie between 10 and 100 nM (Churamani et al., 2012; Gasser et al., 2006; Schmid et al., 2012). On the other hand, Hohenegger et al. (2002) reported concentration-response relationships with RYR1 purified from rabbit skeletal muscles in lipid planar bilayer showing activity of NAADP at concentrations between 30 and 100 nM. Later in 2003, Gerasimenko et al. (2003) found that NAADP evokes Ca^{2+} release from thapsigargin-sensitive nuclear envelope, which is considered to be a continuum of ER with RYR expression. Similarly, Jurkat T cells showed global Ca^{2+} signals upon microinjecting with NAADP (Langhorst et al., 2004). Such signals were reduced either by knocking out

ryr or by introducing ruthenium red, an inhibitor of RYR (Langhorst et al., 2004). Further, upon microinjection of NAADP in Jurkat T cells, initial Ca^{2+} signals were formed with in 1.5 seconds post microinjection very close to the site of injection (Dammermann & Guse, 2005). Such initial signals were found to be similar to the signals observed in the first seconds close to the PM upon TCR/CD3 stimulation with anti-CD3 antibodies (Kunerth et al., 2003). Moreover, Wolf et al. (2015) showed that knockdown of *ryr* in Jurkat T cells and primary murine T cells resulted in either no or significantly fewer Ca^{2+} microdomains closer to the PM upon activation of these T cells. Furthermore, Diercks et al. (Diercks et al., 2018) reported that both BZ194, a reported antagonist of NAADP (Dammermann et al., 2009), and *ryr* knockout decreased the number of Ca^{2+} microdomains formed in first 15 seconds upon activation of primary murine T cells suggesting the involvement of NAADP and RYR at initial phase of T cell activation. In contrast to these findings, microinjection of NAADP did not activate RYR1, which was heterologously expressed in HEK293 cells, rather TPCs responded to the microinjection (Ogunbayo et al., 2011). Further, Wagner et al. (2014) also showed that heterologously expressed RYR1 in HEK293 cells did not respond to NAADP by performing 'on nucleus' patch-clamp recordings.

As mentioned in section 1.3.2, TPCs, that are expressed on membranes of lysosomes, reported to be one of the NAADP-sensitive channels. These voltage-gated ion channels are expressed as both homo and heterodimers forming pseudo-tetrameric complexes (Rietdorf et al., 2011; Zong et al., 2009). Each subunit consists of two hydrophobic domains containing six transmembrane regions and a connecting cytosolic loop (Churamani et al., 2012). TPCs are expressed in mammalian cells as three isoforms: TPC1, 2 and 3. Among these isoforms, TPC1 and TPC2 are widely expressed in mammals, while TPC3 is not found in several prominent mammalian models e.g. humans, mice or rats (Zhu et al., 2010). Brailoiu et al. (2009) reported that microinjection of 10 nM NAADP in human adenocarcinoma cell line SkBr3, that overexpresses TPCs, evoked transient Ca^{2+} signals. Further, they reported that gene silencing of *tpc*1 and *tpc2* affected the NAADP-mediated Ca^{2+} signaling (Brailoiu et al., 2009). Embryonic fibroblasts from TPC1/2 deficient (*tpc1/2*$^{-/-}$) mice showed much affected NAADP-mediated Ca^{2+} signaling, which was rescued completely by re-expression of TPCs (Ruas et al., 2015). These data collectively suggest that TPC1/2 are the channels targeted by NAADP to evoke Ca^{2+} release from lysosomes. On the other hand, double knockout of TPC1 and TPC2 (*tpc1*$^{-/-}$*2*$^{-/-}$) did not affect the Ca^{2+} microdomain formation upon activation of primary murine T cells (Diercks et al., 2018). Further, TPCs have been reported to be primarily Na^{+} selective ion channels and that NAADP does not regulate them, but instead the membrane lipid $PI(3,5)P_2$ does, evoking Na^{+} currents (Cang et al., 2013; Wang et al., 2012). Moreover, it was reported that such $PI(3,5)P_2$ induced Na^{+} currents were significantly reduced in the absence of TPC1/2 and that NAADP stimulation showed no differences in the presence and absence of TPC1/2 (Wang et al., 2012). In addition to these findings, Pitt et al. (2014) proposed that TPC1 does not only mobilize Na^{+} and Ca^{2+}, but also H^{+}

and K^+. They also added that NAADP evokes H^+ release from the lysosomes via TPC1 and that Ca^{2+} releasing property of TPC1 depends on the ionic composition of lysosomes (Pitt et al., 2014).

1.3.4 Unifying hypothesis

Though NAADP has been shown to activate RYRs and TPCs for Ca^{2+} release from ER/SR and lysosomes respectively in various cell types, binding sites of NAADP in RYRs or TPCs has not been reported so far. Gerasimenko et al. (2003) hypothesized that NAADP and cADPR initially bind to distinct receptors, which then either directly or indirectly activate RYRs for Ca^{2+} release from ER. Walseth et al. (2012) and Lin-Moshier et al. (2012) used photoaffinity labelling (PAL) by using a modified NAADP analogue, [^{32}P]-5-N_3-NAADP, as a photoaffinity probe to identify the receptors of NAADP in mammalian cells and sea urchin egg homogenates. Interestingly, they discovered that neither RYR1 nor TPCs were labelled by the probe, but a small cytosolic protein of size 22/23 kDa termed as NAADP binding protein (NAADP-BP) (Lin-Moshier et al., 2012; Walseth et al., 2012). These findings strongly supported the hypothesis framed by Gerasimenko et al. (2003) that NAADP likely does not activate RYRs directly for Ca^{2+} release.

Taken together, a mechanistic action of NAADP-mediated Ca^{2+} signaling is depicted in Figure 6. Upon activation of T cells by an antigen presented by antigen presenting cells, DUOX2 oxidases NAADPH to synthesize NAADP in the cytosol, which then binds to a NAADP-BP to evoke Ca^{2+} release from ER or lysosomes via RYR1 or TPC1/2 respectively (Figure 6).

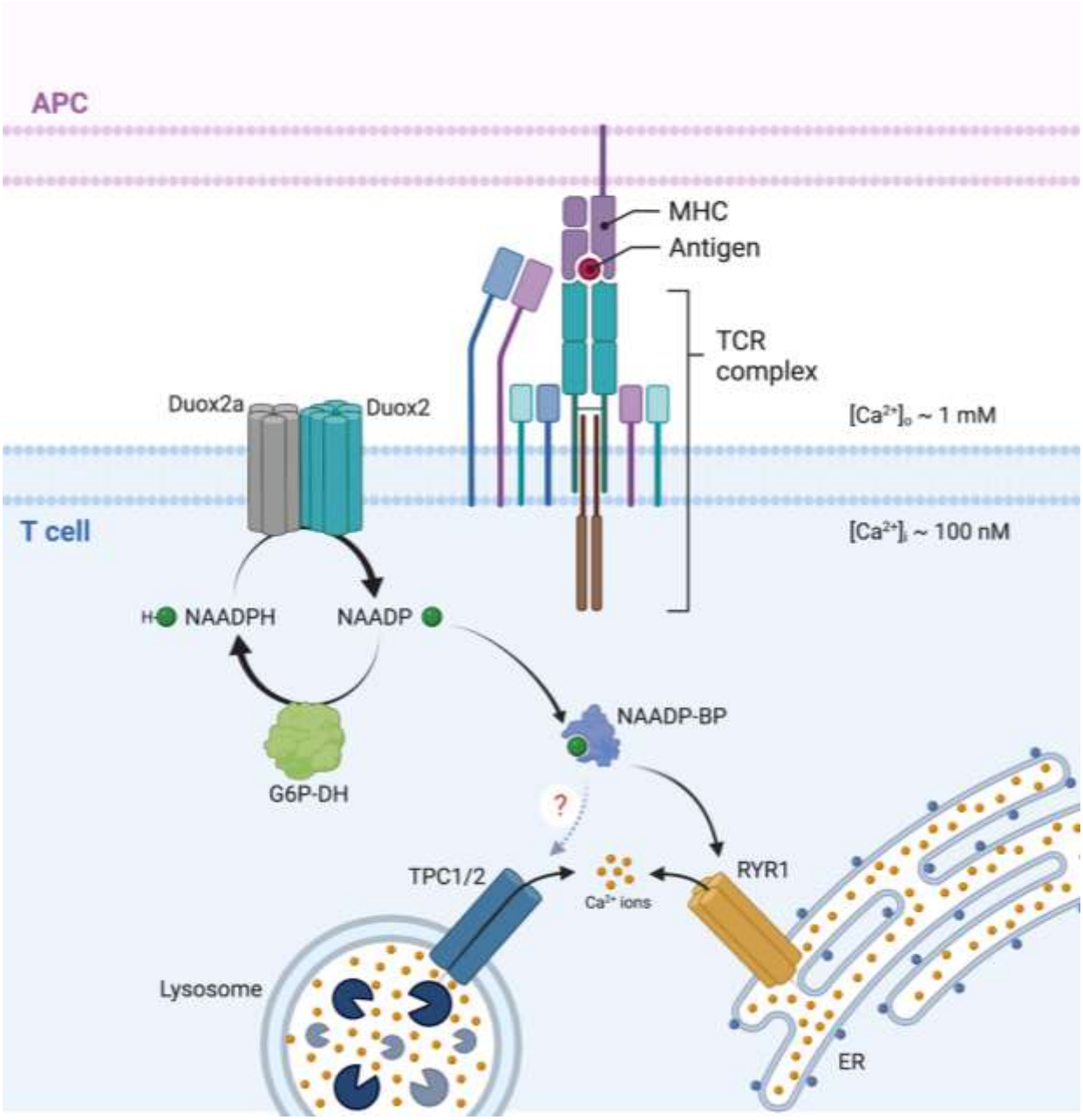

Figure 6: Depiction of NAADP-mediated Ca^{2+} signaling in T cells: Upon activation of T cells by TCR-MHC ligation, NAADP is synthesized in cytosol by DUOX2. Next, NAADP binds to a small cytosolic NAADP-BP, which then as a complex activates RYR1 or TPC1/2 to evoke Ca2+ release from ER or lysosomes respectively (created with biorender.com; modified from Guse, 2012).

Furthermore, Guse (2012) outlined a unifying hypothesis stating the possibilities of existence of different NAADP-BPs in different cell types with different expression patterns of ion channels. Figure 7 shows a schematic representation of the unifying hypothesis outlined for NAADP with regards to its Ca^{2+} signaling role. Such model explains the conflicting and contrasting data discussed in section 1.3.3 regarding the target channels of NAADP.

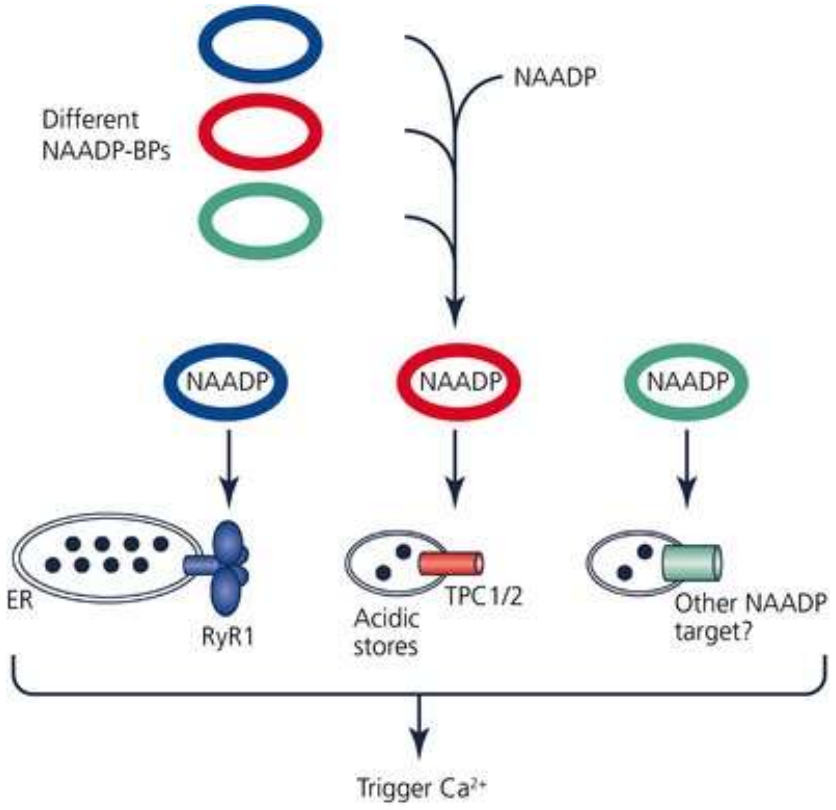

Figure 7: Unifying hypothesis for NAADP targeting different ions channels in different cell types: NAADP is likely to bind to a cell or tissue specific NAADP-BP which then activates the ion channels that are expressed in the particular cell or tissue for Ca^{2+} release events (Guse & Diercks, 2018).

1.3.5 Identification of a NAADP binding protein

NAADP-BPs were highly enriched by subjecting S100 cytosolic fraction of Jurkat T cells to different chromatographic purifications such as anion exchange chromatography, cation exchange chromatography and hydrophobic interaction chromatography. The presence of NAADP-BP was confirmed by performing PAL with [^{32}P]-5-N3-NAADP after each chromatographic step. The previously discovered 22/23 kDa protein (Lin-Moshier et al., 2012; Walseth et al., 2012) and two additional proteins of sizes around 35 and 70 kDa were strongly and specifically labelled by PAL. These proteins were extracted from the SDS-PAGE gel and subjected to trypsin digestion followed by mass spectroscopic analysis. The four most abundant proteins from the 22/23 kDa protein band was identified to be peroxiredoxin-1 (with molecular size of 22.1 kDa), peroxiredoxin-2 (21.9 kDa), methylated-DNA- protein-cysteine methyltransferase (21.6 kDa), and hematological and neurological expressed 1-like protein (HN1L), also called as jupiter microtubule associated homolog 2 (JPT2) (20.1 kDa). Among these proteins, HN1L seemed odd due to its poorly studied physiological function, while the first three proteins were well studied describing their solid physiological functions. Similarly, identifications of the additional proteins of sizes 35 and 70 kDa showed well studied

proteins with known functions. These preliminary data were produced by a previous MD student, Hannes G. Roggenkamp (Institute for Biochemistry and Molecular Cell Biology, UKE, Hamburg, Germany).

As the 22/23 kDa protein was previously discovered as a NAADP-BP in various cell types such as mouse pancreas, HEK293 and SKBR cells (Walseth et al., 2012), suggesting a universal role in NAADP-mediated Ca^{2+} signaling, and HN1L was poorly studied so far, it has been chosen for further characterization to study its role in NAADP signalosome.

2 AIM AND MOTIVATION

The PAL in mammalian cells and sea urchin egg homogenates strongly labelled a small cytosolic protein of size 22/23 kDa (Lin-Moshier et al., 2012; Walseth et al., 2012). Remarkably, no RYRs or TPCs were labelled suggesting that NAADP initially binds to this cytosolic 22/23 kDa protein, which then directly or indirectly activates the ion channels for Ca^{2+} release. Based on these findings, Guse (2012) outlined a unifying hypothesis stating the existence of cell or tissue specific NAADP-BPs targeting the ions channels that are expressed in the cell or tissue for Ca^{2+} release. Accordingly, the 22/23 kDa protein in Jurkat T cells was identified to be HN1L by mass spectroscopic analysis.

The prime objective of this thesis is to provide sufficient evidence to claim HN1L as a signaling protein involved in NAADP mediated Ca^{2+} signaling in T cells. Studies have been performed in this thesis with the following motives:

i. To confirm binding between HN1L and NAADP with recombinantly produced HN1L protein using PAL as binding assay
ii. To analyse the role of HN1L in Jurkat T cells and rat primary T cells by knocking out *hn1l* gene and performing Ca^{2+} imaging.
iii. To assess the association between HN1L and RYR1 using structural and functional studies.

3 MATERIALS AND METHODS

3.1 MEDIA AND BUFFERS

3.1.1 Lysogeny broth (LB) medium

LB medium is the standard medium for the cultivation of *E.coli* and was used for molecular cloning in this thesis. Liquid LB medium was prepared by dissolving commercial purchased LB broth from Carl Roth (Karlsruhe, Germany) following manufacturer's instructions. The medium was then autoclaved and stored at 4 °C until further use. Appropriate antibiotics (depending on bacterial strains (see section 3.2.1) and vectors (see section 3.2.2)) were added to the autoclaved medium prior inoculation of culture. LB agar (Carl Roth, Karlsruhe, Germany) were used to make LB agar plates and appropriate antibiotics were added before solidification.

3.1.2 2xYT medium

2xYT medium (Carl Roth, Karlsruhe, Germany) was used in this thesis to express recombinant protein in *E.coli* rosetta2 (see section 3.2.1) and was prepared following the medium manufacturer's instructions. The medium was then autoclaved and stored at 4 °C until further use. Appropriate antibiotics were added to the autoclaved medium prior inoculation of culture.

3.1.3 SOC medium

Super Optimal broth (SOB) was purchased from (Sigma-Aldrich Biochemie, Hamburg, Germany) and prepared following manufacturer's instructions. Super Optimal broth with Catabolite repression (SOC) was prepared by adding 1mM $MgCl_2$ and 2mM glucose to SOB. The medium was then autoclaved and stored until further use.

3.1.4 Buffers

Table 1 shows the buffers used in this thesis and their compositions.

Table 1: Buffers with composition

Buffers	Composition
50x TAE buffer	2 M Tris, 50 mM EDTA disodium salt, 1 M acetic acid
10x Wash buffer (W)	1 M Tris-HCl, 1.5 M NaCl, 10 mM EDTA, pH 8.0
10x Elution buffer (E)	1 M Tris-HCl, 1.5 M NaCl, 10 mM EDTA, 25 mM desthiobiotin, pH 8.0
10x Regeneration buffer (R)	1 M Tris-HCl, 1.5 M NaCl, 10 mM EDTA, 10 mM HABA pH 8.0
Lysis buffer	20 mM HEPES, 500 mM NaCl, 10mM imidazole, pH 8.0

Wash buffer	20 mM HEPES, 500 mM NaCl, 20mM imidazole, pH 8.0
Elution buffer	20 mM HEPES, 500 mM NaCl, 250mM imidazole, pH 8.0
Storage buffer	20 mM HEPES, 300 mM NaCl, 10% (v/v) glycerol, pH 8.0
4x Stacking buffer	0.5 M Tris-HCl, pH 6.8
4x Separating buffer	1.5 M Tris-HCl, pH 8.8
6x Sample buffer stock	350 mM Tris-HCl (pH 6.8), 34% (v/v) glycerol, 0.0012% (w/v) bromophenol blue
4x SDS sample buffer	73.8% (v/v) 6x Sample buffer stock, 21.1% (v/v) 20% SDS, 5.1% (v/v) β-mercaptoethanol
10x SDS running buffer	250 mM Tris, 1.924 M glycine, 20% (v/v) 20% SDS
10x Transfer buffer	250 mM Tris, 1.924 M glycine
1x Transfer buffer	10% (v/v) 10x transfer buffer, 20% (v/v) methanol
10x TBS buffer	200mM Tris, 1.5 M NaCl, pH 7.5
1x TBST	10% (v/v) 10x TBS buffer, 0.05% (v/v) tween
Blocking milk	50 g/L milk powder in 1xTBST
RSB buffer	10 mM Tris-HCl, 10 mM NaCl, 3 mM $MgCl_2$, pH 7.4
Ca^{2+} measurement buffer	140 mM NaCl, 5 mM KCl, 1 mM $CaCl_2$, 1 mM $MgSO_4$, 1 mM NaH_2PO_4, 20mM HEPES, 5.5mM glucose, pH 7.4

3.2 BACTERIAL STRAINS AND VECTORS

3.2.1 Bacterial strains

Table 2 shows the list of bacteria used in this study and their significances.

Table 2: Significances of the bacterial strains used in this thesis

Strain	Significance	Used as	Reference
E.coli XL1 blue competent cells	endonuclease (endA) deficient; single-strand rescue of phagemid DNA; allow blue-white color screening; preparation of high-quality plasmid DNA.	Cloning host	Agilent
E. coli Rosetta 2 competent cells	BL21 derivatives; enhanced expression of eukaryotic proteins; has compatible chloramphenicol-resistant plasmid supplying tRNAs for 7 rare codons.	Expression host	Novagen

3.2.2 Vectors

The vectors used to produce recombinant HN1L proteins, and their deletion mutants are listed below.

3.2.2.1 pASK-IBA43plus

pASK-IBA43plus vector was purchased from IBA lifesciences (Göttingen, Germany) conferring resistance to ampicillin. Figure 8 shows the vector map of pASK-IBA43plus. This vector was used to express recombinant tagged HN1L proteins.

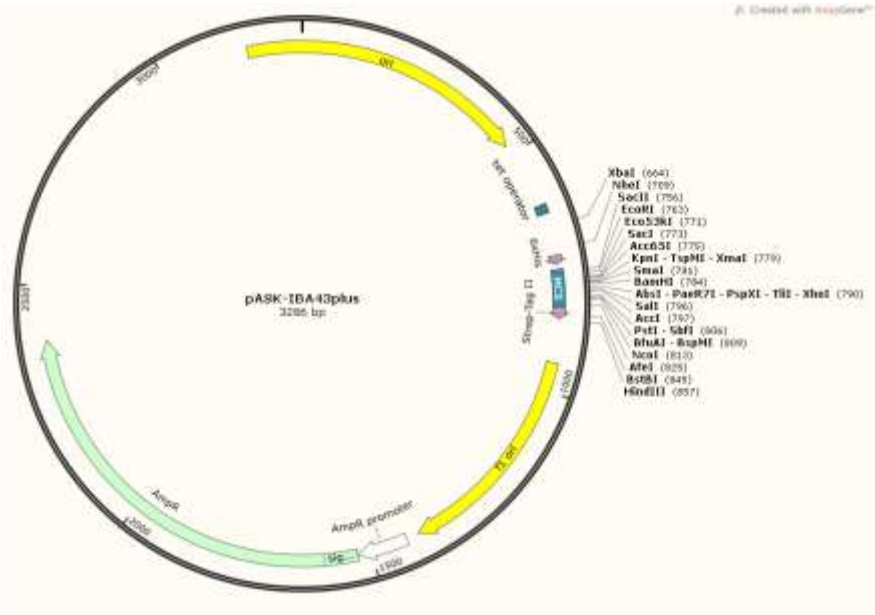

Figure 8: Vector map of pASK-IBA43plus: The vector was manufactured in a way that 6*His tag and strep tag are attached to N- and C-terminus of the recombinant proteins respectively. It confers resistance to ampicillin. The image was prepared in SnapGeneR software.

3.2.2.2 pET-M33

pET M33 vector was kindly provided by the group of Prof. Aymelt Itzen (Institute for biochemistry and signal transduction, UKE, Hamburg, Germany). This vector confers resistance to kanamycin and was used in this thesis to express recombinant tag-free HN1L proteins and their deletion mutants. The proteins were expressed as fusion proteins with 6x his tagged GST with a PreScission protease recognition site between GST and HN1L proteins. The PreScission protease recognition site was employed to cleave off the tags after the purification. Figure 9 shows the vector map of pET M33.

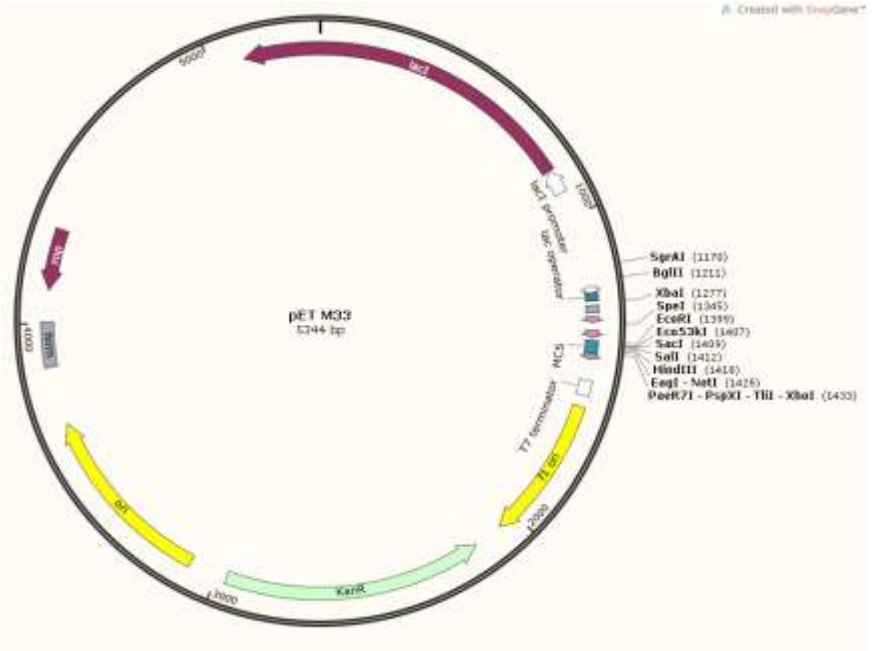

Figure 9: Vector map of pET M33: The vector was used to produce recombinant tag-free HN1L proteins as fusion protein attached with 6*His tag, GST followed by a PreScission protease cleavage site. It confers resistance to kanamycin. The image was prepared in SnapGeneR software.

3.3 MOLECULAR CLONING

This section discusses several molecular cloning techniques that were applied to recombinantly express human *hn1l* genes in bacteria and to make deletion mutants of HN1L.

3.3.1 Restriction enzyme-based cloning

The human *hn1l* genes were codon optimized using IDT codon optimization tool (Integrated DNA technologies, Iowa, USA) for its expression in bacteria and were cloned into pASK-IBA43plus vector using restriction enzyme-based cloning and the generated plasmids were used to recombinantly express tagged HN1L proteins. The following techniques were used in the same order to generate the plasmids.

3.3.1.1 Restriction digestion

The codon optimized *hn1l* genes were ordered Eurofins Scientific (Luxembourg) with restriction sites of BsaI at both ends as flanking sequences. Both pASK-IBA43plus (vector) and codon optimized *hn1l* genes (insert) were digested with the restriction enzyme BsaI by preparing the reaction mixture as shown in Table 3. The mixture was mixed gently and incubated at 37 °C for 1 hour.

Table 3: Reaction mixture composition for BsaI digestion

Components	Amount
Vector / Insert	1 µg
10x CutSmart buffer	5 µL
BsaI-HF	1 µL (5U)
Water, nuclease-free	to 50 µL

3.3.1.2 Agarose gel electrophoresis

The restriction digested products or PCR products were analyzed by running them through 1% (w/v) agarose gel with the help of electric current. The gel was cast by dissolving 1% (w/v) of agarose in 1x Tris-acetate-ethylnediaminetetraacetic acid (TAE) buffer which was diluted from 50X TAE stock buffers (see section 3.1.4). Roti-Safe GelStain (Carl Roth, Karlsruhe, Germany) was added to the gel mixture at warm temperature (before casting) to visualize DNA fragments in the gel. The samples were mixed with commercial 6X loading dye (Thermo Fisher Scientific, Waltham, Massachusetts, USA) and loaded into the agarose gel pockets. Electrophoresis was performed by applying a constant voltage of 120V for 45 minutes using horizontal electrophoresis system using power source (Bio-Rad Laboratories Inc., Hercules California, USA). The gel was visualized and documented with Gel Doc 2000 (Bio-Rad, Hercules California, USA). GeneRuler DNA Ladder Mix (Thermo Fisher Scientific, Waltham, Massachusetts, USA) was used as marker along with the samples.

3.3.1.3 Gel clean-up

After confirmation of the products on an agarose gel, the appropriate bands were extracted from the gel and purified by using a NucleoSpin® Gel and PCR Clean-up (Macherey-Nagel, Düren, Germany) according to the manual. The concentration of the purified product was measured with a` NanoDrop™ One Mikrovolumen-UV/VIS-Spektralphotometer (Thermo Fisher Scientific, Waltham, Massachusetts, USA) by following the manufacturer's protocol.

3.3.1.4 Ligation

The digested and purified vector and insert were ligated together using T4 DNA ligase (Thermo Fisher Scientific, Waltham, Massachusetts, USA). The reaction mixture was prepared as shown in Table 4 and incubated at 28 °C for 1 hour.

Table 4: Reaction mixture composition for ligation of digested vector and insert

Components	Amount
Digested vector*	100 ng
Digested insert*	63.64 ng
10x T4 DNA ligase buffer	2 µL
T4 DNA ligase	1 µL (5U)
Water, nuclease-free	to 20 µL

* Calculated for insert and vector ratio of 1:5

3.3.1.5 Transformation

Frozen competent cells (200 µL per tube) were thawed on ice for 20 minutes. 20 µL of ligated products (or 1 µL of plasmids for re-transformation) were added to the cells and incubated on ice for 30 minutes. Then the mixture was heat-shocked at 42 °C for 45 seconds. In parallel, SOC medium (see section 3.1.3) was warmed up at 37 °C. The mixture was then cooled down on ice for 2 minutes and 800 µL of warmed up SOC medium was added to the cells. For XL1blue competent cells, 60 µL of the culture were then plated on LB agar plates with appropriate antibiotics (see section 3.1.1). For Rosetta2 competent cells, the culture was centrifuged at 10k rpm for 5 minutes and 800 µL of medium was discarded to resuspend the cells with remaining 200 µL medium. The resuspended cells were then plated on LB agar plates with appropriate antibiotics (see section 3.1.1). The plated agar plates were then incubated at 37 °C overnight.

3.3.1.6 Mini-prep (Plasmid extraction)

Up to 5 colonies were randomly selected from the overnight incubated agar plates and was seeded in to 5mL LB medium. They were then incubated at 37 °C overnight. The plasmids from each colony culture were extracted using NucleoSpin® Miniprep (Macherey-Nagel, Düren, Germany) by following the manufacturer's protocol. The concentrations of the extracted plasmids were measured using NanoDrop™ One Mikrovolumen-UV/VIS-Spektralphotometer (Thermo Fisher Scientific, Waltham, Massachusetts, USA) by following the manufacturer's protocol.

3.3.1.7 Sequencing

Sample preparation for sequencing was done as shown in Table 5. A universal primer can also be chosen for sequencing, for which no primer was added to the samples. The mixed samples were then sent to Microsynth Seqlab in Göttingen for sequencing.

Table 5: Sample preparation for sequencing

Components	Amount
Extracted plasmid	400 ng – 1000 ng
Primer (10 µM)	3 µL
Water, nuclease-free	to 15 µL

3.3.1.8 Maxi-prep (Plasmid extraction)

After confirmation of positive clones from sequencing, XL1blue competent cells were transformed with the plasmids as shown in section 3.3.1.5. A primary culture was made with one of the colonies from the overnight incubated agar plates and was grown overnight at 37 °C. 200 mL of LB medium was seeded with the primary culture and incubated at 37°C overnight. Plasmids from the 200 mL culture was extracted using

NucleoSpin® Miniprep (Macherey-Nagel, Düren, Germany) by following the manufacturer's protocol. The concentrations of the extracted plasmids were measured using NanoDrop™ One Mikrovolumen-UV/VIS-Spektralphotometer (Thermo Fisher Scientific, Waltham (Massachusetts), USA) and stored at -20 °C until further use.

3.3.2 Inverse PCR

Deletion mutants of HN1L were created at DNA level using inverse PCR technique. Inverse PCR is a variant of conventional PCR where the primers extend DNA away from each other rather than towards. In this way, the regions to be deleted will not be amplified by PCR.

3.3.2.1 Polymerase Chain Reaction (PCR)

Appropriate forward and reverse primers with phosphorylated 5` end were designed in SnapGeneR software and purchased from Eurofins Scientific (Luxembourg). Phosphorylated 5` ends of primers were important for PCR as the products were re-circularized by ligating the phosphorylated 5` ends of the product. PCRs were carried out using Q5 polymerase (New England Biolabs, Massachusetts, USA) following the pipetting instructions as shown in Table 6 and PCR steps with the conditions as shown in Table 7.

Table 6: Pipetting instructions for PCR using Q5 DNA polymerase.

Component	Amount
Template DNA	1 pg – 10 ng
dNTP's (10mM)	2.5 µL
Forward primer (10 µM)	2.5 µL
Reverse primer (10 µM)	2.5 µL
5x Q5 reaction buffer	10 µL
Q5 DNA polymerase	0.5 µL
Water, nuclease-free	to 50 µL

Table 7: PCR steps with Q5 DNA polymerase and their conditions.

Step	Temp. [°C]	Duration [s]	Cycle
Initiation	98	30	-
Denaturation	98	10	30 x
Annealing	X*	30	30 x
Extension	72	Y*	30 x
Final extension	72	120	-

* X: 3°C above the T_m of the lower T_m primer (T_m+3); Y: Extension time calculated by 30 s /kb

3.3.2.2 Dpn1 digestion

The PCR products were digested with DpnI (New England Biolabs, Massachusetts, USA) to get rid of the template DNA. The reaction mixture was prepared by following the manufacturer's guidelines as shown in Table 8. The mixture was mixed gently and incubated at 37 °C in a heat block for 1 hour.

Table 8: Reaction mixture composition for DpnI digestion

Components	Amount
PCR product	50 µL
10x r1.1 buffer	6 µL
DpnI	1 µL (20 U)
Water, nuclease-free	to 60 µL

The DpnI digested PCR products were then analysed by agarose gel electrophoresis as shown in section 3.3.1.2 and purified from the gel as shown in section 3.3.1.3.

3.3.2.3 Re-circularization of plasmid

The purified DpnI digested PCR products were re-circularized using T4 DNA ligase (Thermo Fisher Scientific, Waltham, Massachusetts, USA). The reaction mixture was prepared as shown in Table 9 and incubated at 28°C for 1 hour.

Table 9: Reaction mixture composition for ligation of digested vector and insert

Components	Amount
DpnI digested PCR product	100 ng
10x T4 DNA ligase buffer	2 µL
T4 DNA ligase	1 µL (5U)
Water, nuclease-free	to 20 µL

The re-circularized plasmid was then used to transform XL1blue competent cells as shown in section 3.3.1.5 followed by sequencing to confirm the sequences as shown in sections 3.3.1.6 and 3.3.1.7. The positive clone from sequencing was then subjected to Maxi-prep for amplification of the plasmid as shown in section 3.3.1.8.

3.3.3 Ligation independent cloning

Ligation independent cloning technique was also used in this study to transfer insert DNA from one plasmid to another. The codon-optimized *hn1l* gene sequences were transferred from pASK-IBA43plus to pET M33, which has a 6*His tag and GST followed by PreScission protease cleavage site, by infusion cloning to produce tag-free recombinant HN1L proteins.

3.3.3.1 In-fusion cloning

Forward and reverse primers, to amplify *hn1l* gene from pASK-IBA43plus, were designed in such a way that the 5` ends of the primers contained 15-base overhangs that were homologous to the downstream and upstream sequences of insertion site in the recipient vector (pET M33) respectively. The 3` ends of both primers were specific to the start and end of *hn1l* gene respectively. To linearise and amplify the recipient vector (pET M33), forward and reverse primers (as in inverse PCR mentioned in section 3.3.2) were designed without any overhangs and specific to the downstream and upstream sequences of the insertion

site respectively. PCRs were carried out to amplify insert and vector DNA as shown in section 3.3.2.1. The PCR products were analysed as shown in section 3.3.1.2 and purified as shown in section 3.3.1.3. The reaction mixture to set up in-fusion cloning reaction was made as shown in Table 10.

Table 10: Reaction mixture composition for In-fusion cloning reaction

Components	Amount
PCR-linearized vector*	1 - 2 µL
PCR-linearized insert*	1 - 2 µL
5x In-fusion HD enzyme premix	2 µL
Water, nuclease-free	to 10 µL

* The total volume of PCR linearized vector and insert was not exceeded 4 µL per 10 µL reaction

The reaction mixture was incubated at 50 °C for 15 minutes and then placed on ice. The whole volume of the mixture was used to transform XL1blue competent cells as shown in section 3.3.1.5 followed by sequencing to confirm the insertion as shown in sections 3.3.1.6 and 3.3.1.7. The positive clone from sequencing was then subjected to Maxi-prep for amplification of the plasmid as shown in section 3.3.1.8.

3.4 RECOMBINANT PROTEIN PRODUCTION

HN1L proteins and their deletion mutants were produced recombinantly in *E.coli* rosetta 2 strain. The extracted plasmids (pASK-IBA43plus or pET M33) with *hn1l* genes were used to transform *E.coli* rosetta 2 competent cells following the protocol given in section 3.3.1.5. The following methods were performed in the same order to produce the recombinant HN1L proteins.

3.4.1 Recombinant over-expression of *hn1l* gene

An isolated colony from the above-mentioned agar plates was cultivated in 5 mL 2xYT medium with appropriate antibiotics (depending on bacterial strains (see section 3.2.1) and vectors (see section 3.2.2) used) by overnight incubation at 37 °C. Shake flask with 200 mL 2xYT medium and appropriate antibiotics (as used for the pre-culture) was then inoculated with the 5 mL of cultivated pre-culture and incubated in a shaker at 37 °C until the culture reaches exponential phase ($0.5<OD_{600}<0.6$). At this stage, over-expression of *hn1l* genes was either induced by 0.2 µg/mL of anhydrotetracycline (AHT) for pASK-IBA43plus vector or by 0.5 mM of IPTG for pET M33 vector. The culture was then incubated overnight at 25 °C with constant shaking.

3.4.2 Protein purification and characterization

This section discusses the methods used to extract, purify and characterize the recombinant proteins produced in *E.coli* rosetta 2.

3.4.2.1 Clarified cell lysate preparation

200mL overnight culture was centrifuged at 5000 g for 15 minutes at 4 °C to pellet the cells. The cell pellet was resuspended either in 5 mL of 1x W buffer (for Strep-tactin chromatographic purification) or in 5mL of lysis buffer (for Ni-NTA chromatographic purification). 400 μg/mL of RNAse, 200 μg/mL of DNAse and 1x protease inhibitor (Roche, Basel, Switzerland) were added to resuspended cell pellet. The cells were disrupted by ultra-sonication using Sonopuls GM 70 (Bandelin Electronic, Berlin, Germany).The instrument was set at 70 % power and 50 % cycle (1 s ON and 1 s OFF). The cell suspension was placed on ice and sonicated thrice for 3 minutes with 1 minute interval. The sonicated cell suspension was then clarified by centrifugation at 4000 g for 1 hour at 4 °C. The supernatant (cell lysate) was collected and stored at 4 °C until further processes.

3.4.2.2 Strep-tactin chromatography

Recombinant HN1L proteins produced using pASK-IBA43plus was purified by strep-tactin chromatography. Strep-tactin© column (IBA lifesciences, Göttingen, Germany) was used to purify the strep-tagged proteins following the manufacturer's protocol.

3.4.2.3 Ni-NTA chromatography

Recombinant HN1L proteins and their deletion mutants produced using pET M33 vector were purified by Ni-NTA chromatography. Ni-NTA agarose (Qiagen) was used to purify the his-tagged proteins following the manufacturer's protocol.

3.4.2.4 Protein concentration measurement

The elution fractions from both chromatographic techniques were concentrated using Vivaspin 20, 10000 MWCO PES (Sartorius, Göttingen, Germany) by centrifuging at 4000 g for 40 minutes at 4 °C. This step was repeated with the addition of 10 mL of storage buffer (see section 3.1.4) to reduce the concentration of either biotin (Strep-tactin chromatographic purification) or imidazole (Ni-NTA chromatographic purification) in the purified protein samples. The concentrated purified proteins were measured for their concentration using NanoDrop™ One Mikrovolumen-UV/VIS-Spektralphotometer (Thermo Fisher Scientific, Waltham, Massachusetts, USA) following the manufacturer's protocol.

3.4.2.5 Removal of tags

The purified recombinant HN1L proteins and their deletion mutants produced using pET M33 vector were subjected to additional treatments to remove 6*his and GST tags. 6xHis tagged PreScission protease was used to cleave off the tags by targeting its recognition sequence between the tags and HN1L proteins. Production of 6xHis tagged PreScission protease was outsourced to Centre for Structural Systems Biology

(CSSB, Hamburg, Germany). The reaction mixture for protease treatment was made as shown in Table 11 and incubated on ice for 48 hours.

Table 11: Reaction mixture composition for protease treatment

Components	Amount
6xHis and GST tagged HN1L proteins*	x µg
6xHis tagged PreScission protease*	y µg
100 mM DTT	10 µL
100 mM EDTA	10 µL
Buffer, 20mM HEPES; 300mM NaCl; pH 7.8	to 1 mL

* y is calculated from x considering protease and substrate ratio of 1:50

The reaction mixture was then diluted to 10 mL with lysis buffer and subjected to Ni-NTA chromatography (see section 3.4.2.3) to remove the 6xHis tagged PreScission protease and 6xHis and GST tags that were cleaved off from HN1L proteins. As HN1L proteins are devoid of 6xHis tag, the flow through and wash fractions were collected. These fractions were then concentrated, and buffer exchanged using Vivaspin 20, 10000 MWCO PES (Sartorius, Göttingen, Germany) as shown in section 3.4.2.4.

3.4.2.6 SDS-PAGE

Purity of the purified recombinant HN1L proteins was analyzed by performing sodium dodecyl sulfate polyacrylamide gel electrophoresis (SDS-PAGE). SDS denatures the proteins and imparts negative charge to the linearized proteins which are then separated based on their molecular masses on polyacrylamide gel. 12.5 % SDS-PAGE gels were used throughout the study. Separating and Stacking are the two parts of the gel which were cast one after another requiring different buffers namely 4x Separating buffer and 4x Stacking buffer respectively (see section 3.1.4). Table 12 shows the composition to cast two 12.5 % SDS-PAGE gels. Separating gel was cast first followed by stacking gel above the separating gel.

Table 12: Composition of mixture to cast 12.5 %SDS-PAGE gels

Components	Separating gel	Stacking gel
Acrylamide solution (40 %) - Mix 29 : 1	4.1 mL	650 µL
4x Separating buffer	2.5 mL	-
4x Stacking buffer	-	1.25 mL
De-ionized water	3.3 mL	3.15 mL
10% SDS	100 µL	50 µL
TEMED	10 µL	5 µL
10% APS	50 µL	25 µL

The casted gel was fixed to the chamber and filled with 1x SDS running buffer (see section 3.1.4). 4x SDS sample buffer (see section 3.1.4) was added to the samples and loaded onto the gel along with protein marker (Spectra™ Multicolour Broad Range Protein Ladder, Thermo Scientific). The electrophoresis was performed at 125 V for 1 hour. After electrophoresis, the gel was removed from the chamber and stained

with Coomassie brilliant blue R-250 solution (Bio-Rad Laboratories Inc., Hercules, California, USA) for 1 hour with gentle shaking. The gel was then destained with de-ionized water overnight.

3.4.2.7 Western blot

Identity of the purified recombinant HN1L proteins and expression levels of HN1L in Jurkat T cells and rat primary T cells were checked by performing wet western blotting. Samples were separated on 12.5 % SDS-PAGE gel as mentioned in section 3.4.2.6. Next, PVDF membrane (Merck Millipore Ltd., Immobilon®-P Transfer Membrane, Germany) was activated by incubating in methanol for 10 minutes followed by incubation in 1x transfer buffer for 5 minutes. The SDS-PAGE gel was removed from the chamber and incubated in 1x transfer buffer for 5 minutes along with whatman filter papers. Transfer stack (gel-membrane sandwich) was made as shown below:

Anode (+)
2x whatman filter paper
PVDF membrane
SDS-PAGE gel
2x whatman filter paper
Cathode (-)

The transfer stack was then placed in a tank filled with 1x transfer buffer and electrophoresis was started with constant current of 200 mA at 4 °C. The transfer of the proteins was confirmed by incubating the PVDF membrane with ponseau S solution (AppliChem, Hessen, Germany) for 5 minutes and washed with de-ionized water. Then, the membrane was incubated in blocking solution for 1 hour at RT to avoid unspecific binding of the primary antibody. The membrane was then incubated in HN1L-specific primary antibody solution (with appropriate dilution in blocking solution) overnight at 4 °C. The membrane was washed thrice with 1x TBST to remove the excess primary antibody followed by incubation in secondary antibody solution (HRP (horseradish peroxidase)-conjugated antibody, 1:5000 dilution in blocking solution) at RT for 1 hour. Excess of secondary antibody were removed by washing the membrane thrice with 1x TBST followed by washing thrice with 1x TBS. The membrane was incubated with a ECL substrate called Super Signal West Pico Chemiluminescent Substrate (Thermo Fisher Scientific, Waltham, Massachusetts, USA) which reacts with HRP to produce chemiluminescence. Such signals were imaged in Image Quant LAS 4000 (GE Healthcare, Freiburg, Germany).

3.5 PHOTOAFFINITY LABELLING

Recombinant CD38 and its inactive mutant and recombinant HN1L proteins and their deletion mutants were incubated with either [^{32}P]-5-N_3-NAADP or [^{32}P]-azide-AIO-NAADP (at concentrations indicated in

figure legends) for 90 minutes at 4 °C. Non-radioactive labelled NAADP or NADP were used at final concentrations mentioned in the figure legends. The probes were photoaffinity-labelled to the proteins by irradiating with UV light (10^{15} quanta/second) on ice in a Rayonet photochemical reactor (Southern New England Ultravioloet Co.). The samples were then mixed with 1x SDS sample buffer and separated in 12.5 % Criterion acrylamide gels by SDS-PAGE. Photoaffinity labelling was analyzed by detecting with Cyclone Phosphor Imager (Packard Instruments). The phosphor images were quantified with OptiQuant software (Packard Instruments) as mentioned in Walseth et al. (2012). These experiments were kindly performed by the group of Prof. Timothy Walseth (Department of Pharmacology, University of Minnesota Medical School, Minneapolis, Minnesota, USA) at their facility as external collaborative research.

3.6 MAMMALIAN CELL CULTURE

Two mammalian cells were used in this thesis to study their NAADP-mediated Ca^{2+} signaling: Jurkat T cells and rat primary $CD4^+$ T cells.

3.6.1 Culture maintenance

Jurkat T cells and their *hn1l* knockout clones were cultured in RPMI 1640 medium containing GlutaMAX-1 and 25 mM HEPES (Gibco, Life Technologies) which was supplemented with 100 U/mL of penicillin and streptomycin and 7.5 % (v/v) newborn calf serum (Biochrom, Merck Millipore). They were cultured either in T25 or T75 cell culture flasks (Sarstedt, Nümbrecht, Germany) by incubating them at 37 °C and 5 % CO_2. Cell densities were maintained between 0.3 and 1.2 * 10^6 cells/mL.

Rat primary $CD4^+$ T cells, specific to β-synuclein ($T_{\beta\text{-syn}}$ cells), were kindly provided by the group of Prof. Alexander Flügel (Department of Neuroimmunology, University Medical Center, Göttingen, Germany). Lewis rats were used to prepare the restimulated $CD4^+$ $T_{\beta\text{-syn}}$ cells as mentioned in Flügel et al. (1999). $T_{\beta\text{-syn}}$ cells, after 4 to 6 days of 2^{nd} or 4^{th} restimulation, were sent to our group on ice. Every 10 million cells were resuspended in 1mL freezing medium in a cryo-vial and froze in liquid nitrogen until further use. The frozen cells were thawed a day before the Ca^{2+} measurement by transferring them to 10 mL DMEM medium. The cells were then pelleted and resuspended in 10mL DMEM medium supplemented with 10 % fetal calf serum (v/v) and incubated at 37 °C and 5 % CO_2 overnight.

3.6.2 Protein preparation

S10 cytosolic fraction was extracted from both Jurkat T cells and rat primary $CD4^+$ T cells to check the expression levels of HN1L by western blotting. Jurkat T cell suspension (~30 million cells) or rat primary $CD4^+$ T cell suspension (~10 million cells) was centrifuged at 518 g for 5 minutes at RT to pellet down the

cells. The cell pellet was resuspended in 1mL of RSB buffer supplemented with protease inhibitors. The cells were disrupted by ultrasonicating thrice for 30 seconds each on ice using Sonopuls GM 70 (Bandelin Electronic, Berlin, Germany) followed by centrifugation at 518 g for 5 minutes at 4 °C to pellet down cell debris. The supernatant was collected and centrifuged at 10000 g for 30 minutes at 4 °C to separate S10 and P10 fractions. Protein concentration in S10 fraction was determined using Nano drop following the manufacturer's protocol. S10 fraction was concentrated by centrifugation using Vivaspin 500, 10000 MWCO PES (Sartorius, Göttingen, Germany) if necessary and stored at -20 °C until further use.

P10 membrane fraction were extracted from both stimulated and unstimulated Jurkat T cells to study the association between RYR and HN1L by immunoprecipitation. Jurkat T cell suspension (20 million cells/experiment) was centrifuged at 518 g for 5 minutes at RT to pellet down the cells. The cells were washed and resuspended in Ca^{2+} measurement buffer (see section 3.1.4) and left unstimulated or stimulated by OKT3 for 5, 10 seconds and 5 minutes. The cell suspensions with different conditions of stimulations were then centrifuged at 518 g for 5 minutes at RT, resuspended in RSB buffer and placed on ice for 10 minutes. The cells were disrupted manually using douncer with 30 strokes followed by centrifugation at 1100 g for 5 minutes at 4 °C to remove the cell nulcei. The supernatant was collected and centrifuged at 10000 g for 30 minutes at 4 °C. The resulting pellet, the P10 fraction, was resuspended in RSB buffer and the protein concentration was determined by Bradford assay (Bio-Rad Laboratories Inc., Hercules California, USA) using different concentration of BSA as standard. Extraction of P10 membrane fraction was kindly performed by Lola Hernandez (Institute for Biochemistry and Molecular Cell Biology, UKE, Hamburg, Germany) as internal collaborative research.

3.6.3 Gene silencing using CRISPR/CAS9

The expression plasmids pX330-Puro-T2A-hCas9 and pCAG-EGxxFP were used to knockout *hn1l* gene in Jurkat T cells by CRISPR-Cas9. The sgRNA (single guide RNA) targeting *hn1l* gene was designed using GenScript guide RNA design tool and purchased from Eurofins Scientific (Luxembourg). The above-mentioned expression plasmids and sgRNA were co-transfected into Jurkat T cells by electroporation. Successfully transfected cells were sorted using Fluorescence-activated cell sorting (FACS) and individualized using the fluorescence of green fluorescent protein. *hn1l* knockout in single clones was confirmed at DNA level by DNA sequencing as mentioned in section 3.3.1.7 and at protein level by western blotting as mentioned in section 3.4.2.7. These experiments were performed by Valerie Wolters (Institute for Biochemistry and Molecular Cell Biology, UKE, Hamburg, Germany).

Similarly, gene silencing of *hn1l* in rat primary $CD4^+$ $T_{\beta\text{-syn}}$ cells was kindly performed by the group of Prof. Alexander Flügel (Department of Neuroimmunology, University Medical Center, Göttingen, Germany) using CRISPR-Cas9. pMPuChe-U6zero (Takara Bio, Shiga, Japan) was used to express the

retroviral sgRNA targeting exon 2 of *hn1l* gene. Control sgRNA was also designed targeting intronic sequence in rat *Rosa26* locus. Lipofectamine 3000 was used to transfect GP+E86 ecotropic packaging cell line with the expression plasmids mentioned above. Survivor packaging cells were sorted by flow cytometry and subcloned by limiting edition. Identification of the clones producing high titer of retroviruses was done by short-term co-culturing with murine thymoma cell line BW5147 and analysing by flow cytometry. These clones were expanded before transducing $T_{\beta\text{-syn}}$ cells which were isolated from rats with transgenic background ubiquitously expressing Cas9 nuclease. More than 95 % of the cells were positive for cherry after two rounds of restimulation in culture. The genomic DNA from these cells were isolated using Mouse Direct PCR kit (Bimake, Houston, USA) and exon 2 of *hn1* gene was amplified by PCR using appropriate primers with OPTI polymerase mastermix (Bimake, Houston, USA). The amplified products were then cloned into pJet1.2 vector (Thermo Fisher Scientific, Waltham, Massachusetts, USA). The amplified products were also used for T7 assay by denaturing them for 5 minutes at 95 °C and reannealing them by stepwise ramping temperature down to 25 °C followed by addition of 15 U of T7 endonuclease (New England Biolabs, Massachusetts, USA) per reaction and incubation at 37 °C for 30 minutes.

3.6.4 Transient over-expression of gene

The coding sequence of human HN1L (accession number: NM_144570) was synthesized by custom gene synthesis and purchased from Eurofins Scientific (Luxembourg). Appropriate primers were designed, purchased and PCR was performed to add restriction sites of XhoI and Bam HI at the beginning and end of the coding sequence respectively. Then the PCR product was cloned into pIRES2-DsRed2 vector by restriction enzyme-based cloning using XhoI and Bam HI restriction enzymes as shown in 4.3.1. The resulting vector with human *hn1l* gene was transfected into C2 clone of Jurkat T cells using Neon transfection system (Invitrogen, Massachusetts, USA) following manufacturer's protocol. The transfected cells were then incubated overnight in RPMI 1640 medium supplemented with 10 % FBS at 37 °C and 5 % CO_2. These experiments were performed by Dr. Ralf Fliegert and Anette Rosche (Institute for Biochemistry and Molecular Cell Biology, UKE, Hamburg, Germany) as internal collaborative research.

3.7 CALCIUM IMAGING

Jurkat T cells and rat primary $CD4^+$ $T_{\beta\text{-syn}}$ cells and their *hn1l* knockout clones were imaged for their global and local Ca^{2+} signals upon TCR/CD3 stimulation.

3.7.1 Measurement of global Ca^{2+} signals

10 million of Jurkat T cells (WT, C2 and C4) or rat primary $CD4^+$ $T_{\beta\text{-syn}}$ cells (WT and *hn1l*$^{-/-}$) per each experiment day were centrifuged at 518 g for 5 minutes at RT and resuspended in 1mL fresh RPMI or DMEM medium respectively followed by incubation at 37 °C for 5 minutes. Fura2-AM was added to the cell suspension at a final concentration of 4 µM and incubated in dark at 37 °C for 15 minutes followed by addition of 4mL fresh medium and incubation in dark at 37 °C for 15 minutes. Fura2-AM loaded cells were then washed with 5 mL Ca^{2+} measurement buffer and resuspended in 800 µL of Ca^{2+} measurement buffer. The cell suspension was left undisturbed at RT for 20 minutes to ensure complete hydrolysis of Fura2-AM.

Coverslips were coated with 5mg/mL of BSA and 0.1 mg/mL of poly-l-lysine (PLL) followed by sticking O-rings with the help of silica gel. Fura2-AM loaded cells were added to the prepared coverslips and allowed to adhere for a few minutes. Jurkat T cells were stimulated with either 1 µg/ml of anti-human CD3 monoclonal antibody (mAb) OKT3 or 10 µM IP_3-AM (SiChem, Bremen) and rat primary $CD4^+$ $T_{\beta\text{-syn}}$ cells were stimulated with 1 µg/ml of anti-rat CD3 mAb (554829, BD Pharmingen). Stimulation with 1.67 µM thapsigargin was carried out for every measurement as a control. To compare the effect of NAADP antagonism and *hn1l* knockout, rat primary $CD4^+$ $T_{\beta\text{-syn}}$ cells were preincubated with 500 µM of BZ194 prior to Fura2-AM loading and imaged global Ca^{2+} signals as mentioned above.

Cells were imaged on a Leica IRBE microscope using a 40x objective lens. Frames were recorded with an electron-multiplying charge-coupled device camera (EM-CCD; C9100-13, Hamamatsu). Sutter DG-4 was used as light source with the filter set shown in Table 13. The experiments with IP_3 stimulation were performed by Anette Rosche (Institute for Biochemistry and Molecular Cell Biology, UKE, Hamburg, Germany) as internal collaborative research.

Table 13: Filter sets used for global Ca^{2+} signal imaging

	Filter
Excitation (ex)	HC 340/26 nm and HC 387/11 nm
Beam splitter (bs)	400DCLP
Emission (em)	510/84 nm

3.7.2 Measurement of local Ca^{2+} signals

5 million cells of Jurkat T cells (WT and C2) or rat primary $CD4^+$ $T_{\beta\text{-syn}}$ cells (WT and *hn1l*$^{-/-}$) per each experiment day were centrifuged at 518 g for 5 minutes at RT and supernatant was discarded. Fluo4-AM and Fura-Red-AM (at final concentrations of 10 µM and 20 µM respectively) were added to 500 µL fresh medium which was used to resuspend the cells. The cell suspension was then incubated in dark at RT for

20 minutes followed by addition of 2 mL fresh medium and incubated in dark at RT for further 30 minutes. Fluo4-AM and Fura-Red-AM loaded cells were then washed with 2mL of Ca^{2+} measurement buffer and resuspended in 400 µL of Ca^{2+} measurement buffer. The cell suspension was left undisturbed at RT for 20 minutes to ensure complete hydrolysis of Fluo4-AM and Fura-Red-AM.

The coverslips were prepared as mentioned in 4.6.1 and loaded cells were seeded on the prepared coverslips. 12.5 µL of Protein G magnetic bead suspension was washed with 500 µL PBS-tween and resuspended in 0.2 mg/mL of anti-CD3 and anti-CD28 (human or rat antibodies). The bead suspension was incubated for 30-60 minutes with constant mixing. The antibody coated beads were then washed twice with 500 µL PBS-tween and resuspended in 500 µL Ca^{2+} measurement buffer. 10 µL of the bead suspension was added to the seeded cells to stimulate them.

Cells were imaged with an exposure time of 25 ms (40 frames/second) in 14-bit mode using an EM-CCD camera (C9100-2, Hamamatsu) and a dual-view module (Optical Insights, PerkinElmer Inc.) to split the emission wavelengths. Sutter DG-4 was used as light source with the filter set shown in Table 14. These experiments were performed by Feng Gu, Franziska Möckl and Aileen Krüger (Institute for Biochemistry and Molecular Cell Biology, UKE, Hamburg, Germany) as internal collaborative research.

Table 14: Filter sets used for local Ca^{2+} signal imaging

	Filter
Excitation (ex)	480/40 nm
Beam splitter (bs)	495 nm
Emission 1 (em1)	542/50 nm
Emission 2 (em2)	650/57 nm

3.8 SUPER RESOLUTION MICROSCOPY

Super-resolution via optical reassignment (SoRa) imaging was performed to study co-localization between RYR and HN1L and TCR/CD3 stimulation-dependent translocation of HN1L in Jurkat T cells. The spinning disc in SoRa microscope helps with fast imaging in confocal mode and produces high resolution images. Jurkat T cells were either left unstimulated or stimulated with 1 µg/mL of OKT3 for 10 seconds and 5 minutes.

The unstimulated Jurkat T cells were seeded on slides coated with 5 mg/mL of BSA and 0.1 mg/mL of PLL to assess colocalization of RYR and HN1L. The cells were then fixed with 4 % (w/v) paraformaldehyde

(Alfa Aesar, Massachusetts, USA) for 15 minutes and permeabilized by incubating with 0.5 % (w/v) saponin (Fluka) for 15 minutes. Non-specific binding sites were blocked by incubating with 10% (v/v) FBS overnight at 4 °C. Anti-HN1L (1:100, HPA041888, Sigma-Aldrich) and anti-RYR (1:100, GTX22868, GeneTex) antiobodies were diluted separately in 3 % (v/v) FBS and incubated for 1 hour at RT. Similarly, anti-rabbit alexa fluor 488 (1:400, A21206. Life Technologies) and anti-mouse alexa fluor 565 (1:400, A11004, Thermo Fischer Scientific (Waltham, Massachusetts, USA)) secondary antibodies were diluted separately in 3 % (v/v) FBS and incubated for 1 hour at RT. The fixed, permeabilized and blocked cells were then stained with the antibodies mentioned above and washed four times with 3% (v/v) FBS. Then, coverslips were mounted on the above-treated cells with Abberior Mount Solid (Abberior) overnight at 4 °C.

To assess stimulation-dependent translocation of HN1L, stimulated Jurkat T cells (for 10 seconds and 5 minutes) were first stained with WGA647 (1:100, W32466, Thermo Fischer scientific (Waltham, Massachusetts, USA)) for 10 minutes to stain PM and then seeded, fixed, permeabilized and blocked as mentioned above. Anti-HN1L primary antibody (1:100, HPA041888, Sigma-Aldrich) and anti-rabbit alexa fluor 488 secondary antibody (1:400, A21206. Life Technologies) were diluted separately in 3 % (v/v) FBS and incubated for 1 hour at RT. The cells were then stained with these antibodies and washed four times with 3 % (v/v) FBS. The coverslips were mounted as mentioned above.

Images were captured using super resolution spinning-disk microscope (Visitron) which was equipped with a CSU-W1 SoRa Optic (2.8 x, Yokogawa), a 100x magnification objective (Zeiss) and a sCMOS camera (Orca-Flash 4.0, C13440-20CU Hamamatsu). Alexa Fluor 488 dye was excited using a 488nm laser and recorded using a 525/50 nm filter, whereas alexa fluor 568 dye was excited using a 561 nm laser and recorded using a 609/54 nm filter. Co-localization of proteins were analyzed using a deconvolution script (Openlab5, PerkinElmer) followed by trainable weka (Waikato environment for knowledge analysis) and watershed segmentations in FIJI (version 1.52p) to have more detailed segmentation of the detected proteins. Co-localization was calculated and quantified using a Matlab script as mentioned in Nauth et al. (2018). Translocation was assessed by calculating the euclidean distance of the proteins to the extracted cell border using cell segmentation approach which is based on an active contour model (also known as snake model). Based on energy forces and constraints, the contour was evolved to encompass the cell with a smooth boundary. These experiments were performed by Lola Hernandez (Institute for Biochemistry and Molecular Cell Biology, UKE, Hamburg, Germany) as internal collaborative research.

3.9 CO-IMMUNOPRECIPITATION OF RYR AND HN1L

The P10 membrane fractions extracted from unstimulated or stimulated Jurkat t cells as mentioned in section 3.6.2 were used to perform co-immunoprecipitation of RYR and HN1L. 4 µg of anti-RYR (GTX22868, GeneTex) was coupled to protein G magnetic beads by incubating them overnight at 4 °C. The magnetic beads were rinsed to remove excess anti-RYR antibody. 50 µL of the bead suspension was then mixed with 400 µg of P10 membrane fraction at 4 °C for 1.5 hours with constant mild shaking. The beads were then washed with 0.1 % of PBS-tween and resuspended in 1x SDS sample buffer followed by heating at 94 °C for 10 minutes to detach proteins from beads. SDS-PAGE and western blotting were performed as mentioned in sections 3.4.2.6 and 3.4.2.7 using gradient 4-20 % SDS-PAGE gel (Bio-Rad Laboratories Inc., Hercules, California, USA). The transfer conditions for HN1L were maintained at 200mA current on ice for 1.5 hours, whereas 200mA current at 4 °C for 18 hours was used for transfer of RYR. Appropriate primary antibodies and secondary antibodies at appropriate dilutions (as mentioned in Figure 22B legends) were used to detect HN1L and RYR using SuperSignal West Pico Chemiluminescent (Thermo Fisher Scientific, Waltham, Massachusetts, USA) as substrate. This experiment was performed by Lola Hernandez (Institute of Biochemistry and Molecular Cell Biology, UKE, Hamburg, Germany) as internal collaborative research.

3.10 CONSTRUCTION OF CRYO-EM GRIDS

RYR1 was purified from rabbit (*Oryctolagus cuniculus*) skeletal muscle by calstabin-affinity chromatography as mentioned in Zalk et al. (2015). The purified RYR1, recombinant tagged HN1L-01, and NAADP were used to construct cryo-EM grids as shown in Zalk et al. (2015). Briefly, 3 µL of each components mentioned above was added to holey carbon grids (C-flat CF-1.2 / 1.3-2C-T, Protochip Inc, North Carolina, USA). The grids were then blotted for approximately 1 second and vitrified by rapidly plunging into liquid ethane at -180 ℃ with a Vitrobot (FEI) as mentioned in Dubochet et al. (1988) and Wagenknecht et al. (1988). This experiment was kindly performed by the group of Dr. Oliver Clarke (Department of Physiology and Cellular Biophysics, Columbia University College of Physicians & Surgeons, New York, USA) at their facility as external collaborative research.

3.11 PLANAR LIPID BILAYER RECORDING

Purified RYR1 was reconstituted into microsomes as described in Lee et al. (1994). These reconstituted microsomes were then fused to planar lipid bilayers by applying a lipid mixture of

phosphatidylethanolamine and phosphatidylcholine (Avanti Polar Lipids, Alabama, USA) in ratio of 5:3 in decane across a 200 µm hole in polysulfonate cups (Warner Instruments, Massachusetts, USA) separating trans and cis chambers. The former chamber was connected to bilayer voltage clamp amplifier and the latter was held at virtual ground. Table 15 shows the composition of trans and cis buffer used in this experiment.

Table 15: Composition of trans and cis solutions used in planar lipid bilayer recording

Buffers	Composition
trans solution	1 mM EGTA, 250 mM HEPES, 50 mM KCl (pH 7.35), 0.64 mM $Ca2^{+}$ (150 nM free Ca^{2+})
cis solution	3 mM $Ca(OH)_2$, 50 mM KCl, 250 mM HEPES (pH 7.35)

10 µM of NAADP and 10 µM recombinant tagged HN1L-01 were added subsequently to above mentioned setup and single-channel currents were recorded 0 mV using a Bilayer Clamp BC-525C (Warner Instruments, Massachusetts, USA) at RT. The recordings were analyzed using Clampfit 10.1 (Molecular Devices, California, USA) and Graphpad Prism software. This experiment was kindly performed by the group of Dr. Oliver Clarke (Department of Physiology and Cellular Biophysics, Columbia University College of Physicians & Surgeons, New York, USA) at their facility as external collaborative research.

4 RESULTS

As mentioned in section 1.3.5, the 22/23 kDa protein in T cells was identified to be HN1L by mass spectroscopic analysis. This section reports evidence to claim that HN1L is a NAADP binding protein and plays an important role in formation of highly dynamic Ca^{2+} microdomains. According to Uniprot (Q9H910 (JUPI2_HUMAN), HN1L is expressed in human as 3 alternatively spliced variants which will be referred as isoforms of HN1L (HN1L-01, HN1L-02 and HN1L-03) in this thesis. Among these isoforms, HN1L-03 is the longest protein with 217 aminoacids and HN1L-02 is the shortest one with 170 aminoacids. HN1L-01 is the predominantly expressed HN1L protein across species with 190 aminoacids. The predominantly expressed (HN1L-01) and the longest (HN1L-03) HN1L isoforms were studied extensively in this thesis.

4.1 BINDING OF NAADP TO RECOMBINANTLY EXPRESSED HN1L

Binding between NAADP and HN1L was assessed using recombinantly expressed HN1L proteins. The gene sequences of HN1L-01 and HN1L-03 were codon optimized for bacterial expression and cloned into pASK-IBA43plus vector as mentioned in section 3.3.1. The vector was designed by the manufacturers in a way that a 6*His tag and a strep tag are attached to the HN1L proteins at N terminus and C terminus respectively. The codon optimized *hn1l* genes in the vector were then expressed recombinantly in bacteria as mentioned in section 3.4.1. The strep tag in the recombinant HN1L proteins was used for their purification as mentioned in section 3.4.2. Figure 10 shows the SDS-PAGE and western blot images of purified recombinant HN1L isoform 1 and 3 with 6*His tag and strep tag at both ends.

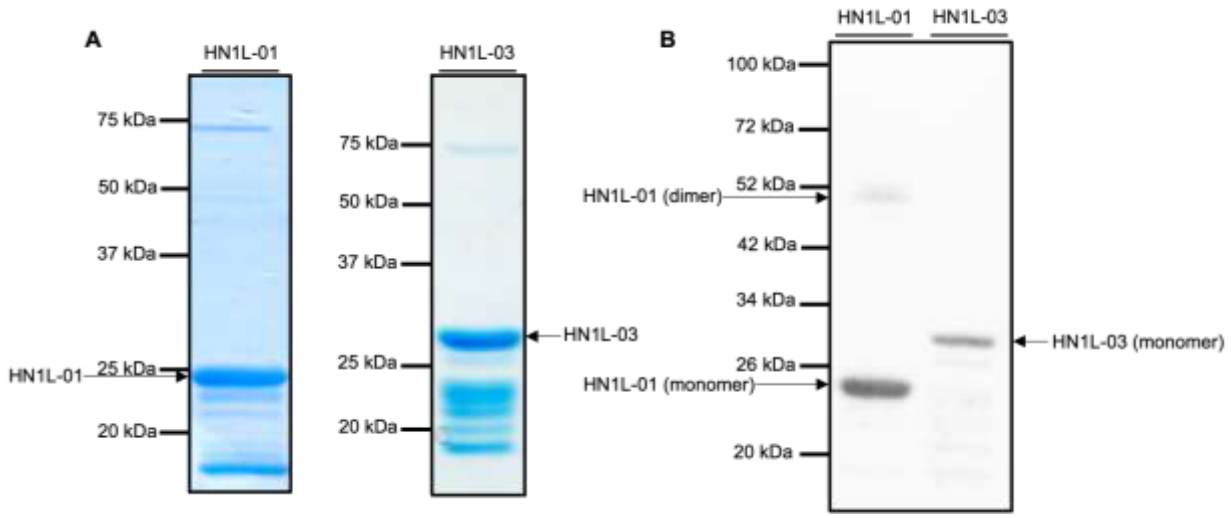

Figure 10: Qualitative assessment of purified recombinant tagged HN1L isoforms 1 and 3: (A) 3 µg of purified proteins were loaded on to 12.5 % SDS-PAGE gel and their purity was checked. (B) 100 ng of purified proteins were used in western blot and their identity was confirmed using the anti-HN1L antibody (1:50000, ab200571, Abcam).

The recombinant HN1L-01 and HN1L-03 run slightly at higher molecular masses (21.43 kDa and 24.39 kDa respectively) than that of reported in Uniprot (20.06 kDa and 23.03kDa respectively) due to the presence of 6*His and strep tags at both ends of the recombinant proteins. Even though the samples were subjected to electrophoresis at reducing condition, dimeric form of HN1L-01 could be seen in western blot image which is not true for HN1L-03. This suggests that the tagged HN1L-01 has more stable dimeric form than that of tagged HN1L-03. Moreover, for both isoforms of HN1L, several protein bands can be seen below the major HN1L protein bands in Figure 10A. The fact, that these smaller protein bands were also detected by anti-HN1L antibody in Figure 10B, proves that these are the degraded products of recombinant HN1L-01 and HN1L-03. These recombinantly expressed HN1L-01 and HN1L-03 isoforms were used to study their binding to NAADP by PAL.

PAL was initially validated by using a previously identified NAADP binding partner, the enzyme CD38. We also used the catalytically inactive E226Q mutant of CD38 in this method expecting a better binding of NAADP as the inactive mutant cannot degrade NAADP and its analog. As shown in the Figure 11A, [^{32}P]-azide-AIO-NAADP labelled WT CD38 much weaker than the E226Q mutant. As only 0.78nM of the probe was used in this experiment, the higher K_m (in micromolar range) of CD38 for its substrates explains such weaker labelling of CD38 by the probe. The stronger labelling of the E226Q mutants is likely due to the inability of the E226Q mutant to degrade the probe. In the presence of 3.3 μM NAADP, the probes were partially displaced in E226Q mutant whereas no displacement was seen for WT CD38. With this successful validation, PAL was performed with recombinant HN1L-01 and HN1L-03. In contrast to CD38, both isoforms of recombinant HN1L were strongly labelled by [^{32}P]-azide-AIO-NAADP. Moreover, dimers and trimers of HN1L-01 were also strongly labelled whereas the oligomeric forms of HN1L-03 were not, which corresponds to the oligomerization of tagged HN1L-01 and HN1L-03 discussed above. The probe, which labelled HN1L-01 and HN1L-03, was successfully displaced by 3.3 μM NAADP leading to a loss of radioactive signals as shown in Figure 11A. Displacement was more effective for dimers and trimers of HN1L-01 than for its monomers. Such displacement of the probe by NAADP clearly suggests that HN1L-01 and HN1L-03 are high affinity NAADP binding proteins.

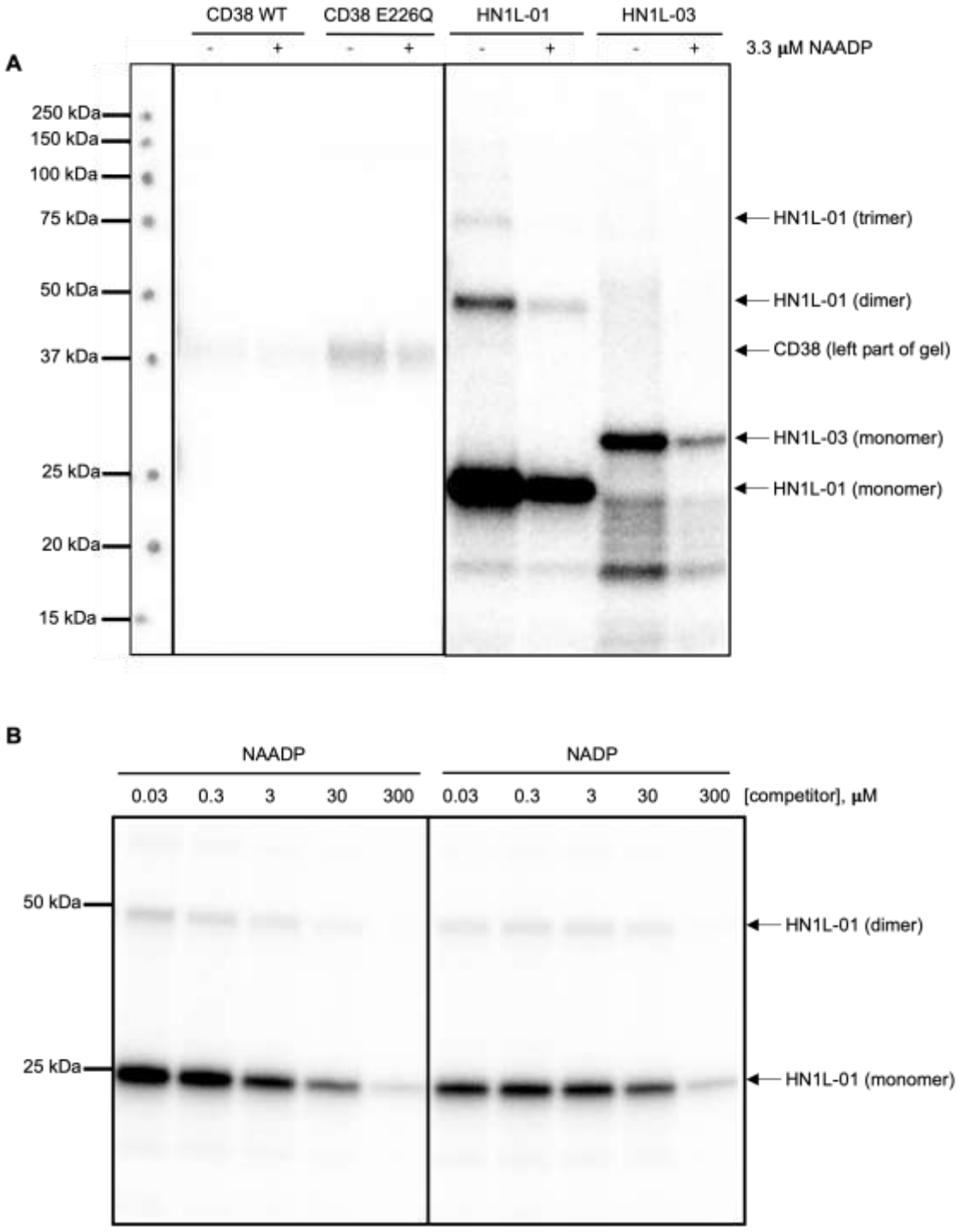

Figure 11: PAL of isoforms of HN1L, WT CD38 and its inactive mutant E226Q: (A) 1µg of purified recombinant proteins (CD38 WT, CD38 E226Q, tagged HN1L-01 and tagged HN1L-03) were subjected to PAL with 0.5nM of [^{32}P]-azide-AIO-NAADP. A representative phosphor image is shown (n=4 independent experiments). (B) PAL of 7.11 µg/mL of tagged HN1L-01 by 0.78nM of [^{32}P]-azide-AIO-NAADP and its displacement by different concentrations of NAADP and NADP as indicated. A representative phosphor image is shown (n=4 independent experiments). This data was produced by the group of Prof. Timothy Walseth (Department of Pharmacology, University of Minnesota Medical School, Minneapolis, Minnesota, USA) at their facility as external collaborative research. This dataset was modified from figure 4 of Roggenkamp et al. (2021).

Furthermore, HN1L-01 was subjected to quantitative displacement PAL experiments with different concentrations of NAADP and NADP ranging from 30nM to 300µM. Figure 11B shows that the dimer of HN1L-01 was already partially displaced from the probe between 30nM and 300nM of NAADP, whereas it was only displaced by NADP between 30 and 300µM. Moreover, the monomeric HN1L-01 was displaced by NAADP at 3 – 30µM and by NADP at 30 – 300µM. Collectively, PAL studies claim that HN1L is a highly specific NAADP binding protein.

4.2 PRODUCTION AND CHARACTERIZATION OF TAG-FREE HN1L AND DELETION MUTANTS THEREOF

Based on the previous findings shown in Figure 11, we next attempted to narrow down the binding site of NAADP in HN1L with its deletion mutants using PAL. For this purpose, tag-free recombinant HN1L proteins were used to mimic native HN1L conditions. The entire bacterial expression system was changed to produce tag-free recombinant proteins as mentioned in section 3.4. Figure 12 shows the SDS-PAGE and western blot images of purified tag-free recombinant HN1L isoform 1 and 3. The tag-free HN1L-01 and HN1L-03 run at almost the same size of native HN1L isoforms (20.22 kDa and 23.18 kDa respectively). The change of bacterial expression system affected the purity of the recombinant HN1L proteins (Figure 12A), but enhanced the oligomerization property of HN1L proteins (Figure 12B) as compared to the tagged recombinant HN1L proteins. Despite reducing conditions during electrophoresis, up to pentameric form of tag-free HN1L-01 and trimeric form of HN1L-03 can be detected in western blot (Figure 12B).

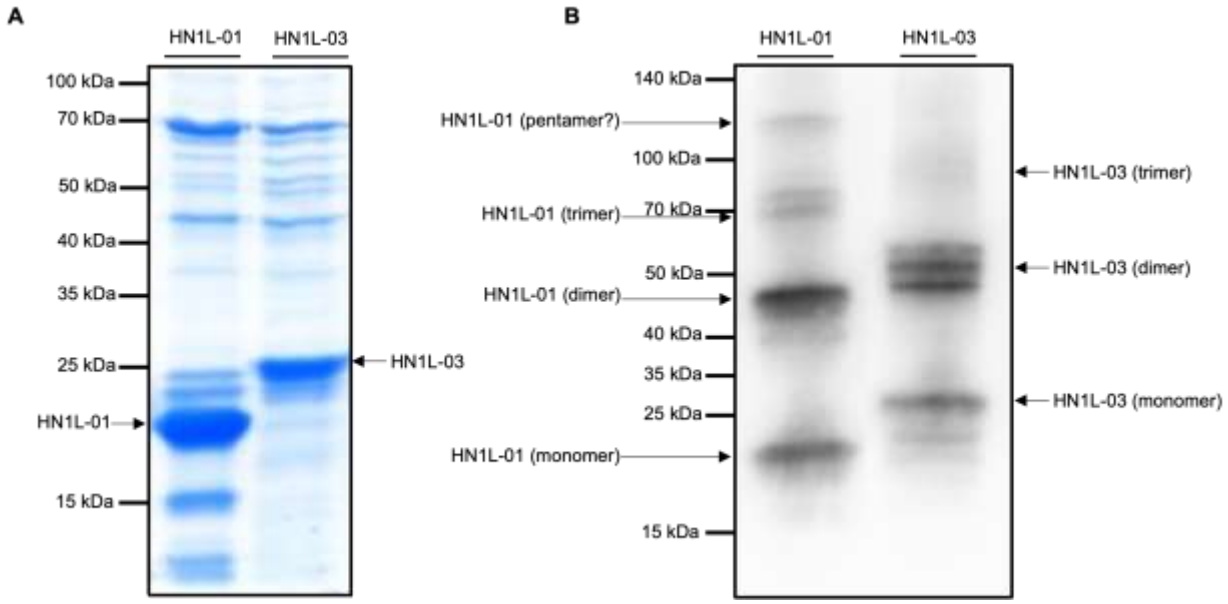

Figure 12: Qualitative assessment of purified recombinant tag-free HN1L isoforms 1 and 3: (A) 3µg of purified proteins were loaded on to 12.5% SDS-PAGE gel and their purity was checked. (B) 100ng of purified proteins were used in western blot and their identity was confirmed using the anti-HN1L antibody (1:50000, ab200571, Abcam).

With the successful validation of the tag-free recombinant protein production, the longest HN1L protein (HN1L-03) was chosen to make deletion mutants. As shown in Figure 13A, four regions were marked which include a jupiter domain (JD) and 3 randomly chosen regions (part-1, part-2 and part-3). Each of these four regions was deleted to make four deletion mutants namely: HN1L-03-ΔJD, HN1L-03-ΔP1, HN1L-03-ΔP2 and HN1L-03-ΔP3 (Figure 13A).

Figure 13B shows SDS-PAGE gel image of purified tag-free HN1L-03 and its deletion mutants and the red boxes indicate HN1L-03 proteins in each purified fraction. The mutants HN1L-03-ΔP2 and HN1L-03-ΔP3 were poorly expressed in bacteria resulting in high impurity levels (Figure 13B). The identity of HN1L-03 proteins (indicated in red boxes) in each purified fraction was confirmed by western blot (Figure 13C). The poorly expressed deletion mutants would not pose a problem in intended usage in PAL because of the method's high sensitivity. These tag-free HN1L and its deletion mutants will be subjected to PAL in future to narrow down the binding site of NAADP.

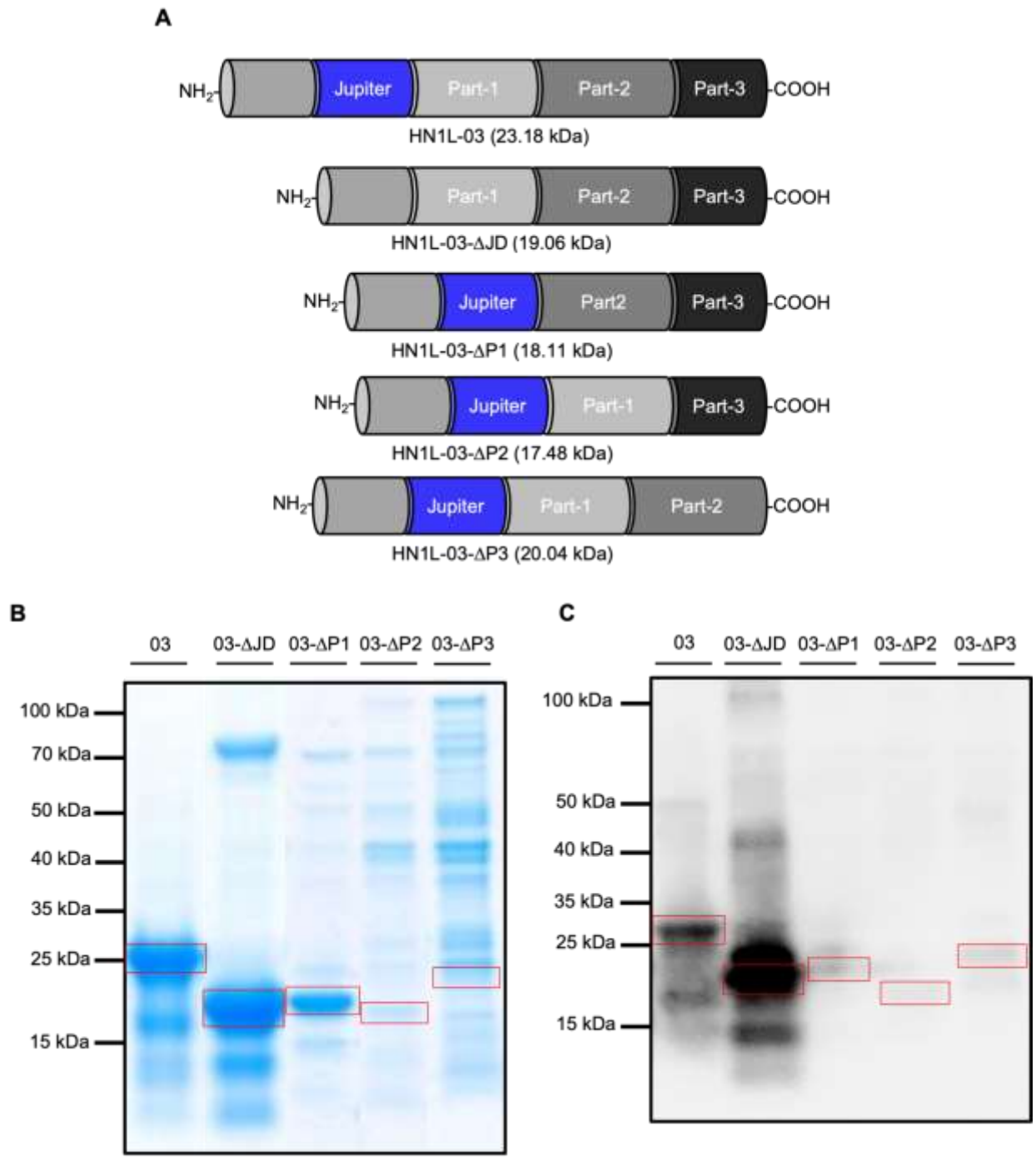

Figure 13: Deletion mutants of tag-free HN1L isoform 3 and their qualitative assessment: (A) Graphical representation of deletion mutants of HN1L isoform 3. (B) 3µg of purified proteins were loaded on to 12.5% SDS-PAGE gel and their purity was checked. (C) 100ng of purified proteins were used in western blot and their identity was confirmed using the anti-HN1L antibody (1:50000, ab200571, Abcam). Red boxes represent HN1L-03 and its deletion mutants.

4.3 EFFECT OF *HN1L* GENE KNOCKOUT

HN1L is a widely expressed protein across species with low tissue specificity. It is predominantly localized in the cytoplasm and at the plasma membrane (JPT2 protein expression summary - The human protein atlas). According to RNA sequencing data from the Human Protein Atlas, it is moderately expressed in both naïve and memory $CD4^+$ and $CD8^+$ T cells and in regulatory T cells (JPT2 protein expression summary - The human protein atlas). This section discusses *hn1l* gene knockout studies performed in Jurkat T cells and rat primary $CD4^+$ T cells.

4.3.1 Jurkat T cells

Jurkat T cells are an immortalized T lymphocyte cell line, which is widely used to study T cell signaling. In this thesis, this cell line was used to determine the role of HN1L in NAADP-mediated Ca^{2+} signaling. HN1L was detected at about 22 kDa in the cytosolic fraction of Jurkat T cells (Figure 14). Although the cytosolic protein fraction was separated by electrophoresis at reducing condition, higher oligomeric forms of HN1L could be detected using anti-HN1L antibody as shown in Figure 14, suggesting stable oligomeric forms of HN1L.

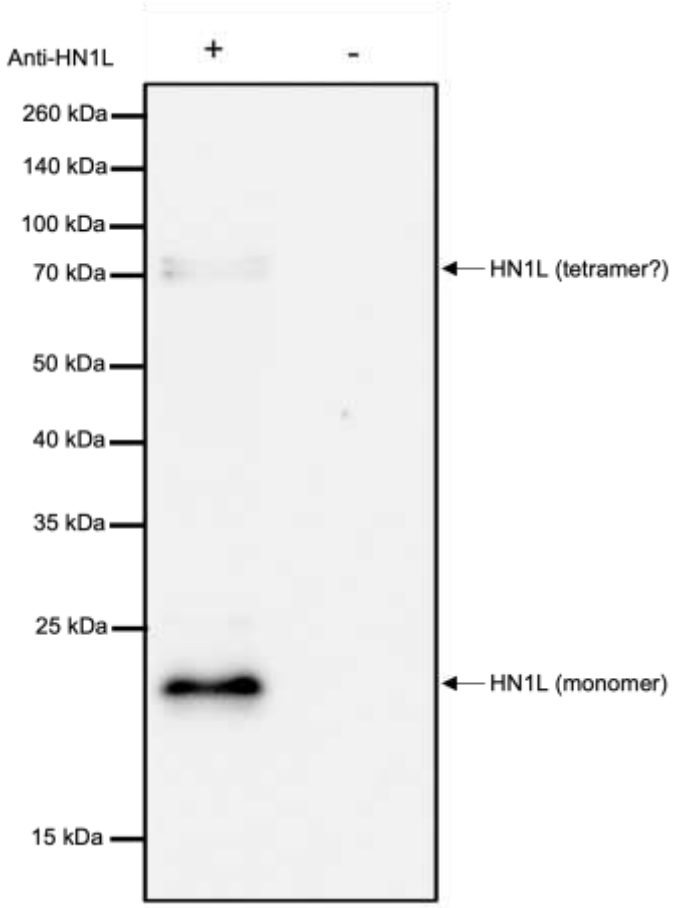

Figure 14: Detection of endogenous HN1L in Jurkat T cell cytosolic fraction: 30 µg of S10 fraction Jurkat T cells was subjected to 12.5 % SDS-PAGE and western blot analysis (n=4 independent experiments). Endogenous HN1L was detected using anti-HN1L antibody (1:200, HPA041888, Atlas antibodies). This dataset was modified from figure 1 of Roggenkamp et al. (2021).

The *hn1l* gene was targeted by Cas-9 mediated approach to knock it out. As shown in Figure 15A, exon 1 of *hn1l* gene was targeted, which caused frameshift mutations in all 3 alleles resulting in the loss of HN1L. Based on this approach, two Jurkat T cell clones were isolated: Clone 2 (C2) and clone 4 (C4). Expression levels of HN1L were compared among WT, C2 and C4 Jurkat T cell clones (Figure 15B). The clone C2 had 13 ± 3-fold decreased HN1L expression level as compared to WT clone, whereas C4 had only 2.9 ± 0.2-fold decreased expression level.

These two clones with differential expression levels of HN1L were analyzed for of their global Ca^{2+} signaling upon TCR/CD3 stimulation. Figure 15C shows that C2 has significantly decreased Ca^{2+} peak, Ca^{2+} plateau and signal onset velocity as compared to WT, whereas only Ca^{2+} peak was affected for C4. The effects on global Ca^{2+} signaling are comparable to the expression levels of HN1L in the clones C2 and C4. *Hn1l* gene was transiently re-expressed in C2 leading to 2.8 ± 0.4-fold over-expression and analyzed for its impact in global Ca^{2+} signaling (Figure 15D). As expected, global Ca^{2+} signaling was rescued, but not completely. A significant increase in signal onset velocity and Ca^{2+} peak amplitude was observed for C2 with transiently re-expressed HN1L. The partial rescue of global Ca^{2+} signaling confirms that HN1L is a major constituent of Ca^{2+} signaling in T cells.

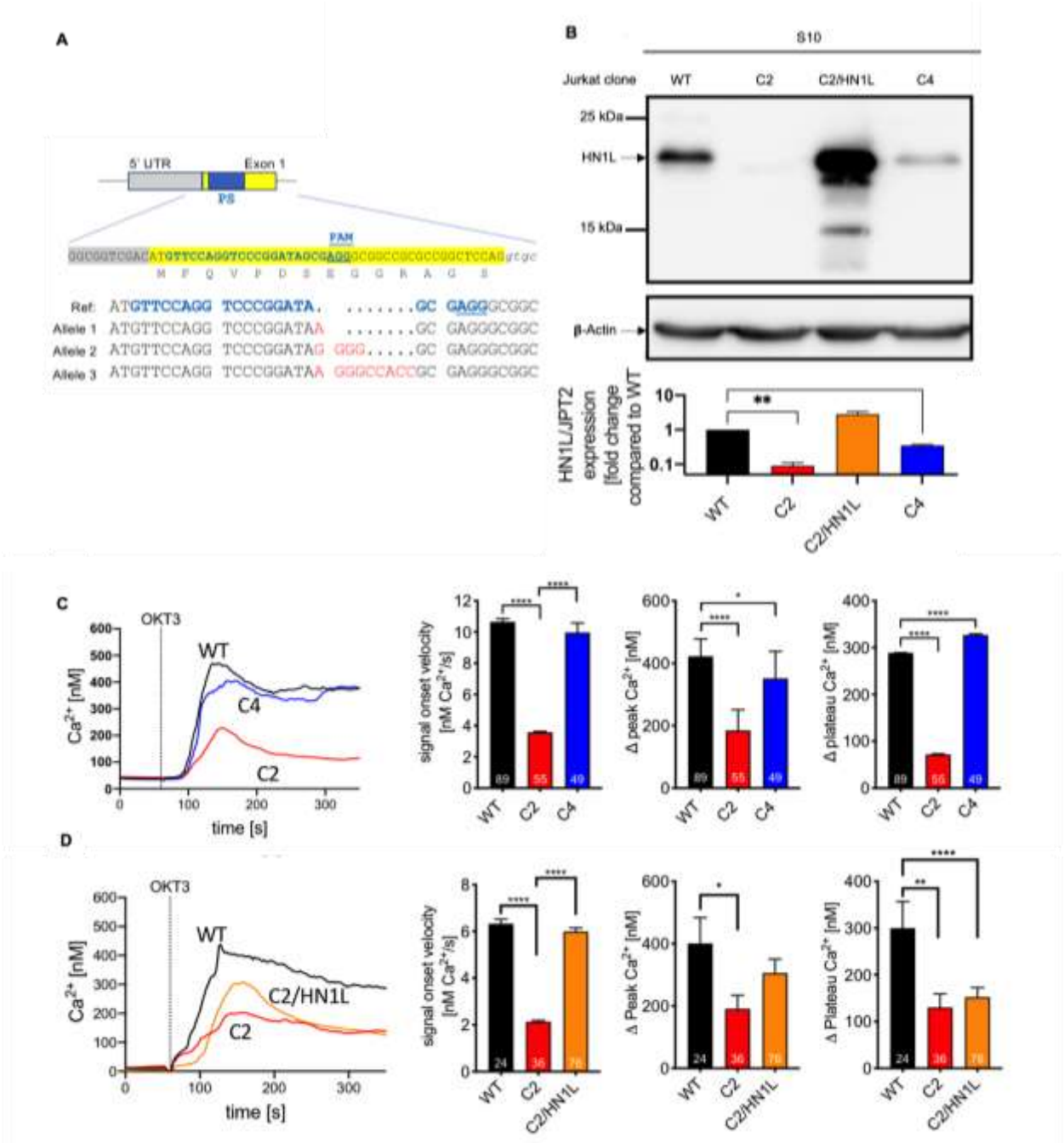

Figure 15: Knockout of HN1L affected TCR/CD3-evoked global Ca^{2+} signaling in Jurkat T cells: (A) The protospacer sequence (PS) of exon1 of human *hn1l* gene was used to perform Cas9-mediated knockout. Frameshift mutations (red font) were caused in all three alleles leading to the loss of HN1L protein in clone 2 (C2). (B) HN1L expression were analyzed in WT, C2, C2 with transient overexpression of HN1L (C2/HN1L) and C4 clones using anti-HN1L antibody (1:200, HPA041888, Atlas antibodies) in western blot analysis. β-actin was used as loading control. 30 µg of S10 fraction from all above-mentioned clones were separated in 12.5 % SDS-PAGE gel and subjected to western blotting (n=3 independent experiments). Densitometric analysis of HN1L bands in above-mentioned clones was performed in ImageJ and depicted in the lower graph as relative expression to WT (set to 1). (C) Global Ca^{2+} signals of WT, C2 and C4 Jurkat T cell clones were analyzed by global Ca^{2+} imaging as mentioned in the methods. Jurkat T cell clones were stimulated with 1 µg/mL anti-CD3 mAb (OKT3). The bar graphs indicate the comparison among the Jurkat T cell clones with respect to signal onset velocity, ΔCa^{2+} peak and ΔCa^{2+} plateau. Data are presented as means ± SEM (WT, n = 89 cells; C2, n = 55 cells; C4, n = 49 cells) from five independent experiments. (D) Global Ca^{2+} signals of WT, C2 and C2 with transient overexpression of HN1L (C2/HN1L) Jurkat T cell clones were analyzed by Ca^{2+} imaging as mentioned in the methods. Jurkat T cell clones were stimulated with 1µg/mL anti-CD3 mAb (OKT3). The bar graphs indicate the comparison

among the Jurkat T cell clones with respect to signal onset velocity, ΔCa^{2+} peak and ΔCa^{2+} plateau. Data are presented as means ± SEM (WT, n = 24 cells; C2, n = 36 cells; C4, n = 76 cells) from three independent experiments. Statistical analysis for (C) and (D) were performed by one-way ANOVA (Kruskal-Wallis test). Asterisks (*) in (B) to (D) refer to significant differences (*P < 0.05, **P < 0.01, ***P < 0.001, ****P < 0.0001). Data shown in (A) were prepared by Valerie Wolters (Institute for Biochemistry and Molecular Cell Biology, UKE, Hamburg, Germany) as internal collaborative research. Data shown in (C) and (D) were prepared by Anette Rosche (Institute for Biochemistry and Molecular Cell Biology, UKE, Hamburg, Germany) as internal collaborative research. This dataset was modified from figure 2 of Roggenkamp et al. (2021).

In T cells, three secondary messengers contribute to global Ca^{2+} signaling upon TCR/CD3 stimulation: NAADP, IP_3 and cADPR. NAADP evokes Ca^{2+} release in seconds, whereas IP_3 comes in to play in minutes and cADPR contributes in ≥ 10 minutes. As the global Ca^{2+} signals were measured for a few minutes, it was necessary to rule out the contribution of IP_3 in global Ca^{2+} signaling. Hence, IP_3 evoked Ca^{2+} signals were analyzed in clone C2 by stimulating with membrane permeable analog of IP_3 called IP_3-acetoxymethyl ester (IP_3-AM). Figure 16A shows that there are no significant differences in signal onset velocity and Ca^{2+} peak amplitude between WT and C2 upon stimulation with IP_3-AM. However, a significant difference in Ca^{2+} plateau phase was observed. Furthermore, impact of *hn1l* gene knockout on store operated Ca^{2+} entry (SOCE) was analyzed by stimulating with thapsigargin (Figure 16B). It was clear that global Ca^{2+} signaling, with respect to Ca^{2+} peak and Ca^{2+} plateau amplitude, in C2 clone was not affected by the loss of HN1L. Collectively, these data suggest that HN1L is a major player only in NAADP-mediated Ca^{2+} signaling, but not in IP_3-mediated Ca^{2+} signaling or in SOCE mediated by STIM1/2 or ORAI.

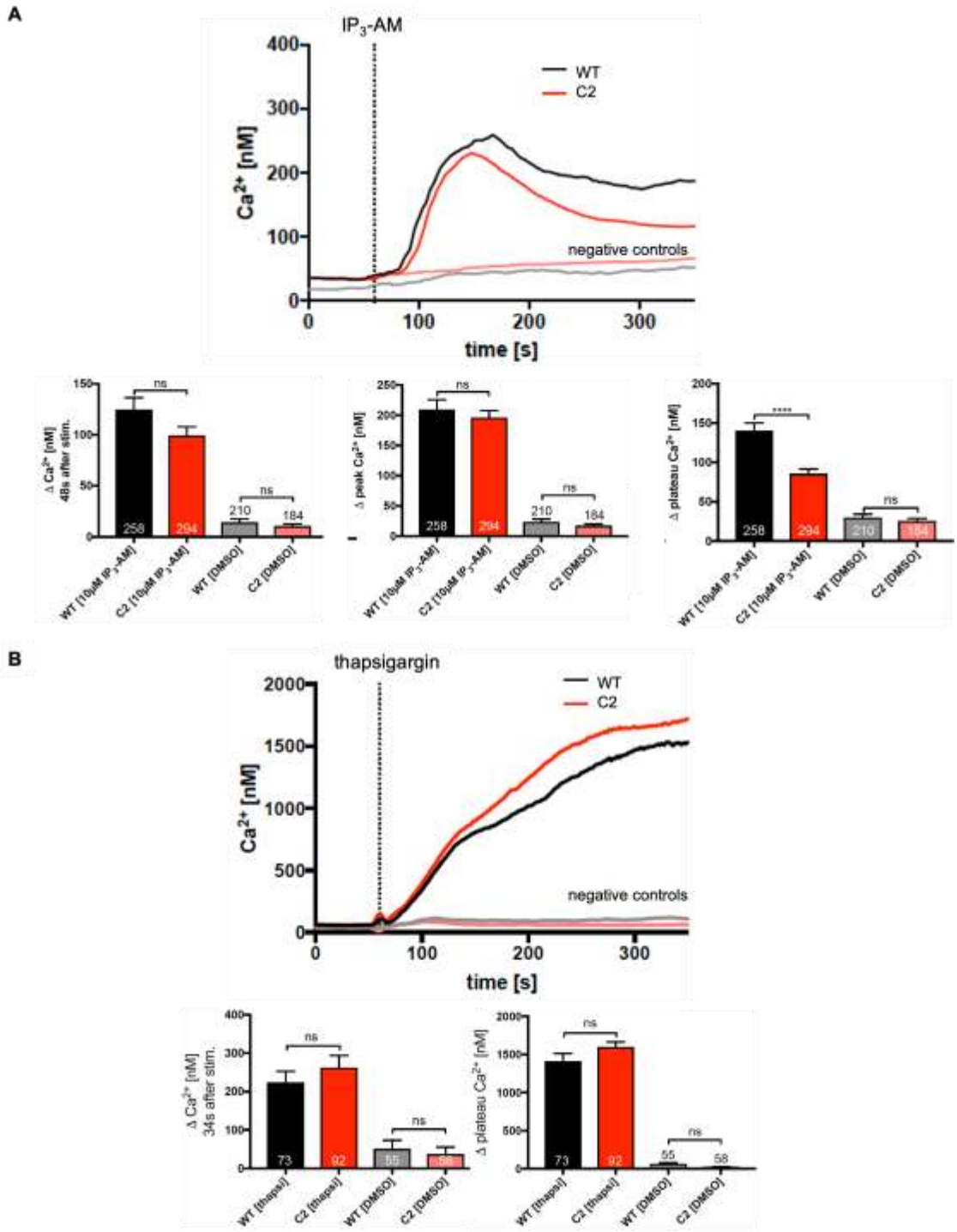

Figure 16: Knockout of HN1L does not affect IP_3 evoked Ca^{2+} signaling or SOCE: (A) Global Ca^{2+} signals of WT and C2 Jurkat T cell clones were analyzed by global Ca^{2+} imaging as mentioned in the methods. Jurkat T cell clones were stimulated with 10 µM IP_3-AM or DMSO (negative control). The bar graphs indicate the comparison among the Jurkat T cell clones with respect to ΔCa^{2+} 48 seconds after stimulation, ΔCa^{2+} peak and ΔCa^{2+} plateau. Data are presented as means ± SEM (WT [IP_3-AM], n = 258 cells; C2 [IP_3-AM], n = 294 cells; WT [DMSO], n = 210 cells; C2 [DMSO], n = 184) from five independent experiments. (B) Global Ca^{2+} signals of WT and C2 Jurkat T cell clones were measured by Ca^{2+} imaging as mentioned in the methods. Jurkat T cell clones were stimulated with 1.67µM thapsigargin or DMSO (negative control). The bar graphs indicate the comparison among the Jurkat T cell clones with respect to ΔCa^{2+} 34 seconds after stimulation and ΔCa^{2+} plateau. Data are presented as means ± SEM (WT [thapsi], n = 73 cells; C2 [thapsi], n = 92 cells; WT [DMSO], n = 55 cells; C2 [DMSO], n = 58) from five independent experiments. Statistical analysis for (A) and (B) were performed by one-way ANOVA with Tukey correction for multiple testing. Asterisks (*)

in (A) and (B) refer to significant differences (ns – non-significant; ****P < 0.0001). These data were prepared by Anette Rosche (Institute for Biochemistry and Molecular Cell Biology, UKE, Hamburg, Germany) as internal collaborative research. This dataset was modified from figure S6 of Roggenkamp et al. (2021).

Next, Ca^{2+} microdomains were analyzed in C2 to study the effect of *hn1l* gene knockout in Ca^{2+} microdomain formation. Fast imaging with directed TCR/CD3 stimulation was used to image Ca^{2+} microdomains. Figure 17A shows two representative cells of WT and C2 clones at top and bottom respectively and beads coated with anti-CD3 antibody (marked as B) which were used to create artificial immune synapse. It is clear that several discrete Ca^{2+} microdomains (warm color) were formed in WT cell (at the region of bead contact site) between 3 and 4 seconds, whereas no Ca^{2+} microdomains were formed in C2 cell until 6 seconds after stimulation. The number of average Ca^{2+} microdomains formed in C2 and WT over the first 15 seconds was calculated and observed that it drastically decreased in C2 clone (Figure 17B). Similarly, the percentage of responding cells was significantly reduced in C2 (Figure 17B). However, the Ca^{2+} concentration in microdomains was not affected in C2 (Figure 17B). Figure 17C shows the kinetics of Ca^{2+} microdomain formation over 10 seconds post bead contact and it reports that C2 clone formed barely detectable Ca^{2+} microdomains, whereas WT clone formed the microdomains between 3 and 4 seconds and remained elevated over the next seconds. Altogether, these analyses of initial Ca^{2+} microdomain formation suggest that HN1L is one of the key proteins that are involved in the early phase of NAADP-mediated Ca^{2+} signaling. Such early involvement of HN1L also explains the delayed onset of global Ca^{2+} signals and reduced Ca^{2+} peak amplitude at later time points in global Ca^{2+} signaling in C2 clone.

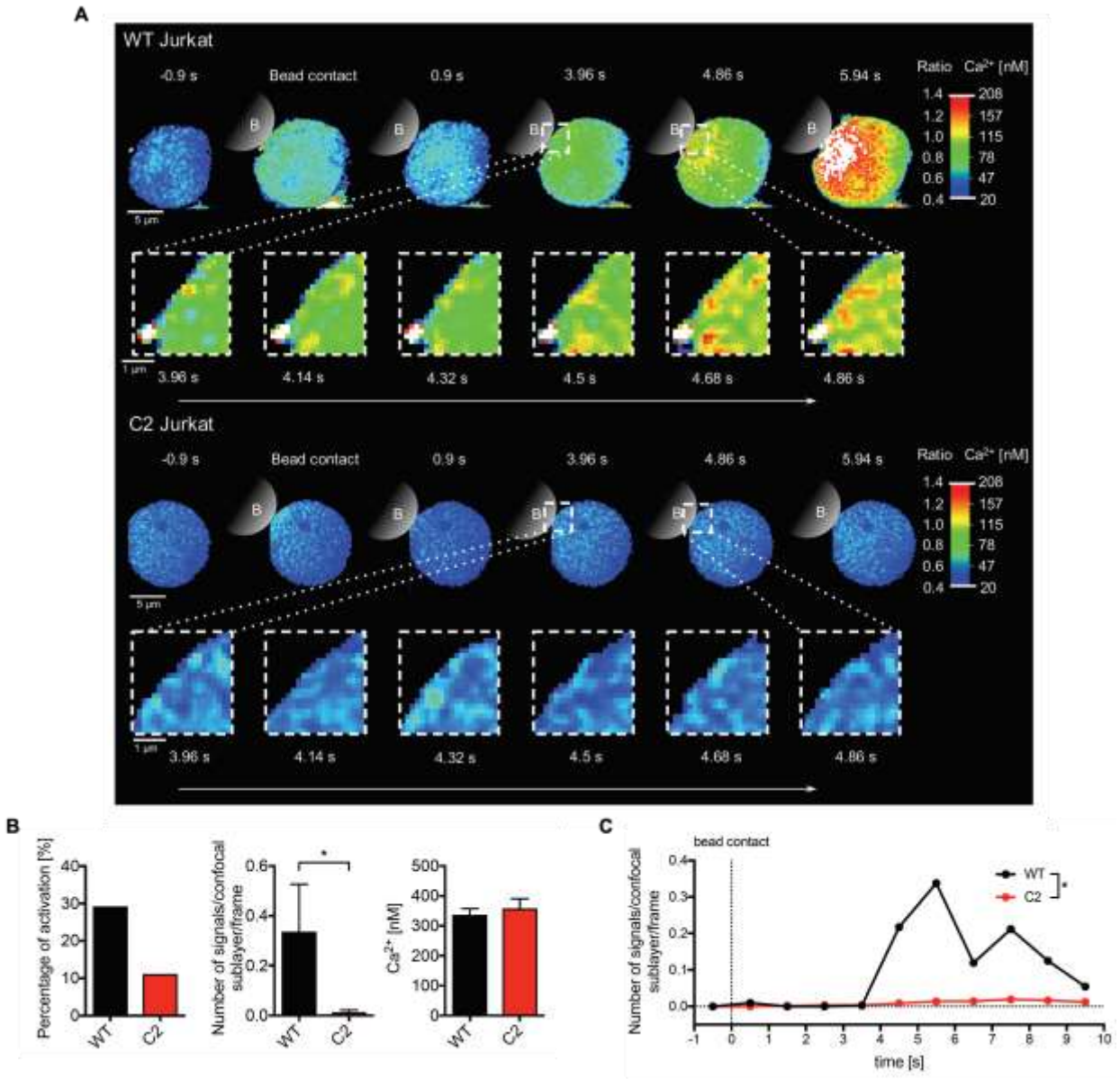

Figure 17: Deletion of HN1L suppresses initial Ca^{2+} microdomains evoked by TCR/CD3 stimulation in Jurkat T cells: (A) Local Ca^{2+} microdomains of WT and C2 Jurkat T cell clones were analyzed by local Ca^{2+} imaging as mentioned in the methods. Representative cells from both WT and C2 clones are shown at full resolution along with the bead (marked as B; coated with anti-CD3 mAb OKT3) used to create artificial immune synapse. (B) The bar graphs indicate the comparison between the Jurkat T cell clones with respect to percentage of activated cells, number of Ca^{2+} microdomains and average Ca^{2+} concentration of the microdomains over the first 15 seconds of stimulation. Data are presented as means ± SEM (WT, n = 23 cells; C2, n = 35 cells). Statistical analyses were performed by non-parametric unpaired two-tailed test (Mann-Whitney). (C) Kinetics of Ca^{2+} microdomain formation in WT and C2 Jurkat T cell clones until 10 seconds after stimulation. Statistical analyses were performed by an unpaired two-tailed *t* test. Asterisks (*) in (B) and (C) refer to significant differences (*P < 0.05). These data were prepared by Feng Gu, Franziska Möckl and Aileen Krüger (Institute for Biochemistry and Molecular Cell Biology, UKE, Hamburg, Germany) as internal collaborative research. This dataset was modified from figure 3 of Roggenkamp et al. (2021).

4.3.2 Rat primary T cells

With the successful *hn1l* gene knockout studies in Jurkat T cells, the system was changed to rat primary T cells for more physiological relevance. *hn1l* gene is expressed in 21 tissues in rats with the highest expression in thymus (Q5BK20 (JUPI2_RAT); Uniprot). $CD4^+$ effector rat T cells ($T_{\beta\text{-SYN}}$ cells), specific to β-synuclein, were used in this thesis to study Ca^{2+} signaling. Cas9-mediated knockout was performed to knockout *hn1l* gene and as shown in Figure 18A, exon 2 of *hn1l* gene was targeted by guide RNA which caused frame shift mutations leading to the loss of HN1L protein. It was confirmed by T7 endonuclease cleavage assay that exon 2 of *hn1l* gene was successfully targeted (Figure 18A). On protein level, a strong reduced expression of HN1L can be observed for knockout clone as compared to WT clone (Figure 18B). In contrast to the expression of HN1L in Jurkat T cells, HN1L was detected in rat T cells at 22 kDa (prominent band as observed in Jurkat T cells) and 24/25 kDa (additional double band).

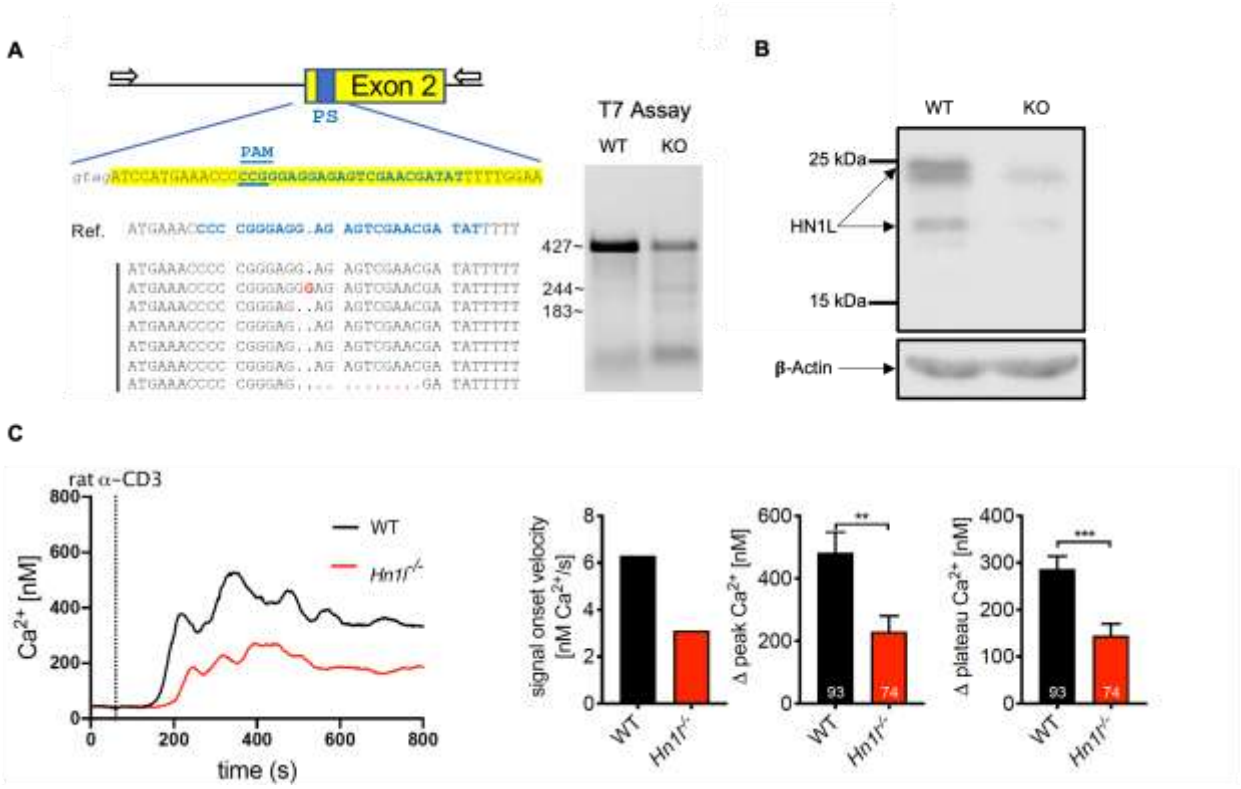

Figure 18: Knockout of HN1L affected TCR/CD3-evoked global Ca^{2+} signaling in rat primary T cells: (A) The protospacer sequence (PS) of exon1 of rat *hn1l* gene was used to perform Cas9-mediated knockout. Primers were used for genomic PCR as indicated by the arrows. Frameshift mutations (red font) were caused as shown in the aligned sequences leading to the loss of HN1L protein in *hn1l* knockout rat primary T cells. The right DNA gel electrophoresis image shows the approximate size of uncleaved and cleaved products of T7 endonuclease cleavage assay. (B) HN1L expression were analyzed in resting rat WT and *hn1l*$^{-/-}$ $T_{\beta\text{-SYN}}$ cells using anti-HN1L antibody (1:500, A304-664A, Bethyl Laboratories) in western blot analysis. 30 µg of S10 fraction from the above-mentioned cells were separated in 12.5% SDS-PAGE gel and subjected to western blotting (n=3 independent experiments). (C) Global Ca^{2+} signals of resting rat WT and *hn1l*$^{-/-}$ $T_{\beta\text{-SYN}}$ cells were measured by global Ca^{2+} imaging as mentioned in the methods. Rat primary T cells were stimulated with 1 µg/mL of rat anti-CD3 mAb (554829, BD Pharmingen). The bar graphs indicate the comparison between the above-mentioned cell types with respect to signal onset velocity, ΔCa^{2+} peak and ΔCa^{2+} plateau. Data are presented as means ± SEM (WT, n = 93 cells; *hn1l*$^{-/-}$, n = 74 cells). Statistical analysis was performed by unpaired two-tailed *t* test. Asterisks (*) refer to significant differences (**P < 0.01, ***P < 0.001). Data shown in (A) were provided by the

group of Prof. Alexander Flügel (Department of Neuroimmunology, University Medical Center, Göttingen, Germany) as external collaborative research. This dataset was modified from figure 5 of Roggenkamp et al. (2021).

As in Jurkat T cells, the impact of *hn1l* gene knockout on TCR/CD3-evoked Ca^{2+} signaling in rat $T_{\beta\text{-SYN}}$ cells was first studied by performing global Ca^{2+} signal measurement. It is clear from Figure 18C that *hn1l*$^{-/-}$ rat $T_{\beta\text{-SYN}}$ cells showed impaired global Ca^{2+} signals with delayed signal onset velocity, reduced ΔCa^{2+} peak and ΔCa^{2+} plateau amplitudes as compared to WT rat $T_{\beta\text{-SYN}}$ cells. The effect of *hn1l* knockout in rat primary T cells is in line with that of in Jurkat T cells, proving the fact that HN1L is indeed a major player in global Ca^{2+} signaling.

Next, role of HN1L in rat T cells at initial phase of T cell activation was analyzed by imaging the Ca^{2+} microdomains in rat $T_{\beta\text{-SYN}}$ cells over first 15 seconds after TCR/CD3 stimulation. Figure 19A shows two representative cells from WT and *hn1l*$^{-/-}$ rat $T_{\beta\text{-SYN}}$ cells with Ca^{2+} microdomain formation after bead contact (TCR/CD3 stimulation). The characteristic WT rat $T_{\beta\text{-SYN}}$ cell (Figure 19A) responded rapidly with increase in discrete Ca^{2+} microdomains close to the region of bead contact site, where as the *hn1l*$^{-/-}$ rat $T_{\beta\text{-SYN}}$ cell, shown below in Figure 19A, responded with fewer Ca^{2+} microdomains in the region of artificial immune synapse. Statistical analysis (Figure 19B) confirmed that the number of Ca^{2+} microdomains formed at the region of artificial immune synapse were significantly reduced in *hn1l*$^{-/-}$ rat $T_{\beta\text{-SYN}}$ cells. Moreover, significantly decreased Ca^{2+} amplitude in microdomains could also be observed for *hn1l*$^{-/-}$ rat $T_{\beta\text{-SYN}}$ cells (right panel of Figure 19B). Collectively, these Ca^{2+} microdomains data strengthens the fact that HN1L connects T cell activation (and NAADP formation) and early Ca^{2+} microdomain formation.

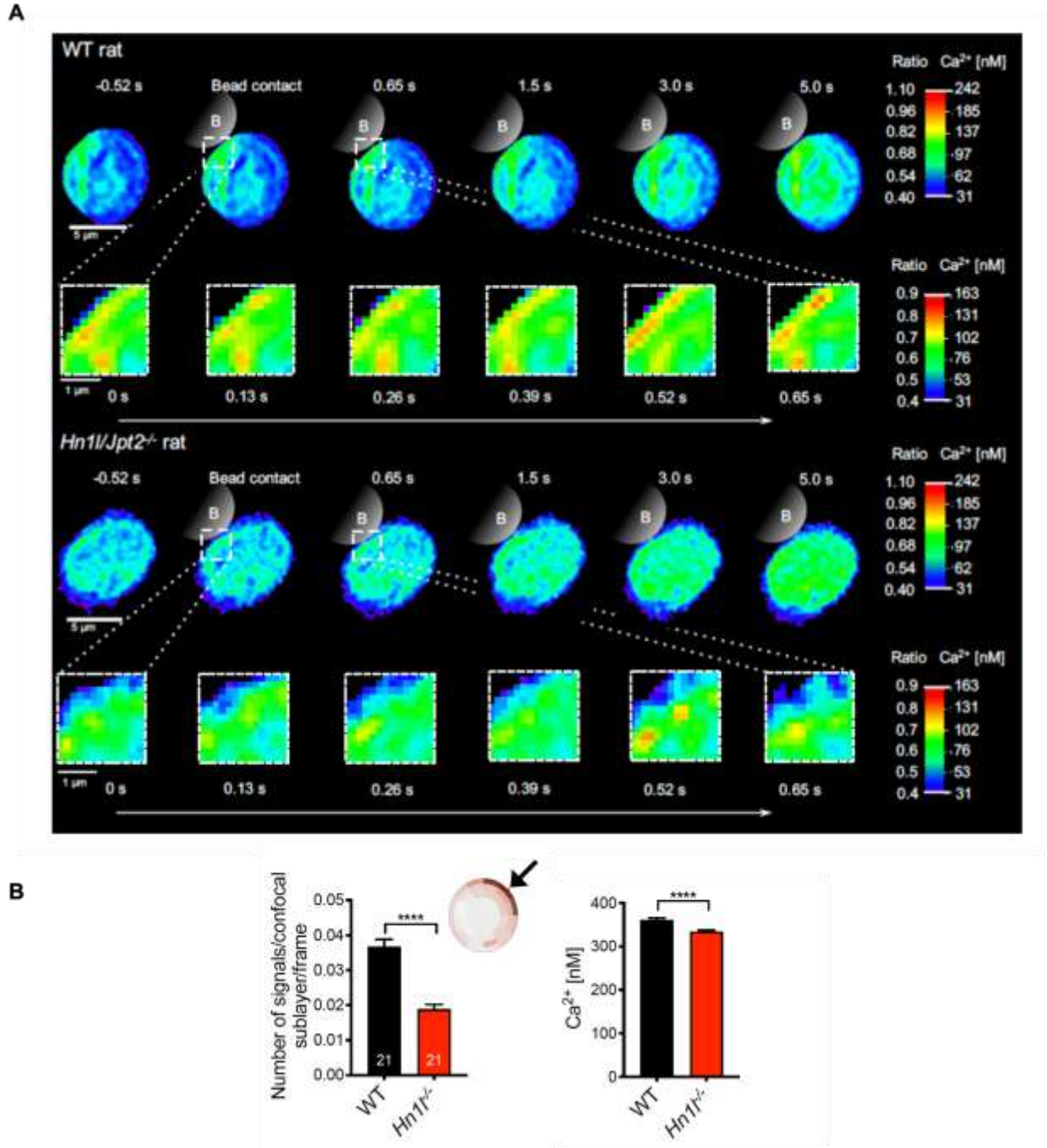

Figure 19: Deletion of HN1L in rat primary T cells diminishes initial Ca^{2+} microdomains evoked by TCR/CD3 stimulation: (A) Local Ca^{2+} microdomains of resting rat WT and *hn1l*$^{-/-}$ $T_{\beta\text{-SYN}}$ cells were analyzed by local Ca^{2+} imaging as mentioned in the methods. Representative cells from both WT and *hn1l*$^{-/-}$ $T_{\beta\text{-SYN}}$ cells are shown at full resolution along with the bead (marked as B; coated with rat anti-CD3 and anti-CD28 mAb) used to create artificial immune synapse. (B) The bar graphs indicate the comparison between the rat primary T cell types with respect to number of Ca^{2+} microdomains and average Ca^{2+} concentration of the microdomains over the first 15 seconds of stimulation. Data are presented as means ± SEM (WT, n = 21 cells; *hn1l*$^{-/-}$, n = 21 cells). Statistical analyses were performed by non-parametric unpaired two-tailed test (Mann-Whitney). Asterisks (*) refer to significant differences (****P < 0.0001). These data were prepared by Feng Gu, Franziska Möckl and Aileen Krüger (Institute for Biochemistry and Molecular Cell Biology, UKE, Hamburg, Germany) as internal collaborative research. This dataset was modified from figure 5 of Roggenkamp et al. (2021).

4.4 NAADP ANTAGONISM ACTS VIA HN1L

Furthermore, antagonist effect of BZ194 on global Ca^{2+} signaling in rat T cells was studied to compare it with the effect of *hn1l* gene knockout. As expected, BZ194 blocked the NAADP-evoked Ca^{2+} signaling in WT rat $T_{\beta\text{-SYN}}$ cells which was similar to the effect of *hn1l* gene knockout with respect to signal onset velocity, ΔCa^{2+} peak and ΔCa^{2+} plateau amplitudes (Figure 20). Moreover, no additional antagonist effect of BZ194 was observed when *hn1l*$^{-/-}$ rat $T_{\beta\text{-SYN}}$ cells were pre-incubated with BZ194 (Figure 20). With this data, we claim that NAADP antagonism by BZ194 acts via HN1L.

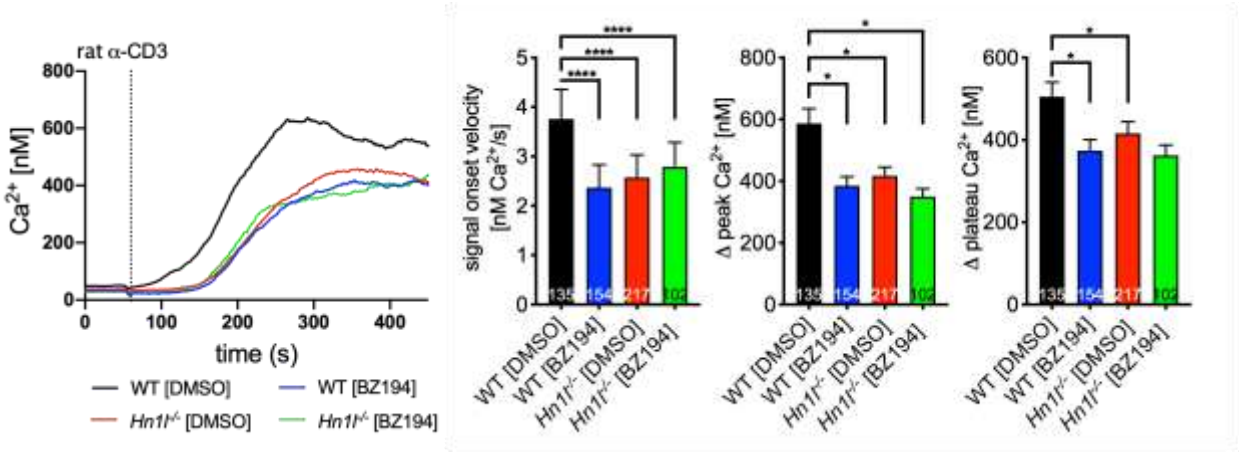

Figure 20: Antagonizing effect of BZ194 on TCR/CD3 evoked global Ca^{2+} signaling is similar to the effect of HN1L deletion in rat primary T cells: Global Ca^{2+} signals of resting rat WT and *hn1l*$^{-/-}$ $T_{\beta\text{-SYN}}$ cells, which were preincubated with 500 µM of BZ194 or DMSO (negative controls), were measured by global Ca^{2+} imaging as mentioned in the methods. Rat primary T cells were stimulated with 1 µg/mL of rat anti-CD3 mAb (554829, BD Pharmingen). The bar graphs indicate the comparison among the above-mentioned cell types with respect to signal onset velocity, ΔCa^{2+} peak and ΔCa^{2+} plateau. Data are presented as means ± SEM (WT [DMSO], n = 135 cells; WT [BZ194], n = 154 cells; *hn1l*$^{-/-}$ [DMSO], n = 217 cells; *hn1l*$^{-/-}$ [BZ194], n = 102 cells). Statistical analysis was performed by one-way ANOVA (Kruskal-Wallis test). Asterisks (*) refer to significant differences (*P < 0.05, ****P < 0.0001). This dataset was modified from figure 5 of Roggenkamp et al. (2021).

4.5 ASSOCIATION OF HN1L AND RYR1

According to our unifying hypothesis, NAADP initially binds to its cytosolic binding protein, which as a complex activates a cell type-specific or tissue-specific NAADP-sensitive Ca^{2+} channel (Guse, 2012). It was previously reported that RYR1 is the target channel of NAADP in T cell (Diercks et al., 2018). This section of thesis deals with the data providing evidence for association of HN1L and RYR1 in T cells.

4.5.1 Co-localization of HN1L and RYR1

Initially, super-resolution imaging was performed to study the localization of HN1L and RYR1 in Jurkat T cells. Figure 21 shows a representative Jurkat T cell in which RYR1 (in red) and HN1L (in green) were

stained with their respective antibodies. It is clear that HN1L can be detected as spots throughout the cytosol and also close to the PM. These spots close to PM were merged with RYR1 spots (shown in white), suggesting that a substantial percentage of RYR1 and HN1L colocalizes together close to PM (Figure 21). In addition, this data claims that HN1L has a role in ER-PM junction and is co-responsible for Ca^{2+} microdomain formation together with RYR1 after TCR/CD3 stimulation.

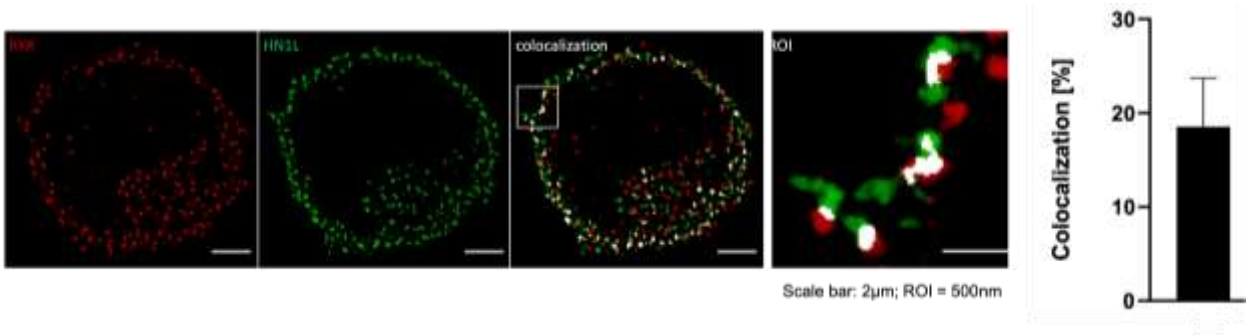

Figure 21: Co-localization of HN1L and RYR1 in Jurkat T cells: Jurkat T cells were fixed, stained and imaged by optical reassignement (SoRa) imaging. A representative Jurkat T cell with HN1L (stained green) and RYR (stained red) is shown. Colocalization of HN1L and RYR was assessed post deconvolution, waikato environment for knowledge analysis (Weka) segmentation and watershed segmentation; and was quantified by a Matlab script. Data are shown as means ± SD (n = 35 cells). Scale bars are set at 2µm and 500nm for the whole cell image and the region of interest (Viita et al.) image respectively. These data were prepared by Lola Hernandez (Institute for Biochemistry and Molecular Cell Biology, UKE, Hamburg, Germany) as internal collaborative research. This dataset was modified from figure 6 of Roggenkamp et al. (2021).

Further, Figure 22A shows that HN1L was translocated towards PM within 10 seconds upon TCR/CD3 stimulation. The translocation was quantified by calculating average distance of individual HN1L spots to PM at different time points. It is clear from right panel of Figure 22A that the stimulation-dependent translocation of HN1L sustained for 5 minutes. To support this data, co-immunoprecipitation of RYR1 and HN1L was performed using membrane fraction of Jurkat T cells. Figure 22B shows that there was a slight increase in co-precipitated HN1L with RYR1 within seconds after TCR/CD3 stimulation. Altogether, these data set claims that there is a strong association of RYR1 and HN1L at ER-PM junction, which is translated to Ca^{2+} microdomain formation after TCR/CD3 stimulation.

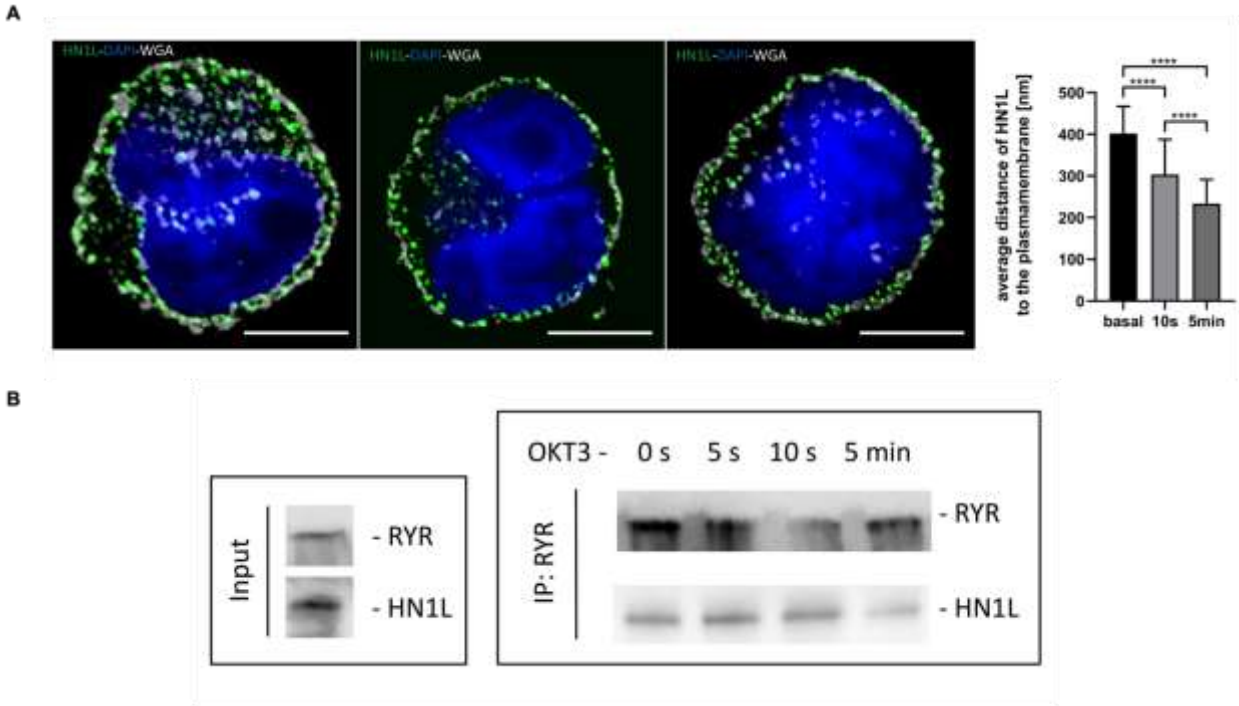

Figure 22: Translocation of HN1L towards PM-ER junction upon TCR/CD3 stimulation in Jurkat T cells: (A) Jurkat T cells, which were stimulated by 1 µg/mL of anti-CD3 mAb (OKT3), were imaged at three time points (0, 10 seconds and 5 minutes after stimulation) by super-resolution imaging. A representative Jurkat T cell with HN1L (stained green) is shown. Average distance of HN1L spots to the plasma membrane was calculated at three time points to assess the translocation of HN1L upon stimulation. Data are shown as means ± SD (basal, n = 36 cells; 10s, n = 36 cells; 5min, n = 49 cells). Statistical analysis was performed using an unpaired two-tailed *t* test. Scale bars are set at 2um. Asterisks (*) refer to significant differences (****P < 0.0001). (B) HN1L was co-immunoprecipitated with RYR (using anti-RYR antibody; GTX22868, GeneTex) from P10 membrane fraction of Jurkat T cells which were stimulated with anti-CD3 (OKT3) for four time durations as mentioned. Both HN1L and RYR were immunoblotted with anti-HN1L antibody (1:5000, ab200571, Abcam) and anti-RYR antibody (1:1000, H-300, Santa Cruz Biotechnology) respectively. A representative input control and a representative immunoblot are shown. Data are shown as means ± SEM (n = 4 independent experiments). Statistical analysis was performed by repeated-measures one-way ANOVA using Dunnett's multiple comparison test and no significant differences were found. These data were prepared by Lola Hernandez (Institute for Biochemistry and Molecular Cell Biology, UKE, Hamburg, Germany) as internal collaborative research. This dataset was modified from figure 6 of Roggenkamp et al. (2021).

4.5.2 HN1L and NAADP binds to bridging solenoid of RYR1

Next, structural studies were performed to look closely how NAADP and HN1L are associated with RYR1. Cryo-EM grids were set up with RYR1 purified from rabbit skeletal muscles, recombinantly expressed HN1L-01 and NAADP. Figure 23A shows the cryo-EM density map of RYR1 with HN1L-01 and NAADP. In the presence of HN1L-01 and NAADP, an extra density can be observed at the cytosolic C-terminal end of RYR1. The zoomed in panels in Figure 23A show the additional density in two orientations and the two domains, namely SPRY2 (domain 2 found in splA kinase and ryanodine receptors) and bridging solenoid (BSol), that interact with HN1L-01 and NAADP. The binding site of HN1L-01 and NAADP at RYR1 is unambiguous and interesting as they bind at interface of two above-mentioned domains. Figure 23B shows apo and holo states of C-terminal end of RYR1 with and without HN1L-01 and NAADP respectively. A clear conformational change in C-terminal end of BSol domain can be observed in the merged images of

apo and holo states indicating that RYR1 is activated by HN1L-01.

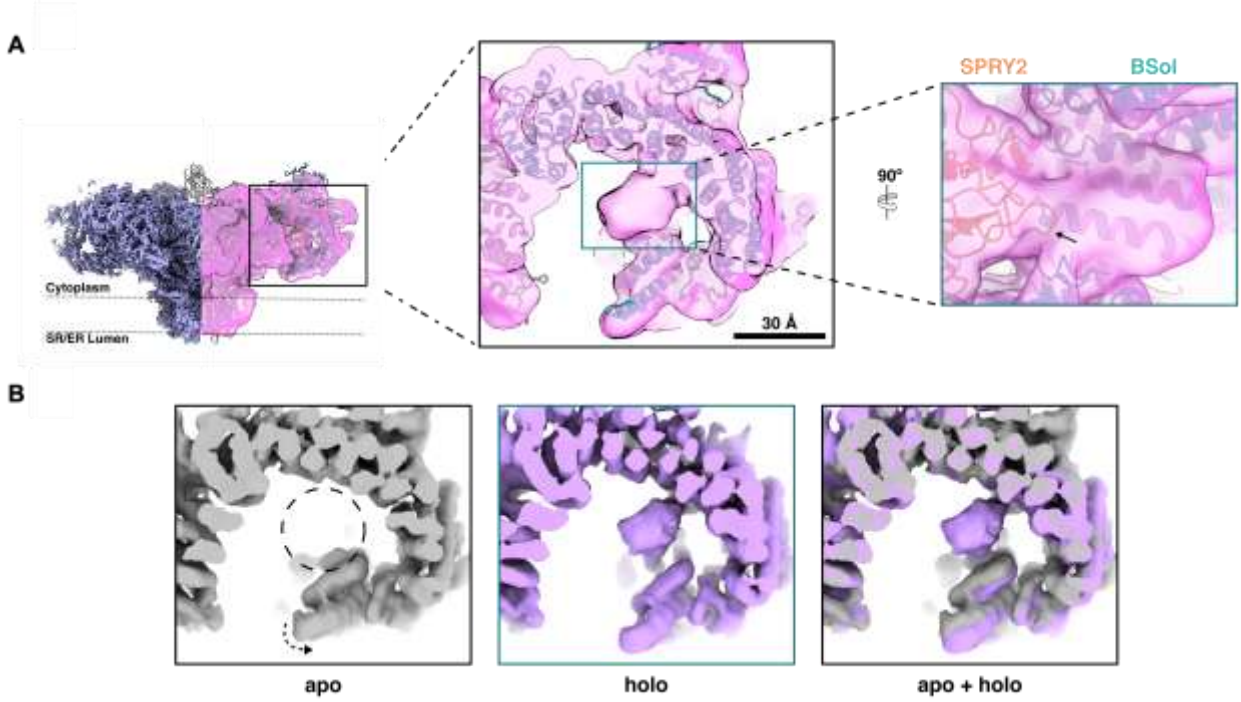

Figure 23: Cryo-EM density map of RYR1 in the absence and presence of HN1L and NAADP: (A) The density map of RYR1-recombinant HN1L-01-NAADP complex was either shown as sharpened (purple) or unsharpened (pink) image. The insets show HN1L-01 density in two orientations (middle and right images) and the domains of RYR1 (SPRY2 and BSol), which interacted with HN1L-01 and NAADP, are shown in ribbon representation (in orange and neon blue respectively). Scale bar is set at 30 Å for the middle image. (B) Comparison of the classes with and without HN1L and NAADP and the associated change in conformation of the C-terminal end of the BSol domain are shown. These data were provided by the group of Dr. Oliver Clarke (Department of Physiology and Cellular Biophysics, Columbia University College of Physicians & Surgeons, New York, USA) as external collaborative research.

4.5.3 Opening of RYR1 by HN1L/JPT2 and NAADP

The question, if the conformational change in BSol domain of RYR1 upon binding of HN1L and NAADP is enough for opening of the channel, was answered by performing functional lipid planar bilayer recordings with RYR1 and subsequent addition of NAADP and HN1L-01. 1 µM Ca^{2+} activated RYR1 in the lipid bilayer with an open probability (P_o) of 0.013 (Figure 24). P_o was significantly increased to 0.046 in the presence of 10 µM NAADP (Figure 24). Upon subsequent addition of 10 µM HN1L-01, the P_o of RYR1 drastically increased to 0.222 (Figure 24). Taken together, the structural (Figure 23) and functional data (Figure 24) claim that upon TCR/CD3 stimulation of T cells, HN1L and NAADP binds to RYR1 for Ca^{2+} release from ER within seconds. Such Ca^{2+} release is observed as Ca^{2+} microdomains in high resolution microscopy.

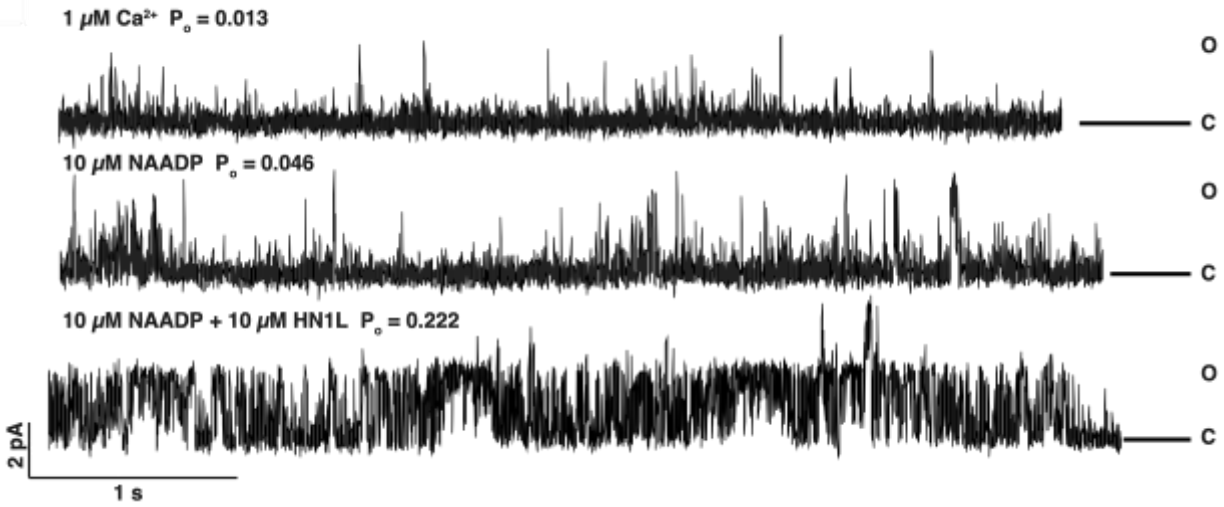

Figure 24: Bilayer recordings showing that HN1L increases the open probability of RYR1: The open probability of RYR1 was measured by planar bilayer recordings with 1 μM Ca^{2+}, 10 μM NAADP and 10 μM NAADP + 10 μM HN1L. A representative recording (n = 3 experiments) is shown. These data were provided by the group of Dr. Oliver Clarke (Department of Physiology and Cellular Biophysics, Columbia University College of Physicians & Surgeons, New York, USA) as external collaborative research.

5 DISCUSSION

Since the discovery of NAADP as a new member of second messenger family, it has been reported as the most potent endogenous Ca^{2+} mobilizing second messenger. Though NAADP was deeply studied in different cell types, its mechanism of action remained unclear, and its receptors were controversially discussed. Some groups proposed that NAADP elicit Ca^{2+} release from acidic stores via two-pore channels (TPCs) (Calcraft et al., 2009; Ruas et al., 2015), while other groups reported that NAADP activates ryanodine receptors (RYRs) to release Ca^{2+} from ER (Dammermann et al., 2009; Hohenegger et al., 2002). However, it was hypothesized that NAADP may not directly interact with the ion channels and may initially bind to a small cytosolic protein (NAADP binding protein) of size 22/23 kDa to activate the ion channels for Ca^{2+} release from ER or acidic stores (Guse, 2012; Lin-Moshier et al., 2012; Walseth et al., 2012). In Jurkat T cells, the 22/23 kDa protein was identified to be HN1L by mass spectrometric analysis. This thesis reports evidence to claim that (i) HN1L is a NAADP-BP in T cells, (ii) HN1L plays an important signaling role in NAADP mediated Ca^{2+} signaling and (iii) HN1L interacts with RYR1 for the formation of Ca^{2+} microdomains during activation of T cells.

hn1l and *hn1* were initially reported as evolutionary conserved genes involving in embryonic development (Zhou et al., 2004). *hn1l* is located on 16p13.3 with three splicing encoding three spliced variants with sizes 18.42, 20.06 and 23.07 kDa respectively (Zhou et al., 2004). Among these spliced variants, the last two (referred as HN1L-01 and HN1L-03 in this thesis) were widely expressed in almost all tissues except lung (Zhou et al., 2004). Later, *hn1l* was reported as a putative oncogene involving in small cell lung cancer (Li et al., 2017). Further, Li's group (2017) added that knockdown of *hn1l* mediated by short hairpin RNA caused cell cycle arrest, blocked adherent and nonadherent colony formation and inhibited tumor growth in nude mice proposing a key role of HN1L in the regulation of cell growth. It has been also reported that the number of breast cancer stem cells were decreased and tumor growth was inhibited in the absence of HN1L (Liu et al., 2018). Multiple functions of HN1L in the silkworm *Bombyx mori* have been reported such as cell cycle regulation and anti-apoptotic activity during viral infection (Lei et al., 2019). HN1L has a microtubule binding domain (referred as jupiter domain in this thesis) which interacts with tubulin-γ 1 (Hein et al., 2015) and other cytoskeletal proteins such as α-actin (Viita et al., 2019).

5.1 NAADP BINDS TO HN1L *IN VITRO*

Recombinant HN1L proteins with tags were produced in bacteria and were used to study their binding to NAADP using PAL. The tagged recombinant HN1L proteins were longer than native HN1L and showed stable oligomerization properties, especially the tagged recombinant HN1L-01 (Figure 10). PAL of

recombinant CD38 and its inactive mutant validated the system to use it to assess the binding between recombinant HN1L proteins and NAADP. PAL of tagged recombinant HN1L-01 and HN1-03 showed a strong labelling by the probes which were displaced by NAADP in micromolar (for monomers) or in nanomolar range (for oligomers), whereas NADP displaced the probes at micromolar concentrations for both monomers and oligomers suggesting that HN1L is a specific and high affinity NAADP binding protein (Figure 11). This is in line with data presented by Gunaratne and his group (2021), who also identified HN1L as NAADP binding protein in erythrocytes, reporting that the PAL probes labelling HN1L were displaced by NAADP at 100 nM. Displacement of probes in monomers by micromolar concentrations of NAADP could be due to missing or erroneous posttranslational modifications (Sahdev et al., 2008). Moreover, it has been reported that enzymatic activity of several recombinant proteins was compromised in the presence of His tag (Majorek et al., 2014; Panek et al., 2013; Araújo et al., 2000) suggesting that the presence of affinity tags in the recombinant HN1L proteins could also be a reason for poor displacement by NAADP.

Mierendorf et al., (1998) reported that pET expression system is likely the best system to express recombinant proteins in *E.coli* and hence, a pET M33 expression vector was used to express recombinant HN1L proteins. To further improve the quality of recombinant HN1L proteins, they were fused with GST, which acts as chaperone to avoid erroneous protein folding and improves the protein yield (Harper & Speicher, 2011). As discussed above, presence of tags could hinder the activity of the recombinant proteins and thus demanding removal of the tags after protein purification by introducing a protease cleavage site between tag and protein (Waugh, 2011). The tag-free recombinant HN1L proteins, produced using the improved expression system, showed better oligomerization for both isoforms and reduced degraded HN1L proteins (Figure 12). Moreover, the four deletion mutants of HN1L-03 (with a span of around 50 aminoacids deleted in each mutant) were also produced using this expression system. PAL or other sensitive binding assays with these deletion mutants would narrow down the binding site of NAADP to around 50 aminoacids in HN1L.

5.2 HN1L BRIDGES NAADP AND Ca^{2+} MICRODOMAIN FORMATION

The partial or complete deletion of HN1L in Jurkat T cells significantly affected the global Ca^{2+} signals formed upon activation of the cells (Figure 15). The signature of such impaired global Ca^{2+} signals were almost identical to that of global Ca^{2+} signals formed when NAADP signaling was blocked by BZ194 or when the NAADP forming enzyme (DUOX2) was deleted (Dammermann et al., 2009; Gu et al., 2021). Moreover, a complete recovery of signal onset velocity and partial recovery of Ca^{2+} peak amplitude of global Ca^{2+} signals were observed when *hn1l* was re-expressed in Jurkat T cells that were devoid of HN1L

(Figure 15C). Such partial recovery of global Ca^{2+} signals was likely due to the overexpression of *hn1l*. According to Prelich and colleagues (2012), such overexpression of a gene leads to a dominant-negative phenotype. Furthermore, *hn1l* knockout did not affect the IP_3-mediated Ca^{2+} release and store operated Ca^{2+} entry (Figure 16) demonstrating that HN1L functions as a signaling protein only in NAADP signaling cascade. As NAADP initiates the Ca^{2+} release by forming Ca^{2+} microdomains during the first 20 seconds post stimulation (Wolf et al., 2015), role of HN1L in Ca^{2+} microdomains formation was assessed. As expected, *hn1l* knockout reduced the number of Ca^{2+} microdomains observed within first seconds of T cell activation (Figure 17) proving that HN1L connects NAADP and initial Ca^{2+} microdomains in T cells.

As rats have several similarities to humans with regards to anatomy and physiology (Bryda, 2013), their T cells were utilized in this thesis to study the role of HN1L in NAADP mediated Ca^{2+} signaling. Similar to the data from Jurkat T cells, reduced expression of HN1L in rat primary T cells affects the global Ca^{2+} signaling with regards to signal onset velocity, Ca^{2+} peak and Ca^{2+} plateau (Figure 18C). The similar phenotype of *hn1l* knockout in a new and physiologically relevant system strengthens the findings that HN1L is indeed an important signaling protein involving in NAADP-medium global Ca^{2+} signaling. In both systems, the effects of *hn1l* knockout at later stages of global Ca^{2+} signaling were weaker and more divergent. This is likely due to the fact that IP_3-mediated Ca^{2+} release and store operated Ca^{2+} entry contribute to global Ca^{2+} signals in a few minutes of T cell activation (Guse et al., 1993). It was also clear from *hn1l* knockout study in Jurkat T cells that the global Ca^{2+} signals mediated by IP_3 and ORAI1 remained unaltered in the absence of HN1L (Figure 16). Further, similar to the *hn1l* knockout phenotype observed in Jurkat T cells, the reduced expression of HN1L in rat primary T cells caused a decrease in number of Ca^{2+} microdomains formed within first seconds of T cell activation (Figure 19). Additionally, the antagonist effect of BZ194 (Dammermann et al., 2009) in rat primary T cells was observed to be similar to *hn1l* knockout phenotype and no further antagonist effect was observed in *hn1l* knockout rat primary T cells (Figure 20). Similarly, Gu et al. reported that both BZ194 and deletion of DUOX2 (NAADP forming enzyme) caused almost similar phenotype in Ca^{2+} signaling explaining the comparable roles of HN1L and DUOX2 in NAADP mediated Ca^{2+} signaling. Together, the phenotypes observed in both cell systems claim that HN1L is actively involved in the initial phase of T cell activation forming Ca^{2+} microdomains and initial global Ca^{2+} signals. Gunaratne and his group (2021) reported a suppressed Ca^{2+} response to NAADP stimulation in HEK293 and USOS cell lines in the absence of HN1L which is in line with our findings mentioned above.

5.3 ASSOCIATION OF HN1L AND RYR1

Using super resolution imaging, it was shown that a substantial percentage of HN1L and RYR1 were colocalized close to the PM in non-stimulated Jurkat T cells (Figure 21). It was previously reported that ORAI1 and STIM1/STIM2 form complexes at ER-PM junctions for Ca^{2+} entry in non-stimulated T cells (Diercks et al., 2018). Upon stimulation, RYR1 at the ER-PM junction is activated by NAADP to evoke Ca^{2+} release from ER (Diercks et al., 2018). The colocalization data reveals that a fraction of cytosolic HN1L is membrane bound to RYR1 at ER-PM junction in T cells and upon stimulation, NAADP activates RYR1 via the membrane bound HN1L for the Ca^{2+} release from ER. Moreover, the co-immunoprecipitation data with RYR1 and HN1L showed that there was a time-dependent increase in HN1L immunoprecipitated with RYR1 upon stimulation (Figure 22B). This demonstrates that upon activation of T cells, NAADP binds to the cytosolic HN1L, which as a complex bind to RYR1 to evoke Ca^{2+} release. This finding was supported by the data showing that HN1L started to translocate towards PM within 10 seconds of stimulation (Figure 22A). Taken together, we state a new model that HN1L is localized in both cytosol (as a free protein) and at ER-PM junction (as membrane bound protein) in non-stimulated T cells. Upon stimulation, NAADP is formed by an enzyme called DUOX2 (Gu et al., 2021) and binds to both cytosolic and membrane bound HN1L followed by activation of RYR1 to release Ca^{2+} from ER (Figure 25).

The structure studies confirmed that HN1L and NAADP binds to RYR1 which was showed as an extra density in cryo-EM structure of RYR1 (Figure 23). It was found that HN1L and NAADP interacts with SPRY2 and bridging solenoid (BSol) domains of RYR1. SPRY2 domain of RYR1 is one of three SPRY domains found in the N-terminal 1/3 of each of its four subunits in a tetrameric RYR1 (Tae et al., 2011). This domain was reported to be important for excitation-contraction (EC) coupling by which Ca^{2+} is released from sarcoplasmic reticulum (SR) in skeletal muscle (Tae et al., 2011). BSol domain is the largest domain among the three major α-solenoid regions in RYR1 (Zalk et al., 2015) and it was reported that N-lobe of calmodulin binds to this domain for the activation of RYR1 (Woll et al., 2021). The specific sequences of SPRY2 and BSol domains that interact with NAADP/HN1L complex could not be resolved from the structure. Moreover, structure prediction by AlphaFold shows that HN1L is an intrinsically disordered protein (IDP) explaining the poor resolution of NAADP/HN1L complex on RYR1 (Jumper et al., 2021). However, it was clear that the NAADP/HN1L complex binds to the above-mentioned regions of RYR1, which are reported to be important for its activation and Ca^{2+} release events (Tae et al., 2011; Woll et al., 2021).

Furthermore, upon addition of 10 µM of NAADP and HN1L, the open probability of RYR1 drastically increased as compared to the addition of 1 µM Ca^{2+} (Figure 24). However, such high concentration of NAADP does not reflect the physiological condition in cytosol (Churamani et al., 2012; Gasser et al., 2006;

Schmid et al., 2012), and thus demanding further bilayer recordings with 10 – 100 nM NAADP. Moreover, Hohenegger et al. (2002) reported that NAADP increased the open probability of purified skeletal muscle RYR with an EC_{50} of ~ 30 nM. Though NAADP does not directly interact or activate RYR (Gerasimenko et al., 2003; Lin-Moshier et al., 2012; Walseth et al., 2012), Hohenegger et al. (2002) showed that NAADP alone activates the purified RYR by lipid planar bilayer recordings. This is likely due to the fact that HN1L might be pre-bound to the purified RYR in the preparation from skeletal muscles. The colocalization data between HN1L and RYR (Figure 21) strongly supports the above-mentioned argument. Furthermore, it was previously reported that RYR1 requires at least ~100nM Ca^{2+} to be in open state with lowest P_o (Zalk & Marks, 2017). At 100 µM Ca^{2+}, RYR1 is considered to be in a highly activated state with open probability greater than 0.85 (Po > 0.85) (Wei et al., 2016). Although NAADP/HN1L does not lead to the highly opened state of RYR1, it does open enough to activate the channel. All these solid data claims that HN1L is associated with RYR1 which acts as NAADP receptor in T cells.

However, a discrepancy between RYR1 and TPCs as the NAADP receptor still exists. Several groups have reported that NAADP interacts with RYR to evoke Ca^{2+} release from ER/SR in various cell types (Mojzisová et al., 2001; Hohenegger et al., 2002; Gerasimenko et al., 2003; Langhorst et al., 2004; Wolf et al., 2015; Diercks et al., 2018). On the other hand, TPCs have also been reported as NAADP-sensitive channels that are responsible for Ca^{2+} release from acidic stores (Brailoiu et al., 2009; Calcraft et al., 2009; Zong et al., 2009; Ruas et al., 2015). Further, Gunaratne and co-workers (2021) claim that HN1L interacts with TPC1, but not with TPC2, in erythrocytes for Ca^{2+} release from acidic Ca^{2+} stores. The unifying hypothesis for the mechanism of NAADP action, suggesting NAADP and its binding protein activates different Ca^{2+} channels in different cell types or tissues, explains the contrasting discovery of NAADP receptors discussed above (Guse, 2012; Guse & Diercks, 2018). The identification of HN1L as NAADP binding protein in different cell types by two independent groups indicates that HN1L is indeed an essential component of the NAADP signalosome. Moreover, participation of other NAADP-BPs in NAADP signalosome is also possible. Zhang and his group (2021) recently identified Sm-like protein 12 (LSM12) as an NAADP binding protein in HEK293 cell lines and reported that it interacts with TPC2 to evoke Ca^{2+} release from acidic stores. TPC1, TPC2 and NAADP were used as baits in affinity purification followed by a stable isotope labeling by amino acids in cell cultures (SILAC)-based quantitative proteomic approach to identify their mutually interacting proteins (Zhang et al., 2021). LSM12 stood out as a unique interacting protein shared by TPC1, TPC2 and NAADP (Zhang et al., 2021). They have also added that NAADP binds to LSM12 via its Lsm domain (Zhang et al., 2021). Further collaborative research with these groups is required to explain the identity of different NAADP binding proteins in different cell types.

6 CONCLUSION AND OUTLOOK

Our group previously identified HN1L as the 22/23 kDa protein, which showed displacement by NAADP in PAL (Lin-Moshier et al., 2012; Walseth et al., 2012), in T cells. In this thesis, recombinant HN1L proteins produced in bacteria were used to assess its binding to NAADP using PAL. The PAL data suggests that HN1L is a specific and high affinity NAADP binding protein and that NAADP binds at C-terminal end of HN1L. Functional studies in Jurkat T cells and rat primary T cells demonstrated that HN1L is an important signaling protein being essentially involved in the initial signaling phase of T cell activation. Further, this thesis proves that HN1L connects NAADP production and Ca^{2+} microdomain formation observed within first seconds of T cell activation. Lastly, the proof of association between HN1L and RYR1 (NAADP receptor) in T cells was shown using super resolution microscopy and cryo-EM structural study. Altogether, this thesis claims that HN1L is indeed a NAADP binding protein playing a signaling protein role in NAADP-mediated Ca^{2+} signalling by evoking Ca^{2+} release from ER via RYR1 (summarized in Figure 25).

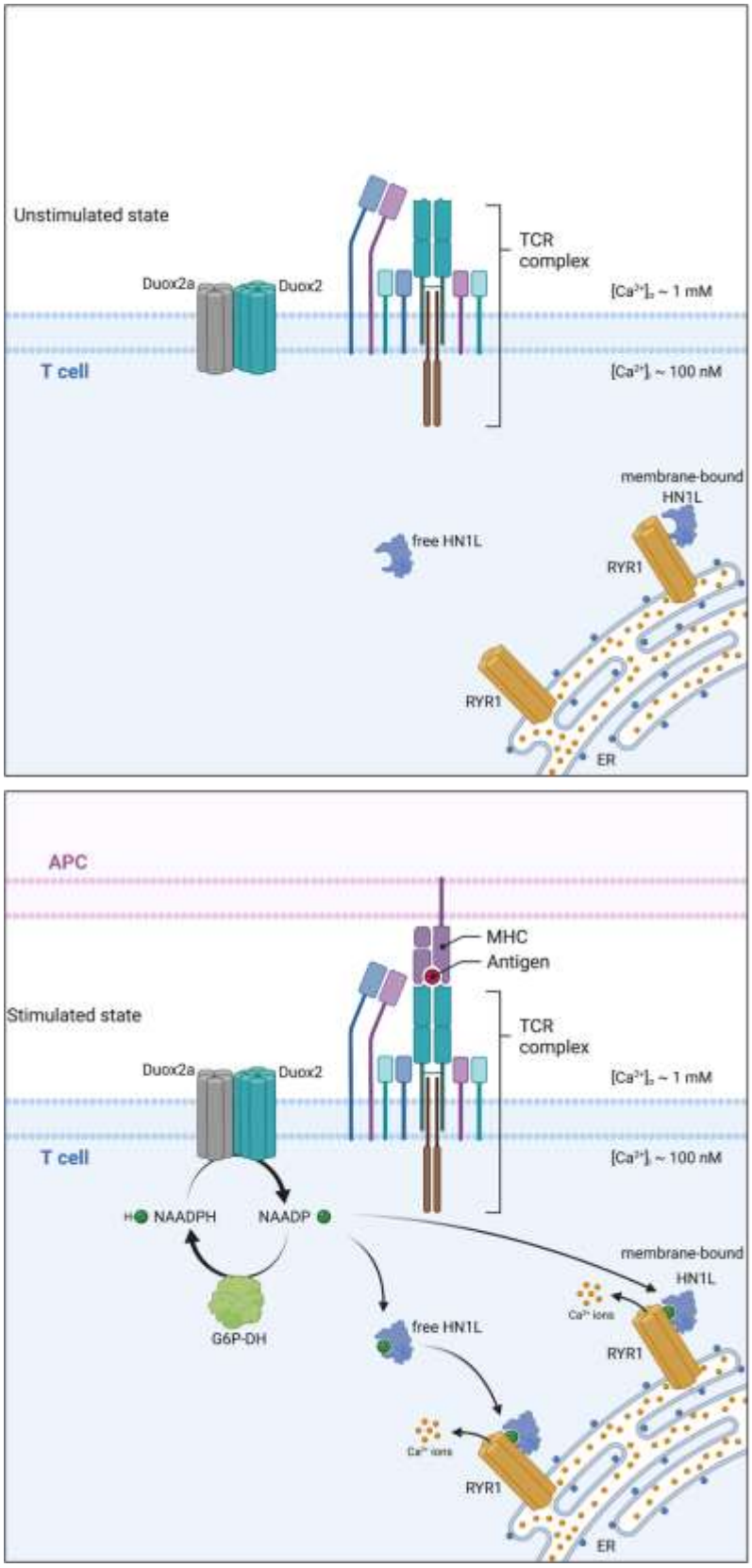

Figure 25: Proposed model to depict the mechanistic action of HN1L during activation of T cells: In unstimulated state (upper panel), HN1L is either present in cytosol as free protein or on ER membranes as membrane-bound protein (bound to RYR1). Upon stimulation (lower panel), DUOX2 forms NAADP in the cytosol, which then binds to both free HN1L and membrane-bound HN1L resulting in Ca^{2+} release from ER via RYR1.

All the data shown in this thesis represent only the tip of an iceberg and lot more research must be performed to provide concrete data to clearly understand spatiotemporal aspects of Ca^{2+} signaling in T cells.

6.1 DETERMINATION OF NAADP BINDING SITE

The deletion mutants of HN1L (Figure 13) must be subjected to PAL to narrow down the binding site of NAADP followed by precise determination of the binding site of NAADP in HN1L. As the recombinant proteins expressed in mammalian expression system includes all the post translational modifications needed for a eukaryotic protein (McKenzie & Abbott, 2018), PAL must be validated and performed with the same. Moreover, a non-radioactive and more sensitive alternative to PAL, e.g. size exclusion HPLC using 5-N_3-ε-NAADP as probe, would open several approaches to closely study its binding to NAADP and other prospective binding partners such as LSM12.

Ponsioen et al. (2004) developed Epac (Exchange protein directly activated by cAMP)-based FRET sensors using a part of cAMP-binding Rap-1 activating protein (Epac) sandwiched between donor and acceptor fluorescent proteins to detect the levels of cyclic adenosine monophosphate (cAMP). Likewise, upon finding the specific binding site of NAADP in HN1L, a FRET sensor could be made with HN1L to measure the concentrations of NAADP in different cell types in real time. Such FRET sensor would be beneficial to explore further in NAADP biology.

Further, an improved construction of cryo-EM grids with RYR1, NAADP and recombinant HN1L produced in mammalian expression system would help us to resolve the structure of extra density observed in RYR1 and determine the binding site of NAADP/HN1L in RYR1. As NAADP/HN1L binds adjacent to the binding site of calmodulin in RYR1, further research to study the connection between HN1L and calmodulin would be interesting.

6.2 CONNECTION BETWEEN HN1L AND LSM12

As LSM12 was also identified as a NAADP-BP (Zhang et al., 2021), it would be interesting to study its role in T cells and compare the effects of *lsm12* and *hn1l* knockouts in Ca^{2+} signaling. The kinetics of NAADP binding to HN1L and LSM12 must be determined to compare the binding affinities of each to NAADP. Fusion of different fluorescent proteins to HN1L and LSM12 would help us to localize the

proteins in a cell and to compare the translocation of HN1L and LSM12 during the initial phase of T cell activation. Such experiments would reveal if HN1L and LSM12 co-participate in NAADP mediated Ca^{2+} signaling. Finally, collaborative research with the groups of Gunaratne and Zhang would be really interesting to share our ideas and research converging different NAADP signaling pathways to envision a unifying NAADP signalosome.

7 BIBLIOGRAPHY

Aarhus, R., Graeff, R. M., Dickey, D. M., Walseth, T. F., & Lee, H. C. (1995). ADP-ribosyl cyclase and CD38 catalyze the synthesis of a calcium-mobilizing metabolite from NADP. *J Biol Chem*, *270*(51), 30327-30333. https://doi.org/10.1074/jbc.270.51.30327

Araújo, A. P., Oliva, G., Henrique-Silva, F., Garratt, R. C., Cáceres, O., & Beltramini, L. M. (2000). Influence of the histidine tail on the structure and activity of recombinant chlorocatechol 1,2-dioxygenase. *Biochem Biophys Res Commun*, *272*(2), 480-484. https://doi.org/10.1006/bbrc.2000.2802

Berridge, M. J., Lipp, P., & Bootman, M. D. (2000). The versatility and universality of calcium signalling. *Nat Rev Mol Cell Biol*, *1*(1), 11-21. https://doi.org/10.1038/35036035

Bezprozvanny, I., Watras, J., & Ehrlich, B. E. (1991). Bell-shaped calcium-response curves of Ins(1,4,5)P3- and calcium-gated channels from endoplasmic reticulum of cerebellum. *Nature*, *351*(6329), 751-754. https://doi.org/10.1038/351751a0

Brailoiu, E., Churamani, D., Cai, X., Schrlau, M. G., Brailoiu, G. C., Gao, X., Hooper, R., Boulware, M. J., Dun, N. J., Marchant, J. S., & Patel, S. (2009). Essential requirement for two-pore channel 1 in NAADP-mediated calcium signaling. *J Cell Biol*, *186*(2), 201-209. https://doi.org/10.1083/jcb.200904073

Bryda, E. C. (2013). The Mighty Mouse: the impact of rodents on advances in biomedical research. *Mo Med*, *110*(3), 207-211.

Calcraft, P. J., Ruas, M., Pan, Z., Cheng, X., Arredouani, A., Hao, X., Tang, J., Rietdorf, K., Teboul, L., Chuang, K. T., Lin, P., Xiao, R., Wang, C., Zhu, Y., Lin, Y., Wyatt, C. N., Parrington, J., Ma, J., Evans, A. M., . . . Zhu, M. X. (2009). NAADP mobilizes calcium from acidic organelles through two-pore channels. *Nature*, *459*(7246), 596-600. https://doi.org/10.1038/nature08030

Cang, C., Zhou, Y., Navarro, B., Seo, Y. J., Aranda, K., Shi, L., Battaglia-Hsu, S., Nissim, I., Clapham, D. E., & Ren, D. (2013). mTOR regulates lysosomal ATP-sensitive two-pore Na(+) channels to adapt to metabolic state. *Cell*, *152*(4), 778-790. https://doi.org/10.1016/j.cell.2013.01.023

Carafoli, E. (1991). Calcium pump of the plasma membrane. *Physiol Rev*, *71*(1), 129-153. https://doi.org/10.1152/physrev.1991.71.1.129

Chini, E. N., Beers, K. W., & Dousa, T. P. (1995). Nicotinate adenine dinucleotide phosphate (NAADP) triggers a specific calcium release system in sea urchin eggs. *J Biol Chem*, *270*(7), 3216-3223. https://doi.org/10.1074/jbc.270.7.3216

Churamani, D., Hooper, R., Brailoiu, E., & Patel, S. (2012). Domain assembly of NAADP-gated two-pore channels. *Biochem J*, *441*(1), 317-323. https://doi.org/10.1042/bj20111617

Churchill, G. C., Okada, Y., Thomas, J. M., Genazzani, A. A., Patel, S., & Galione, A. (2002). NAADP mobilizes Ca(2+) from reserve granules, lysosome-related organelles, in sea urchin eggs. *Cell*, *111*(5), 703-708. https://doi.org/10.1016/s0092-8674(02)01082-6

Clapham, D. E. (2007). Calcium signaling. *Cell*, *131*(6), 1047-1058. https://doi.org/10.1016/j.cell.2007.11.028

Clapper, D. L., Walseth, T. F., Dargie, P. J., & Lee, H. C. (1987). Pyridine nucleotide metabolites stimulate calcium release from sea urchin egg microsomes desensitized to inositol trisphosphate. *J Biol Chem*, *262*(20), 9561-9568.

Dammermann, W., & Guse, A. H. (2005). Functional ryanodine receptor expression is required for NAADP-mediated local Ca2+ signaling in T-lymphocytes. *J Biol Chem*, *280*(22), 21394-21399. https://doi.org/10.1074/jbc.M413085200

Dammermann, W., Zhang, B., Nebel, M., Cordiglieri, C., Odoardi, F., Kirchberger, T., Kawakami, N., Dowden, J., Schmid, F., Dornmair, K., Hohenegger, M., Flügel, A., Guse, A. H., & Potter, B. V. (2009). NAADP-mediated Ca2+ signaling via type 1 ryanodine receptor in T cells revealed by a synthetic NAADP antagonist. *Proc Natl Acad Sci U S A*, *106*(26), 10678-10683. https://doi.org/10.1073/pnas.0809997106

Diercks, B. P., Werner, R., Weidemüller, P., Czarniak, F., Hernandez, L., Lehmann, C., Rosche, A., Krüger, A., Kaufmann, U., Vaeth, M., Failla, A. V., Zobiak, B., Kandil, F. I., Schetelig, D., Ruthenbeck, A., Meier, C., Lodygin, D., Flügel, A., Ren, D., . . . Guse, A. H. (2018). ORAI1, STIM1/2, and RYR1 shape subsecond Ca(2+) microdomains upon T cell activation. *Sci Signal*, *11*(561). https://doi.org/10.1126/scisignal.aat0358

Dubochet, J., Adrian, M., Chang, J. J., Homo, J. C., Lepault, J., McDowall, A. W., & Schultz, P. (1988). Cryo-electron microscopy of vitrified specimens. *Q Rev Biophys*, *21*(2), 129-228. https://doi.org/10.1017/s0033583500004297

Ernst, I. M., Fliegert, R., & Guse, A. H. (2013). Adenine Dinucleotide Second Messengers and T-lymphocyte Calcium Signaling. *Front Immunol*, *4*, 259. https://doi.org/10.3389/fimmu.2013.00259

Feske, S. (2007). Calcium signalling in lymphocyte activation and disease. *Nat Rev Immunol*, *7*(9), 690-702. https://doi.org/10.1038/nri2152

Flügel, A., Willem, M., Berkowicz, T., & Wekerle, H. (1999). Gene transfer into CD4+ T lymphocytes: green fluorescent protein-engineered, encephalitogenic T cells illuminate brain autoimmune responses. *Nat Med*, *5*(7), 843-847. https://doi.org/10.1038/10567

Foskett, J. K., White, C., Cheung, K. H., & Mak, D. O. (2007). Inositol trisphosphate receptor Ca2+ release channels. *Physiol Rev*, *87*(2), 593-658. https://doi.org/10.1152/physrev.00035.2006

Galione, A., & Churchill, G. C. (2002). Interactions between calcium release pathways: multiple messengers and multiple stores. *Cell Calcium*, *32*(5-6), 343-354. https://doi.org/10.1016/s0143416002001902

Galione, A., Lee, H. C., & Busa, W. B. (1991). Ca(2+)-induced Ca2+ release in sea urchin egg homogenates: modulation by cyclic ADP-ribose. *Science*, *253*(5024), 1143-1146. https://doi.org/10.1126/science.1909457

Gasser, A., Bruhn, S., & Guse, A. H. (2006). Second messenger function of nicotinic acid adenine dinucleotide phosphate revealed by an improved enzymatic cycling assay. *J Biol Chem*, *281*(25), 16906-16913. https://doi.org/10.1074/jbc.M601347200

Gerasimenko, J. V., Maruyama, Y., Yano, K., Dolman, N. J., Tepikin, A. V., Petersen, O. H., & Gerasimenko, O. V. (2003). NAADP mobilizes Ca2+ from a thapsigargin-sensitive store in the nuclear envelope by activating ryanodine receptors. *J Cell Biol*, *163*(2), 271-282. https://doi.org/10.1083/jcb.200306134

Gerasimenko, J. V., Sherwood, M., Tepikin, A. V., Petersen, O. H., & Gerasimenko, O. V. (2006). NAADP, cADPR and IP3 all release Ca2+ from the endoplasmic reticulum and an acidic store in the secretory granule area. *J Cell Sci*, *119*(Pt 2), 226-238. https://doi.org/10.1242/jcs.02721

Gilabert, J. A. (2012). Cytoplasmic calcium buffering. *Adv Exp Med Biol*, *740*, 483-498. https://doi.org/10.1007/978-94-007-2888-2_20

Gu, F., Krüger, A., Roggenkamp, H. G., Alpers, R., Lodygin, D., Jaquet, V., Möckl, F., Hernandez, C. L., Winterberg, K., Bauche, A., Rosche, A., Grasberger, H., Kao, J. Y., Schetelig, D., Werner, R., Schröder, K., Carty, M., Bowie, A. G., Huber, S., . . . Guse, A. H. (2021). Dual NADPH oxidases DUOX1 and DUOX2 synthesize NAADP and are necessary for Ca(2+) signaling during T cell activation. *Sci Signal*, *14*(709), eabe3800. https://doi.org/10.1126/scisignal.abe3800

Gunaratne, G. S., Brailoiu, E., He, S., Unterwald, E. M., Patel, S., Slama, J. T., Walseth, T. F., & Marchant, J. S. (2021). Essential requirement for JPT2 in NAADP-evoked Ca(2+) signaling. *Sci Signal*, *14*(675). https://doi.org/10.1126/scisignal.abd5605

Guse, A. H. (2012). Linking NAADP to ion channel activity: a unifying hypothesis. *Sci Signal*, *5*(221), pe18. https://doi.org/10.1126/scisignal.2002890

Guse, A. H., da Silva, C. P., Berg, I., Skapenko, A. L., Weber, K., Heyer, P., Hohenegger, M., Ashamu, G. A., Schulze-Koops, H., Potter, B. V., & Mayr, G. W. (1999). Regulation of calcium signalling in T lymphocytes by the second messenger cyclic ADP-ribose. *Nature*, *398*(6722), 70-73. https://doi.org/10.1038/18024

Guse, A. H., & Diercks, B. P. (2018). Integration of nicotinic acid adenine dinucleotide phosphate (NAADP)-dependent calcium signalling. *J Physiol*, *596*(14), 2735-2743. https://doi.org/10.1113/jp275974

Guse, A. H., Ernst, I. M., & Fliegert, R. (2013). NAADP signaling revisited. *Curr Top Med Chem*, *13*(23), 2978-2990. https://doi.org/10.2174/15680266113136660212

Guse, A. H., Roth, E., & Emmrich, F. (1993). Intracellular Ca2+ pools in Jurkat T-lymphocytes. *Biochem J*, *291 (Pt 2)*(Pt 2), 447-451. https://doi.org/10.1042/bj2910447

Harper, S., & Speicher, D. W. (2011). Purification of proteins fused to glutathione S-transferase. *Methods Mol Biol*, *681*, 259-280. https://doi.org/10.1007/978-1-60761-913-0_14

Hein, M. Y., Hubner, N. C., Poser, I., Cox, J., Nagaraj, N., Toyoda, Y., Gak, I. A., Weisswange, I., Mansfeld, J., Buchholz, F., Hyman, A. A., & Mann, M. (2015). A human interactome in three quantitative dimensions organized by stoichiometries and abundances. *Cell*, *163*(3), 712-723. https://doi.org/10.1016/j.cell.2015.09.053

Hohenegger, M., Suko, J., Gscheidlinger, R., Drobny, H., & Zidar, A. (2002). Nicotinic acid-adenine dinucleotide phosphate activates the skeletal muscle ryanodine receptor. *Biochem J*, *367*(Pt 2), 423-431. https://doi.org/10.1042/bj20020584

Hosoi, E., Nishizaki, C., Gallagher, K. L., Wyre, H. W., Matsuo, Y., & Sei, Y. (2001). Expression of the Ryanodine Receptor Isoforms in Immune Cells. *The Journal of Immunology*, *167*(9), 4887-4894. https://doi.org/10.4049/jimmunol.167.9.4887

Howard, M., Grimaldi, J. C., Bazan, J. F., Lund, F. E., Santos-Argumedo, L., Parkhouse, R. M., Walseth, T. F., & Lee, H. C. (1993). Formation and hydrolysis of cyclic ADP-ribose catalyzed by lymphocyte antigen CD38. *Science*, *262*(5136), 1056-1059. https://doi.org/10.1126/science.8235624

Iwai, M., Michikawa, T., Bosanac, I., Ikura, M., & Mikoshiba, K. (2007). Molecular basis of the isoform-specific ligand-binding affinity of inositol 1,4,5-trisphosphate receptors. *J Biol Chem*, *282*(17), 12755-12764. https://doi.org/10.1074/jbc.M609833200

Jumper, J., Evans, R., Pritzel, A., Green, T., Figurnov, M., Ronneberger, O., Tunyasuvunakool, K., Bates, R., Žídek, A., Potapenko, A., Bridgland, A., Meyer, C., Kohl, S. A. A., Ballard, A. J., Cowie, A., Romera-Paredes, B., Nikolov, S., Jain, R., Adler, J., . . . Hassabis, D. (2021). Highly accurate protein structure prediction with AlphaFold. *Nature*, *596*(7873), 583-589. https://doi.org/10.1038/s41586-021-03819-2

Kunerth, S., Mayr, G. W., Koch-Nolte, F., & Guse, A. H. (2003). Analysis of subcellular calcium signals in T-lymphocytes. *Cell Signal*, *15*(8), 783-792. https://doi.org/10.1016/s0898-6568(03)00015-9

Langhorst, M. F., Schwarzmann, N., & Guse, A. H. (2004). Ca2+ release via ryanodine receptors and Ca2+ entry: major mechanisms in NAADP-mediated Ca2+ signaling in T-lymphocytes. *Cell Signal*, *16*(11), 1283-1289. https://doi.org/10.1016/j.cellsig.2004.03.013

Ledbetter, M. W., Preiner, J. K., Louis, C. F., & Mickelson, J. R. (1994). Tissue distribution of ryanodine receptor isoforms and alleles determined by reverse transcription polymerase chain reaction. *J Biol Chem*, *269*(50), 31544-31551.

Lee, H. B., Xu, L., & Meissner, G. (1994). Reconstitution of the skeletal muscle ryanodine receptor-Ca2+ release channel protein complex into proteoliposomes. *J Biol Chem*, *269*(18), 13305-13312.

Lee, H. C. (2005). Nicotinic acid adenine dinucleotide phosphate (NAADP)-mediated calcium signaling. *J Biol Chem*, *280*(40), 33693-33696. https://doi.org/10.1074/jbc.R500012200

Lee, H. C., & Aarhus, R. (1991). ADP-ribosyl cyclase: an enzyme that cyclizes NAD+ into a calcium-mobilizing metabolite. *Cell Regul*, *2*(3), 203-209. https://doi.org/10.1091/mbc.2.3.203

Lee, H. C., & Aarhus, R. (1995). A derivative of NADP mobilizes calcium stores insensitive to inositol trisphosphate and cyclic ADP-ribose. *J Biol Chem*, *270*(5), 2152-2157. https://doi.org/10.1074/jbc.270.5.2152

Lei, J., Hu, D., Xue, S., Mao, F., Obeng, E., Quan, Y., & Yu, W. (2019). HN1L is essential for cell growth and survival during nucleopolyhedrovirus infection in silkworm, Bombyx mori. *PLoS One*, *14*(5), e0216719. https://doi.org/10.1371/journal.pone.0216719

Lewis, A. M., Aley, P. K., Roomi, A., Thomas, J. M., Masgrau, R., Garnham, C., Shipman, K., Paramore, C., Bloor-Young, D., Sanders, L. E., Terrar, D. A., Galione, A., & Churchill, G. C. (2012). β-Adrenergic receptor signaling increases NAADP and cADPR levels in the heart. *Biochem Biophys Res Commun*, *427*(2), 326-329. https://doi.org/10.1016/j.bbrc.2012.09.054

Li, L., Zeng, T. T., Zhang, B. Z., Li, Y., Zhu, Y. H., & Guan, X. Y. (2017). Overexpression of HN1L promotes cell malignant proliferation in non-small cell lung cancer. *Cancer Biol Ther*, *18*(11), 904-915. https://doi.org/10.1080/15384047.2017.1385678

Lin-Moshier, Y., Walseth, T. F., Churamani, D., Davidson, S. M., Slama, J. T., Hooper, R., Brailoiu, E., Patel, S., & Marchant, J. S. (2012). Photoaffinity labeling of nicotinic acid adenine dinucleotide phosphate (NAADP) targets in mammalian cells. *J Biol Chem*, *287*(4), 2296-2307. https://doi.org/10.1074/jbc.M111.305813

Liu, Y., Choi, D. S., Sheng, J., Ensor, J. E., Liang, D. H., Rodriguez-Aguayo, C., Polley, A., Benz, S., Elemento, O., Verma, A., Cong, Y., Wong, H., Qian, W., Li, Z., Granados-Principal, S., Lopez-Berestein, G., Landis, M. D., Rosato, R. R., Dave, B., . . . Chang, J. C. (2018). HN1L Promotes Triple-Negative Breast Cancer Stem Cells through LEPR-STAT3 Pathway. *Stem Cell Reports*, *10*(1), 212-227. https://doi.org/10.1016/j.stemcr.2017.11.010

Majorek, K. A., Kuhn, M. L., Chruszcz, M., Anderson, W. F., & Minor, W. (2014). Double trouble-Buffer selection and His-tag presence may be responsible for nonreproducibility of biomedical experiments. *Protein Sci*, *23*(10), 1359-1368. https://doi.org/10.1002/pro.2520

Masgrau, R., Churchill, G. C., Morgan, A. J., Ashcroft, S. J., & Galione, A. (2003). NAADP: a new second messenger for glucose-induced Ca2+ responses in clonal pancreatic beta cells. *Curr Biol*, *13*(3), 247-251. https://doi.org/10.1016/s0960-9822(03)00041-1

McKenzie, E. A., & Abbott, W. M. (2018). Expression of recombinant proteins in insect and mammalian cells. *Methods*, *147*, 40-49. https://doi.org/10.1016/j.ymeth.2018.05.013

Mierendorf, R. C., Morris, B. B., Hammer, B., & Novy, R. E. (1998). Expression and Purification of Recombinant Proteins Using the pET System. *Methods Mol Med*, *13*, 257-292. https://doi.org/10.1385/0-89603-485-2:257

Mojzisová, A., Krizanová, O., Záciková, L., Komínková, V., & Ondrias, K. (2001). Effect of nicotinic acid adenine dinucleotide phosphate on ryanodine calcium release channel in heart. *Pflugers Arch*, *441*(5), 674-677. https://doi.org/10.1007/s004240000465

Nagaleekar, V. K., Diehl, S. A., Juncadella, I., Charland, C., Muthusamy, N., Eaton, S., Haynes, L., Garrett-Sinha, L. A., Anguita, J., & Rincón, M. (2008). IP3 receptor-mediated Ca2+ release in naive CD4 T cells dictates their cytokine program. *J Immunol*, *181*(12), 8315-8322. https://doi.org/10.4049/jimmunol.181.12.8315

Nauth, T., Huschka, F., Schweizer, M., Bosse, J. B., Diepold, A., Failla, A. V., Steffen, A., Stradal, T. E. B., Wolters, M., & Aepfelbacher, M. (2018). Visualization of translocons in Yersinia type III protein secretion machines during host cell infection. *PLoS Pathog*, *14*(12), e1007527. https://doi.org/10.1371/journal.ppat.1007527

O'Connell, P. J., Klyachko, V. A., & Ahern, G. P. (2002). Identification of functional type 1 ryanodine receptors in mouse dendritic cells. *FEBS Lett*, *512*(1-3), 67-70. https://doi.org/10.1016/s0014-5793(01)03321-x

Ogunbayo, O. A., Zhu, Y., Rossi, D., Sorrentino, V., Ma, J., Zhu, M. X., & Evans, A. M. (2011). Cyclic adenosine diphosphate ribose activates ryanodine receptors, whereas NAADP activates two-pore domain channels. *J Biol Chem*, *286*(11), 9136-9140. https://doi.org/10.1074/jbc.M110.202002

Panek, A., Pietrow, O., Filipkowski, P., & Synowiecki, J. (2013). Effects of the polyhistidine tag on kinetics and other properties of trehalose synthase from Deinococcus geothermalis. *Acta Biochim Pol*, *60*(2), 163-166.

Pitt, S. J., Lam, A. K., Rietdorf, K., Galione, A., & Sitsapesan, R. (2014). Reconstituted human TPC1 is a proton-permeable ion channel and is activated by NAADP or Ca2+. *Sci Signal*, *7*(326), ra46. https://doi.org/10.1126/scisignal.2004854

Ponsioen, B., Zhao, J., Riedl, J., Zwartkruis, F., van der Krogt, G., Zaccolo, M., Moolenaar, W. H., Bos, J. L., & Jalink, K. (2004). Detecting cAMP-induced Epac activation by fluorescence resonance energy transfer: Epac as a novel cAMP indicator. *EMBO Rep*, *5*(12), 1176-1180. https://doi.org/10.1038/sj.embor.7400290

Prelich, G. (2012). Gene overexpression: uses, mechanisms, and interpretation. *Genetics*, *190*(3), 841-854. https://doi.org/10.1534/genetics.111.136911

Rietdorf, K., Funnell, T. M., Ruas, M., Heinemann, J., Parrington, J., & Galione, A. (2011). Two-pore channels form homo- and heterodimers. *J Biol Chem*, *286*(43), 37058-37062. https://doi.org/10.1074/jbc.C111.289835

Roggenkamp, H. G., Khansahib, I., Hernandez, C. L., Zhang, Y., Lodygin, D., Krüger, A., Gu, F., Möckl, F., Löhndorf, A., Wolters, V., Woike, D., Rosche, A., Bauche, A., Schetelig, D., Werner, R., Schlüter, H., Failla, A. V., Meier, C., Fliegert, R., . . . Guse, A. H. (2021). HN1L/JPT2: A signaling protein that connects NAADP generation to Ca(2+) microdomain formation. *Sci Signal*, *14*(675). https://doi.org/10.1126/scisignal.abd5647

Rossi, D., & Sorrentino, V. (2002). Molecular genetics of ryanodine receptors Ca2+-release channels. *Cell Calcium*, *32*(5-6), 307-319. https://doi.org/10.1016/s0143416002001987

Ruas, M., Davis, L. C., Chen, C. C., Morgan, A. J., Chuang, K. T., Walseth, T. F., Grimm, C., Garnham, C., Powell, T., Platt, N., Platt, F. M., Biel, M., Wahl-Schott, C., Parrington, J., & Galione, A. (2015). Expression of Ca^{2+}-permeable two-pore channels rescues NAADP signalling in TPC-deficient cells. *Embo j*, *34*(13), 1743-1758. https://doi.org/10.15252/embj.201490009

Sahdev, S., Khattar, S. K., & Saini, K. S. (2008). Production of active eukaryotic proteins through bacterial expression systems: a review of the existing biotechnology strategies. *Mol Cell Biochem*, *307*(1-2), 249-264. https://doi.org/10.1007/s11010-007-9603-6

Schmid, F., Fliegert, R., Westphal, T., Bauche, A., & Guse, A. H. (2012). Nicotinic acid adenine dinucleotide phosphate (NAADP) degradation by alkaline phosphatase. *J Biol Chem*, *287*(39), 32525-32534. https://doi.org/10.1074/jbc.M112.362715

Schwarzmann, N., Kunerth, S., Weber, K., Mayr, G. W., & Guse, A. H. (2002). Knock-down of the type 3 ryanodine receptor impairs sustained Ca2+ signaling via the T cell receptor/CD3 complex. *J Biol Chem*, *277*(52), 50636-50642. https://doi.org/10.1074/jbc.M209061200

Sei, Y., Gallagher, K. L., & Basile, A. S. (1999). Skeletal muscle type ryanodine receptor is involved in calcium signaling in human B lymphocytes. *J Biol Chem*, *274*(9), 5995-6002. https://doi.org/10.1074/jbc.274.9.5995

Song, E. K., Lee, Y. R., Kim, Y. R., Yeom, J. H., Yoo, C. H., Kim, H. K., Park, H. M., Kang, H. S., Kim, J. S., Kim, U. H., & Han, M. K. (2012). NAADP mediates insulin-stimulated glucose uptake and insulin sensitization by PPARγ in adipocytes. *Cell Rep*, *2*(6), 1607-1619. https://doi.org/10.1016/j.celrep.2012.10.018

Steen, M., Kirchberger, T., & Guse, A. H. (2007). NAADP mobilizes calcium from the endoplasmic reticular Ca(2+) store in T-lymphocytes. *J Biol Chem*, *282*(26), 18864-18871. https://doi.org/10.1074/jbc.M610925200

Streb, H., Irvine, R. F., Berridge, M. J., & Schulz, I. (1983). Release of Ca2+ from a nonmitochondrial intracellular store in pancreatic acinar cells by inositol-1,4,5-trisphosphate. *Nature*, *306*(5938), 67-69. https://doi.org/10.1038/306067a0

Tae, H., Wei, L., Willemse, H., Mirza, S., Gallant, E. M., Board, P. G., Dirksen, R. T., Casarotto, M. G., & Dulhunty, A. (2011). The elusive role of the SPRY2 domain in RyR1. *Channels (Austin)*, *5*(2), 148-160. https://doi.org/10.4161/chan.5.2.14407

Taylor, C. W., Genazzani, A. A., & Morris, S. A. (1999). Expression of inositol trisphosphate receptors. *Cell Calcium*, *26*(6), 237-251. https://doi.org/10.1054/ceca.1999.0090

Toyoshima, C., & Nomura, H. (2002). Structural changes in the calcium pump accompanying the dissociation of calcium. *Nature*, *418*(6898), 605-611. https://doi.org/10.1038/nature00944

Trebak, M., & Kinet, J. P. (2019). Calcium signalling in T cells. *Nat Rev Immunol*, *19*(3), 154-169. https://doi.org/10.1038/s41577-018-0110-7

Tu, H., Wang, Z., & Bezprozvanny, I. (2005). Modulation of mammalian inositol 1,4,5-trisphosphate receptor isoforms by calcium: a role of calcium sensor region. *Biophys J*, *88*(2), 1056-1069. https://doi.org/10.1529/biophysj.104.049601

Viita, T., Kyheröinen, S., Prajapati, B., Virtanen, J., Frilander, M. J., Varjosalo, M., & Vartiainen, M. K. (2019). Nuclear actin interactome analysis links actin to KAT14 histone acetyl transferase and mRNA splicing. *J Cell Sci*, *132*(8). https://doi.org/10.1242/jcs.226852

Wagenknecht, T., Grassucci, R., & Frank, J. (1988). Electron microscopy and computer image averaging of ice-embedded large ribosomal subunits from Escherichia coli. *J Mol Biol*, *199*(1), 137-147. https://doi.org/10.1016/0022-2836(88)90384-1

Wagner, L. E., 2nd, Groom, L. A., Dirksen, R. T., & Yule, D. I. (2014). Characterization of ryanodine receptor type 1 single channel activity using "on-nucleus" patch clamp. *Cell Calcium*, *56*(2), 96-107. https://doi.org/10.1016/j.ceca.2014.05.004

Walseth, T. F., Lin-Moshier, Y., Jain, P., Ruas, M., Parrington, J., Galione, A., Marchant, J. S., & Slama, J. T. (2012). Photoaffinity labeling of high affinity nicotinic acid adenine dinucleotide phosphate (NAADP)-binding proteins in sea urchin egg. *J Biol Chem*, *287*(4), 2308-2315. https://doi.org/10.1074/jbc.M111.306563

Wang, X., Zhang, X., Dong, X. P., Samie, M., Li, X., Cheng, X., Goschka, A., Shen, D., Zhou, Y., Harlow, J., Zhu, M. X., Clapham, D. E., Ren, D., & Xu, H. (2012). TPC proteins are phosphoinositide-activated sodium-selective ion channels in endosomes and lysosomes. *Cell*, *151*(2), 372-383. https://doi.org/10.1016/j.cell.2012.08.036

Waugh, D. S. (2011). An overview of enzymatic reagents for the removal of affinity tags. *Protein Expr Purif*, *80*(2), 283-293. https://doi.org/10.1016/j.pep.2011.08.005

Wei, R., Wang, X., Zhang, Y., Mukherjee, S., Zhang, L., Chen, Q., Huang, X., Jing, S., Liu, C., Li, S., Wang, G., Xu, Y., Zhu, S., Williams, A. J., Sun, F., & Yin, C. C. (2016). Structural insights into Ca(2+)-activated long-range allosteric channel gating of RyR1. *Cell Res*, *26*(9), 977-994. https://doi.org/10.1038/cr.2016.99

Wolf, I. M., Diercks, B. P., Gattkowski, E., Czarniak, F., Kempski, J., Werner, R., Schetelig, D., Mittrücker, H. W., Schumacher, V., von Osten, M., Lodygin, D., Flügel, A., Fliegert, R., & Guse, A. H. (2015). Frontrunners of T cell activation: Initial, localized Ca2+ signals mediated by NAADP and the type 1 ryanodine receptor. *Sci Signal*, *8*(398), ra102. https://doi.org/10.1126/scisignal.aab0863

Woll, K. A., Haji-Ghassemi, O., & Van Petegem, F. (2021). Pathological conformations of disease mutant Ryanodine Receptors revealed by cryo-EM. *Nat Commun*, *12*(1), 807. https://doi.org/10.1038/s41467-021-21141-3

Yamasaki, M., Thomas, J. M., Churchill, G. C., Garnham, C., Lewis, A. M., Cancela, J. M., Patel, S., & Galione, A. (2005). Role of NAADP and cADPR in the induction and maintenance of agonist-evoked Ca2+ spiking in mouse pancreatic acinar cells. *Curr Biol*, *15*(9), 874-878. https://doi.org/10.1016/j.cub.2005.04.033

Zalk, R., Clarke, O. B., des Georges, A., Grassucci, R. A., Reiken, S., Mancia, F., Hendrickson, W. A., Frank, J., & Marks, A. R. (2015). Structure of a mammalian ryanodine receptor. *Nature*, *517*(7532), 44-49. https://doi.org/10.1038/nature13950

Zalk, R., Lehnart, S. E., & Marks, A. R. (2007). Modulation of the ryanodine receptor and intracellular calcium. *Annu Rev Biochem*, *76*, 367-385. https://doi.org/10.1146/annurev.biochem.76.053105.094237

Zalk, R., & Marks, A. R. (2017). Ca(2+) Release Channels Join the 'Resolution Revolution'. *Trends Biochem Sci*, *42*(7), 543-555. https://doi.org/10.1016/j.tibs.2017.04.005

Zhang, J., Guan, X., Shah, K., & Yan, J. (2021). Lsm12 is an NAADP receptor and a two-pore channel regulatory protein required for calcium mobilization from acidic organelles. *Nat Commun*, *12*(1), 4739. https://doi.org/10.1038/s41467-021-24735-z

Zhou, G., Wang, J., Zhang, Y., Zhong, C., Ni, J., Wang, L., Guo, J., Zhang, K., Yu, L., & Zhao, S. (2004). Cloning, expression and subcellular localization of HN1 and HN1L genes, as well as characterization of their orthologs, defining an evolutionarily conserved gene family. *Gene*, *331*, 115-123. https://doi.org/10.1016/j.gene.2004.02.025

Zhu, M. X., Ma, J., Parrington, J., Galione, A., & Evans, A. M. (2010). TPCs: Endolysosomal channels for Ca2+ mobilization from acidic organelles triggered by NAADP. *FEBS Lett*, *584*(10), 1966-1974. https://doi.org/10.1016/j.febslet.2010.02.028

Zong, X., Schieder, M., Cuny, H., Fenske, S., Gruner, C., Rötzer, K., Griesbeck, O., Harz, H., Biel, M., & Wahl-Schott, C. (2009). The two-pore channel TPCN2 mediates NAADP-dependent Ca(2+)-

release from lysosomal stores. *Pflugers Arch*, *458*(5), 891-899. https://doi.org/10.1007/s00424-009-0690-y

EIDESSTATTLICHE VERSICHERUNG

Name: Khansahib Vorname: Imrankhan

Hiermit erkläre ich an Eides statt, dass ich die vorliegende Dissertationsschrift selbst verfasst und keine anderen als die angegebenen Quellen und Hilfsmittel benutzt habe.

Hamburg, 11.04.2022 

Ort, Datum Unterschrift

ACKNOWLEDGEMENT

Firstly, I wish to express my immense gratitude to Prof. Dr. Andreas H. Guse, head of the Institute of Biochemistry and Molecular Cell Biology, who provided excellent supervision, motivation and support to complete my PhD thesis. This thesis was possible through SFB1328, project A01.

Further, I would like to thank Prof. Dr. Hans Willi Mitrücker, who kindly provided consent to evaluate my thesis.

I wish to extend my thanks to our collaboration partners,

- Group of Prof. Timothy Walseth (Department of Pharmacology, University of Minnesota Medical School, Minneapolis, Minnesota, USA) who performed PAL experiments for us.
- Group of Prof. Alexander Flügel (Department of Neuroimmunology, University Medical Center, Göttingen, Germany) who provided us the rat primary T cells and performed gene knockout in the same.
- Group of Dr. Oliver Clarke (Department of Physiology and Cellular Biophysics, Columbia University College of Physicians & Surgeons, New York, USA) who performed structural and bilayer recording experiments for us.

I wish to show my appreciation and special thanks to my colleagues of the Calcium signaling group who contributed to this thesis as internal collaborative research: Lola Hernandez, Yunpeng Zhang, Hannes G. Roggenkamp, Feng Gu, Franziska Möckl, Aileen Krüger, Anette Rosche and Valeria Wolters.

Moreover, I would also like to thank all other colleagues of the Calcium signaling group, especially Dr. Björn-Philipp Diercks, Dr. Anke Löhndorf, Dr. Mariella Weiß, Dr. Ralf Fliegert, Andreas Bauche and Dr. Sukanya Arcot Kannabiran for all their constructive discussions and support to complete my thesis. Special appreciation and thanks to Dr. Mariella Weiß and Dr. Björn-Philipp Diercks for proofreading this thesis.

I wish to convey regards to my friends, especially Srimeenakshi Sankaranarayan, who provided constant support and affection throughout my time to complete this thesis.

Finally, I would like to thank my family members without whom I could not have achieved this position in my life. Their constant love and support served as fuel to complete my thesis away from home.